The Dissertation Committee for Daniel Blazevski
Certifies that this is the approved version of the following dissertation:

ON THE ROLE OF INVARIANT OBJECTS IN APPLICATIONS OF DYNAMICAL SYSTEMS

Committee:

Thomas Chen, Supervisor

Rafael de la Llave, Supervisor

Hans Koch

Phil Morrison

Cesar Ocampo

Natasa Pavlovic

Alexis Vasseur

ON THE ROLE OF INVARIANT OBJECTS IN APPLICATIONS OF DYNAMICAL SYSTEMS

by

Daniel Blazevski, B.S.; M.A.

DISSERTATION

Presented to the Faculty of the Graduate School of

The University of Texas at Austin

in Partial Fulfillment

of the Requirements

for the Degree of

DOCTOR OF PHILOSOPHY

THE UNIVERSITY OF TEXAS AT AUSTIN

May 2012

Dedicated to my parents, Danca and Krume.

Acknowledgments

The amount of gratitude I have for Rafael de la Llave is related to the number of degrees of freedom considered in a recent paper of ours: They are both infinite. I consider myself honored to have been his student and I greatly admire and appreciate his patience, encouragement, wisdom, work ethic, vast knowledge, and dedication. In many aspects, he has and will continue to serve as a inspiration for me to follow. I am grateful that he encouraged me to take courses in other departments and to spend time in a national laboratory. As he is well aware, these experiences were a significant part of this dissertation, and I am very grateful that he led me to pursue such interdisciplinary research. None of the work that I have accomplished as a graduate student would have been possible with his efforts. Thanks, Rafael.

I would also like to thank Thomas Chen for serving as my co-supervisor. I am grateful for the interesting conversations we have had and his interest in my research and for his interest in my academic well-being. I would also like to thank Hans Koch, Phil Morrison, Cesar Ocampo, Natasa Pavlovic and Alexis Vasseur for serving on my committee.

I am grateful that I had the opportunity to enroll in courses with Cesar Ocampo. Through these courses my computational abilities were strongly en-

hanced. I was also pleasantly surprised to learn that sophisticated techniques from dynamical systems can be used for very practical problems. His demonstrated a great interest and patience in teaching me techniques from computing and engineering that were standard for many students in the courses I took from him, and for this I am very grateful. Lastly, I would like to thank him for his enthusiasm and interest in the project we worked on together.

I was fortunate to have met Phil Morrison as a graduate student. I appreciate him teaching me plasma physics, I was able to learn a lot from him and I am grateful his was willing to teach me various topics in plasma physics even though I knew very little about the subject when I met him. I am also very grateful that he played an important role in me starting a collaboration with Diego del-Castillo-Negrete.

My work with Diego del-Castillo-Negrete has been a great experience thus far. I admire his willingness to embark on a project with me to study magnetically confined plasma even though I only knew little about the subject. I am amazed at how much I have learned from working with him. I am grateful that he taught me so many interesting topics in dynamical systems, plasma physics, non-locality and for expanding my computational tools. I would also like to thank Luis Chacon of Oak Ridge National Laboratory for sharing his code to compute parallel heat transport, and for teaching me how to use the code and other computational tools.

Dan Knopf has been an excellent graduate advisor, and I am very

grateful for his efforts, especially in dealing the bureaucracy involved in me spending a semester at the Georgia Institute of Technology. I would like to thank Sandra Catlett, Mark North, and Nancy Lamm for being very helpful over the years. I would also like to thank Maorong Zou for kindness in helping me with the math department's computer system at UT, and also for spending several hours repairing my laptop. I am also very grateful to have had the experience of advising Jennifer Franklin on a project related to my research interests. She has worked very hard on the project, and I hope she continues to succeed in her pursuits.

I would also like to thank Rafael de la Llave's former and current students Renato Calleja, Jason Mireles James, Timothy Blass and Mikel de Viana for having taught me concepts from dynamical systems for their ongoing support and encouragement. I am glad we are able to continue being good friends and continue having interesting discussions. I would also like to thank Hector Lomelli and Xifeng Su for their discussions and support. I would also like to thank the many long-term visitors Rafael had over the years, namely Maciej Capinski, Alejandro Luque, Jordi Luis-Figueras and Fabricio Macia. They made for a more enjoyable and broad experience, and I am glad to have had the pleasure to meet and collaborate with them. Also, I have met some great people in the Working Dynamical Systems seminar, and I would like to thank them for their enthusiasm in participating the seminar. I am also grateful for the happy hour that often followed the seminar, this set up a very positive

environment for working with Rafael and his students and I got to know many interesting visiting researchers during the post-seminar happy hour. I would also like to thank my friends Jacob Glenn-Levin, Nick Rauh, Mio Alter, Sean Bowman, Hector Chang, Davi Maximo, Rory Rother and Mark Norfleet for their support and the good times we had.

I would like to thank my family. My sister Kiki was always willing to help in a time of need and always believed in me and wanted and inspired me to do great things. Thanks, sis. My cousins Robert, Borce, Michael and Nikki, my aunts Ilinka and Sonja, my uncles Dusko and Zive, grandmas Mitana and Bogina, a big thanks to all of you for you support, your love, and for believing in me.

Lastly, I would like to thank my parents, Danca and Krume. I am still amazed by the fact that neither of you, my aunts, my uncles, nor my grandparents have a college degree, yet you were able to raise me to get a PhD in mathematics and to write a dissertation that I am very proud of. Words cannot express how grateful and proud of you I am that you endured struggles having moved from Macedonia to the United States in your youth. Without your support, your perseverance, your love, this dissertation would not have been possible, any success I have or will have is yours. Thanks.

ON THE ROLE OF INVARIANT OBJECTS IN APPLICATIONS OF DYNAMICAL SYSTEMS

Publication No. _____

Daniel Blazevski, Ph.D.
The University of Texas at Austin, 2012

Supervisors: Thomas Chen
Rafael de la Llave

In this dissertation, we demonstrate the importance of invariant objects in many areas of applied research. The areas of application we consider are chemistry, celestial mechanics and aerospace engineering, plasma physics, and coupled map lattices.

In the context of chemical reactions, stable and unstable manifolds of fixed points separate regions of phase space that lead to a certain outcome of the reaction. We study how these regions change under the influence of exposing the molecules to a laser.

In celestial mechanics and aerospace engineering, we compute periodic orbits and their stable and unstable manifolds for a object of negligible mass (e.g. a satellite or spacecraft) under the presence of Jupiter and two of its moons, Europa and Ganymede. The periodic orbits serve as convenient spot

to place a satellite for observation purposes, and computing their stable and unstable manifolds have been used in constructing low-energy transfers between the two moons.

In plasma physics, an important and practical problem is to study barriers for heat transport in magnetically confined plasma undergoing fusion. We compute barriers for which heat cannot pass through. However, such barriers break down and lead to robust partial barriers. In this latter case, heat can flow across the barrier, but at a very slow rate.

Finally, infinite dimensional coupled map lattice systems are considered in a wide variety of areas, most notably in statistical mechanics, neuroscience, and in the discretization of PDEs. We assume that the interaction amont the lattice sites decays with the distance of the sites, and assume the existence of an invariant whiskered torus that is localized near a collection of lattice sites. We prove that the torus has invariant stable and unstable manifolds that are also localized near the torus. This is an important step in understanding the global dynamics of such systems and opens the door to new possible results, most notably studying the problem of energy transfer between the sites.

Table of Contents

List of Tables

List of Figures

Chapter 1

Introduction

In this dissertation we present new results on the use of invariant objects to understand applied dynamical systems. We focus on four distinct areas of applications: chemistry, celestial mechanics and aerospace engineering, heat transport in fusion plasmas, and coupled map lattices. I cannot think of a more concise and accurate description of the role of invariant objects in dynamical systems than the one given by Carles Simò [68]:

> Objects which play a key role for the organization of the dynamics (or the so called *skeleton* of the system) are the *invariant objects* under the action of the dynamics: periodic orbits, invariant tori, invariant stable and unstable manifolds, etc. They give a key to predict or to interpret the behavior of most of the points in the *phase space*, following Poincarè's idea that it is better to study the full set of orbits rather than individual ones

Chapter 2 contains a paper [11] that has appeared in *Journal of Physics A: Mathematical and Theoretical* co-authored by Dr. Rafael de la Llave. The last section of Chapter 2 contains more recent work with Jennifer Franklin [14],

a undergraduate student at the University of Texas at Austin. This project was started as a summer research project that I was advising her on and we now plan on submitting this work to a peer-reviewed journal for publication. Chapter 3 consists of a project [9] done in collaboration with aerospace engineering professor Dr. Cesar Ocampo. Our work has been accepted for publication in *Physica D: Nonlinear phenomena*. In Chapter 4 we discuss a project done in collaboration with Dr. Diego del-Castilo-Negrete, a scientist at Oak Ridge National Laboratory. This project is expected to result in the publication or two papers [13, 12] submitted to peer-reviewed journals. Chapter 5 contains a draft of a paper [10] done in collaboration with Rafael de la Llave, and we plan on submitting our work to a peer-reviewed journal for publication.

In Chapter 2 we develop a classical time-dependent scattering theory for general systems subject to a non-autonomous perturbation that is localized in time, and then apply the theory thus developed to the problem of laser-driven molecular reactions. The results of this chapter are based off of published work with Rafael de la Llave. In this case, the role of invariant objects is that stable and unstable manifolds normally hyperbolic invariant manifolds separate regions of phase space that lead to a certain outcome of a reaction, and we want to understand how these regions are modified by exposing the molecules to a laser for a short time. The final section of Chapter 2 uses the theoretical framework thus developed in to use scattering theory to carry out numerical computations of invariant manifolds for the laser-driven Henon-Heilies system, a system considered by chemists in [56]. This work is the continuation of a summer project in which I was advising undergraduate

student Jennifer Franklin.

In Chapter 3 we consider the motion of an object with negligible mass, e.g. a spacecraft, in the presence of three massive bodies. The specific model we consider is the Jupiter-Europa-Ganymede-spacecraft system, though the techniques can be generalized to other restricted four-body systems. We give numerical calculations of Lyapunov-like periodic orbits and their stable and unstable manifolds for the system. Due to the non-autonomous nature of the equations of motion, this task is more subtle than in the restricted three-body problem. The key ingredient to our algorithm to construct periodic orbits is the Laplace resonance, which states that $\omega_E \approx 2\omega_G$, where ω_E, ω_G are the frequencies of motion of Europa and Ganymede about Jupiter, respectively. The computations of the stable and unstable manifolds shows that the unstable manifold

In Chapter 4, we consider the problem of heat transport in magnetically confined plasma. We give numerical computations of transport barriers, i.e. invariant objects associated to the magnetic field lines. We observe that heat cannot be transported across the barrier in the case that the barrier is a smooth curve. Once the curve breaks down, there are still robust partial cantor-like transport barriers. In these partial barriers, heat can move across the barriers, but the rate at which this occurs is much slower than the diffusivity rates away from the barriers.

Finally, in Chapter 5 we prove the existence of localized stable manifolds for lattice systems with decaying interaction. This is joint work with Dr.

Rafael de la Llave. In finite dimensional systems using stable and unstable manifolds of whiskered KAM tori has proved to be a robust mechanism for demonstrating the energy transfer between weakly coupled systems. Recently Dr. de la Llave and collaborators proved a KAM-type theorem for whiskered tori in infinite dimensional coupled map lattices. They assume that the interaction amont lattice sites decays with the distance of the lattice sites and they are then able to prove that the tori they construct are localized near a certain collection of lattice sites. In our work we assume the existence of a infinite dimensional whiskered torus and prove that it has a stable and unstable manifold that is localized near the torus.

Chapter 2

Time-dependent scattering theory for ODEs and applications to reaction dynamics

2.1 Introduction

Many physical situations are described by an ODE subject to a time dependent perturbation which is localized in space and time. That is, a system whose evolution is given by finding trajectories of a time-dependent vector field

$$\mathcal{V}(x,t) = \mathcal{U}(x,t) + \mathcal{F}(x,t) \tag{2.1}$$

where $\mathcal{F}(x,t)$ is localized in space and time (e.g. $|\mathcal{F}(x,t)| \leq C\exp(-\lambda|t|)$). All the vector fields in this chapter are assumed to be defined on $\mathbb{R}^n$.

Notice that we do not assume that $\mathcal{F}$ is uniformly small. Indeed, in the motivating examples we have in mind $\mathcal{F}$ will not, for instance, depend on a parameter ϵ whose value is taken to be sufficiently small. Indeed, the examples we have in mind include: exposing molecules to a laser, an ion passing near a molecule, and similarly the passage of a comet of a a planet-satellite system. These phenomenon have been studied in chemistry and astronomy using a variety of methods (e.g. transition state theory [56] and adiabatic perturbation theory [75, 39, 52]. The goal of this chapter is to present a treatment based

on scattering theory. Since the perturbation is localized in time, it is easy to guess that a trajectory of the full system will behave, both in the past and in the future, like a trajectory of the unperturbed system. It is then natural to write the future (or past) asymptotic states as functions of the present states. This is were the *wave maps* $\Omega_{\pm}^{t_0}$ come in: $\Omega_{+}^{t_0}$ (resp. $\Omega_{-}^{t_0}$) is a function on the phase space that takes the present states of a system as an input and output the future (resp. past) states. The composition $s^{t_0} = \Omega_{+}^{t_0} \circ (\Omega_{-}^{t_0})^{-1}$, called the *scattering map*, computes the future states knowing the past states is also of physical interest.

In section 2, working in the context of general time-dependent vector fields in $\mathbb{R}^n$, we give conditions on $\mathcal{U}$ and $\mathcal{V}$ that ensure the existence, smoothness, and invertibility of the wave maps $\Omega_{\pm}^{t_0}$ and scattering map s^{t_0}. The wave maps $\Omega_{+}^{t_0}$ (resp. $\Omega_{-}^{t_0}$) compute a systems asymptotic future (resp. past) knowing the present state of the system. The scattering map $s^{t_0} = \Omega_{+}^{t_0} \circ (\Omega_{-}^{t_0})^{-1}$ computes the asymptotic future knowing the asymptotic past. The method to prove existence uses deformation theory [19] and is analogous to Cook's method in quantum mechanics [64]. We also give conditions on the vector fields, $\mathcal{V}_\sigma$, $\mathcal{U}_\sigma$ and the flow $U_{t_0}^t$ that implies that the wave maps are invertible, a property called *asymptotic completeness* in quantum mechanical scattering theory. Note that our conditions do not involve the flow $V_{t_0}^t$, which is very convenient since this implies we can use scattering theory to understand $V_{t_0}^t$ knowing only the vector fields and $U_{t_0}^t$.

Using scattering theory, we then show that the existence, smoothness and invertibility yields intertwining relations for the wave maps $\Omega_{\pm}^{t_0}$ and we

show that the dynamics of $\mathcal{U}$ and $\mathcal{V}$ are conjugate when viewed as autonomous vector fields on the extended space $\mathbb{R}^n \times \mathbb{R}$.

Based on of the intertwining relations results and the applications we have in mind, we develop a notion of a time-dependent normally hyperbolic invariant manifold and discuss how we can use $\Omega_{\pm}^{t_0}$ to compute such manifolds and their corresponding stable/unstable manifolds.

In Section 3 we give perturbative calculations of the scattering map. Thus, we will consider vector fields of the form

$$\mathcal{V}(x,t) = \mathcal{U}(x,t) + \epsilon \mathcal{F}(x,t) \tag{2.2}$$

In this setting we show that the scattering map is the time-ϵ map of a vector field $\mathcal{S}_\epsilon$ and give explicit formulas for $\mathcal{S}_\epsilon$. The result is analogous to Fermi's Golden Rule in quantum mechanics as considered in [61, 64, 72, 73].

We also show that, in the case of Hamiltonian systems, $\mathcal{S}_\epsilon$ has a corresponding Hamiltonian S_ϵ. The results and methods of proof are similar to the perturbative calculations of scattering map for a normally hyperbolic manifold [**?**].

In Section 4, we apply the theory developed to a problem in transition state theory. In [56] they consider the problem of understanding how the dynamics of reaction between molecules behaves under the influence of a laser pulse. In their work, they compute time-dependent invariant manifolds using normal form theory. We give an alternate method to compute the manifolds that were computed in [56] using scattering theory.

We also give perturbative calculations of the quantity called the *branching ratio* in [56] which measures the fraction of initial conditions which go into different scattering channels. In quantum mechanics this is called the *branching fraction* (see [1]) but we will stick with the name "branching ratio" used in [56].

2.2 Definitions and existence/smoothness results

In this section will work with general time-dependent ODE's, and consider more specific cases later. Let $\mathcal{U}_t$ and $\mathcal{V}_t$ be two time-dependent vector fields on $\mathbb{R}^n$, and let $U_{t_0}^t$ and $V_{t_0}^t$ be the corresponding flows. Thus $U_{t_0}^t$ satisfies the equation

$$\begin{aligned} \frac{d}{dt} U_{t_0}^t(x) &= \mathcal{U}_t(U_{t_0}^t(x)), \\ U_{t_0}^{t_0}(x) &= x \end{aligned} \tag{2.3}$$

and moreover, $U_{t_0}^t \circ U_s^{t_0} = U_s^t$. Of course, $V_{t_0}^t$ satisfies a similar equation.

We define the *wave maps* by

$$\Omega_{\pm}^{t_0} = \Omega_{\pm}^{t_0}(U, V) = \lim_{t \to \pm\infty} U_t^{t_0} \circ V_{t_0}^t$$

The intuition is that $\Omega_+^{t_0}$ (resp. $\Omega_-^{t_0}$) gives the orbital elements in the future (resp. past) given the present orbital elements. Assuming that $\Omega_-^{t_0}$ is invertible, the *scattering map* which is defined by

$$s^{t_0} = \Omega_+^{t_0} \circ \left(\Omega_-^{t_0}\right)^{-1}$$

gives the future orbital elements knowing the past. To make the intuition of

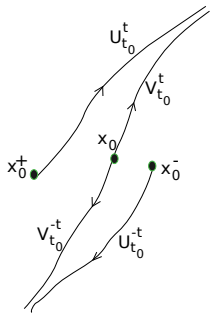

Figure 2.1: Pictorial description of the wave and scattering maps. For a given point x_0 let $x_0^{\pm} := \Omega_{\pm}^{t_0}$. Then $V_{t_0}^t(x_0)$ converges in the future (resp. past) to $U_{t_0}^t(x_0^+)$ (resp. $U_{t_0}^{-t}(x_0^-)$) and the scattering map takes x_0^- as an input and outputs x_0^+.

wave maps a bit more concrete notice that for large $T > 0$ we have

$$U_{t_0}^{\pm T}(\Omega_{\pm}^{t_0}(x)) \approx V_{t_0}^{\pm T}(x)$$

Thus, the wave maps give us a precise way of describing how, for large times, the flow $V_{t_0}^t$ behaves like the flow for $U_{t_0}^t$, though the flows may be quite distinct for short times (See Figure 2.1).

Notice that the wave maps depend on the starting time t_0 of the non-autonomous flow $U_{t_0}^t$. This is what makes the theory different from scattering theory for time independent vector fields. This will become especially relevant in the next section when discussing the intertwining relations and conjugacy.

Before we give conditions that ensure the existence, smoothness, invertibility of the wave maps, we recall the definition the function space $C^k(B_R)$,

where B_R refers to the ball of radius R in $\mathbb{R}^n$

$$C^k(B_R) = \{f : B_R \to \mathbb{R}^n : \sup_j \sup_{x \in B_R} \|D^j f(x)\| < \infty\}$$

Here $\|D^j f(x)\|$ refers to the norm of the $D^j f(x)$ as a $j-$multilinear map, that is the smallest of all real number M such that

$$|D^j f(x)(v_1, \ldots, v_j)| \leq M|v_1| \cdots |v_j|$$

and $|v_i|$ simply refers to the Euclidean norm of v_i. For a function in $C^k(B_R)$ we define its C^k norm as

$$\|f\|_{C^k} = \sup_j \sup_{x \in B_R} \|D^j f(x)\|$$

We now impose conditions on $U_{t_0}^t$ and $V_{t_0}^t$ that ensure that the wave maps and scattering map exist, are smooth, depend smoothly on parameters, and are invertible. The proof of existence is similar to Cook's method [64] in quantum mechanical scattering theory and also relies heavily on deformation theory. Let us recall briefly a basic definition from deformation theory that we will use here. The details and propositions that we use are in Appendix A. Let f_a be a family diffeomorphisms, and define the vector field $\mathcal{F}_a$ by

$$\frac{d}{da} f_a = \mathcal{F}_a \circ f_a$$

$\mathcal{F}_a$ is called the *vector field generating* f_a.

Theorem 2.2.1. *Suppose that the following condition on the flows* $U_{t_0}^t$ *and* $V_{t_0}^t$ *is satisfied:*

The integrals

$$I_{\pm}(t_0) = \int_{t_0}^{\pm\infty} \| \left(DU_{\sigma}^{t_0}(\mathcal{V}_{\sigma} - \mathcal{U}_{\sigma}) \right) \circ V_{t_0}^{\sigma} \|_{C^k(B_R)} d\sigma < \infty$$

Then:

(1) the wave maps

$$\Omega_{\pm}^{t_0} = \lim_{t \to \pm\infty} U_t^{t_0} \circ V_{t_0}^t$$

exist and are in $C^k(B_R)$ for every R.

(2) Suppose that $k > 1$ and that the limits

$$\lim_{t_0 \to \infty} I_+(t_0) = \lim_{t_0 \to -\infty} I_-(t_0) = 0$$

hold. Then $\Omega_{\pm}^{t_0}$ are invertible, and their inverses are in $C^k(B_R)$ for every $R > 0$

Proof of (1): First, we show that $\Omega_+^{t_0}$ exists. Define $\Omega_+^{(t_0,T)} := U_T^{t_0} \circ V_{t_0}^T$. Since the maps $V_{t_0}^t$ and $U_{t_0}^t$ are diffeomophisms we can use deformation theory (c.f. appendix A) to construct the vector field generating $\Omega_+^{(t_0,T)}$. Using Proposition A.0.8 from the appendix and the fact that $\mathcal{U}_t$ and $\mathcal{V}_t$ generate $U_{t_0}^t$ and $V_{t_0}^t$ respectively we have that the generator, $\mathcal{O}_T^+$, of $\Omega_+^{(t_0,T)}$ is given by

$$\mathcal{O}_T^+ = -(U_T^{t_0})_* \mathcal{U}_T + (U_T^{t_0})_* \mathcal{V}_T = (U_T^{t_0})_* (\mathcal{V}_T - \mathcal{U}_T) \tag{2.4}$$

The Fundamental Theorem of Calculus implies that

$$\Omega_+^{(t_0,T+1)} - \Omega_+^{(t_0,T)} = \int_T^{T+1} \mathcal{O}_\sigma^+ \circ \Omega_+^{(t_0,\sigma)} d\sigma \tag{2.5}$$

and hence

$$\sum_{N>t_0}^{\infty} \|\Omega_+^{(t_0,N+1)} - \Omega_+^{(t_0,N)}\|_{C^k(B_R)} \leq \int_{t_0}^{\infty} \|\mathcal{O}_\sigma^+ \circ \Omega_+^{(t_0,\sigma)}\|_{C^k(B_R)} d\sigma$$
$$= \int_{t_0}^{\infty} \|(U_\sigma^{t_0})_*(\mathcal{V}_\sigma - \mathcal{U}_\sigma) \circ \Omega_+^{(t_0,\sigma)}\|_{C^k(B_R)} d\sigma = \int_{t_0}^{\infty} \| \left(DU_\sigma^{t_0}(\mathcal{V}_\sigma - \mathcal{U}_\sigma)\right) \circ V_{t_0}^\sigma \|_{C^k(B_R)} d\sigma \tag{2.6}$$

Since we are assuming the integral converges we conclude that

$$\sum_{N>t_0}^{\infty} \|\Omega_+^{(t_0,N+1)} - \Omega_+^{(t_0,N)}\|_{C^k(B_R)} < \infty$$

and it follows that $\Omega_+^{(t_0,N)}$ converges to a function $\Omega_+^{(t_0,\infty)}$. Moreover, since

$$\|\Omega_+^{(t_0,\infty)} - \Omega_+^{(t_0,T)}\|_{C^k(B_R)} \leq \int_T^{\infty} \| \left(DU_\sigma^{t_0}(\mathcal{V}_\sigma - \mathcal{U}_\sigma)\right) \circ V_{t_0}^\sigma \|_{C^k(B_R)} ds$$

we conclude that $\|\Omega_+^{(t_0,\infty)} - \Omega_+^{(t_0,T)}\|_{C^k(B_R)} \to 0$ as $T \to \infty$ *and* $T \in \mathbb{R}$, which proves the existence of $\Omega_+^{t_0}$.

Similarly, for $\Omega_-^{t_0}$ one considers the family of maps $\Omega_-^{(t_0,T)} = U_{t_0}^{-T} \circ V_{-T}^{t_0}$, which is generated by the vector field $\mathcal{O}_T^- = -\mathcal{O}_{-T}^+$. Using an argument analogous for $\Omega_+^{t_0}$, the existence and smoothness off $\Omega_-^{t_0}$ follows provided that

$$\int_{-t_0}^{\infty} \|(DU_{-\sigma}^{t_0}(\mathcal{V}_{-\sigma} - \mathcal{U}_{-\sigma})) \circ V_{t_0}^{-\sigma}\|_{C^k(B_R)} d\sigma = \int_{-\infty}^{t_0} \|(DU_\sigma^{t_0}(\mathcal{V}_\sigma - \mathcal{U}_\sigma)) \circ V_{t_0}^\sigma\|_{C^k(B_R)} d\sigma \tag{2.7}$$

is finite.

Proof of (2) Now we show that $\Omega_\pm^{t_0}$ are invertible and their inverses are C^k. We prove invertibility for $\Omega_+^{t_0}$, and note that proving invertbility for $\Omega_-^{t_0}$

is similar. We first note that it suffices to prove that $\Omega_+^{t_0}$ is invertible for one value of t_0 . Indeed, we have the following identity

$$\Omega_+^s = U_{t_0}^s \circ \Omega_+^{t_0} \circ V_s^{t_0} \tag{2.8}$$

The proof (2.8) follows straight from the definition of the wave maps. We will discuss (2.8) in more detail in section 2.2. For now we notice that it implies that Ω_+^s is invertible as long as $\Omega_+^{t_0}$ is invertible for some t_0, as claimed.

Now we prove that there is one value of t_0 for which $\Omega_+^{t_0}$ is invertible. Notice that $\Omega_+^{(t_0,t)} - \Omega_+^{(t_0,s)} = \int_s^t \mathcal{O}_\sigma^+ \circ \Omega_+^{(t_0,\sigma)} d\sigma$ Since $\Omega_+^{(t_0,t_0)}(x) = U_{t_0}^{t_0} V_{t_0}^{t_0}(x) = x$ we have that $\Omega_+^{(t_0,t)} - x = \int_{t_0}^t \mathcal{O}_\sigma^+ \circ \Omega_+^{(t_0,\sigma)} d\sigma$ and hence taking the limit as $t \to \infty$ we have that

$$\Omega_+^{t_0} - x = \int_{t_0}^\infty \mathcal{O}_\sigma^+ \circ \Omega_+^{(t_0,\sigma)} d\sigma$$

It follows that

$$\| \Omega_+^{t_0} - \text{ Id } \|_{C^k(B_R)} \leq \int_0^\infty \| (U_\sigma^{t_0})_* (\mathcal{V}_\sigma - \mathcal{U}_\sigma) \circ \Omega_+^{(t_0,\sigma)} \|_{C^k(B_R)} d\sigma \tag{2.9}$$

However, assumption (2) is that the integral tends to zero as $t_0 \to \infty$ for every $R > 0$. Thus given any $y \in \mathbb{R}^{2n}$ with $|y| < R$ and $\epsilon > 0$ we can find a t_0 large enough so that $\| \Omega_+^{t_0} - \text{ Id } \|_{C^k(B_{2R})} < \epsilon$ Thus $\Omega_+^{t_0}$ can be made as close to the identity on any given ball. The next lemma tells us that this implies that $\Omega_+^{t_0}$ is invertible provided $k \geq 2$.

Lemma 2.2.2. *Suppose that $F : \mathbb{R}^n \to \mathbb{R}^n$ is in $C^1(B_R)$. There is a $\epsilon_0 > 0$ such that if $\epsilon < \epsilon_0$ and*

$$\| F - \ Id \ \|_{C^k(B_R)} < \epsilon$$

Then for any $y \in B_{\frac{R}{2}}$ the equation

$$F(x) = y$$

has a solution $x \in B_R$.

Proof: The idea is that $|F(y) - y| < \epsilon$, that is y is an approximate solution to $F(x) = y$, and hence we can use Newton's method to solve the equation $F(x) = y$. Thus we consider

$$G(x) = x - DF(y)^{-1}(F(x) - y)$$

since $G(x) = x$ implies $F(x) = y$. One can show that, for ϵ sufficiently small, G satisfies the hypothesis of the Contraction Mapping Theorem in a ball $B(r; y)$ for some $r > 0$.

□

We now apply Lemma 2.2.2 to $F = \Omega_+^{t_0}$, which satisfies the hypotheses of the lemma provided t_0 is large enough to conclude that $\Omega_+^{t_0}$ is invertible, and $(\Omega_\pm^{t_0})^{-1}$ is in $C^k(B_R)$ for every $R > 0$.

□

Now let us state a corollary that explains when the conditions of the theorem are satisfied.

Corollary 2.2.3. *Suppose that $\mathcal{U}_t$ and $\mathcal{V}_t$ are $C^k(B_R)$ for every $R > 0$ and some integer $k > 0$. Moreover suppose that $\mathcal{U}_t - \mathcal{V}_t$ is compactly supported in time, that is, $\mathcal{U}_t - \mathcal{V}_t \equiv 0$ for $t \notin [T_1, T_2]$. The wave maps $\Omega_\pm^{t_0}$ exist, are in $C^k(B_R)$ for every $R > 0$ and are invertible.*

Proof: The conditions of Theorem 1 were that $I_{\pm}(t_0) = \int_{t_0}^{\pm\infty} \| \left(DU_{\sigma}^{t_0}(\mathcal{V}_{\sigma} - \mathcal{U}_{\sigma})\right) \circ V_{t_0}^{\sigma} \|_{C^k(B_R)} d\sigma < \infty$ and $\lim_{t_0 \to \infty} I_+(t_0) = \lim_{t_0 \to -\infty} I_-(t_0) = 0$. In the case that $\mathcal{V}_{\sigma} - \mathcal{U}_{\sigma}$ is compactly supported in time $I_{\pm}(t_0)$ are integrals over finite intervals and are also compactly supported with respect to t_0. $\square$

Corollary 2.2.4. *The integrals*

$$I_{\pm}(t_0) = \int_{t_0}^{\pm\infty} \| \left(DU_{\sigma}^{t_0}(\mathcal{V}_{\sigma} - \mathcal{U}_{\sigma})\right) \circ V_{t_0}^{\sigma} \|_{C^k(B_R)} d\sigma$$

are finite provided that

(1)

$$I_{\pm}(t_0) = \int_{t_0}^{\pm\infty} \| \left(DU_{\sigma}^{t_0}(\mathcal{V}_{\sigma} - \mathcal{U}_{\sigma})\right) \circ V_{t_0}^{\sigma} \|_{C^0(B_R)} d\sigma$$

are finite and

(2)

$$\| \left(DU_{\sigma}^{t_0}(\mathcal{V}_{\sigma} - \mathcal{U}_{\sigma})\right) \circ V_{t_0}^{\sigma} \|_{C^{k+1}(B_R)} \leq M$$

where M is independent of σ. It follows that the wave maps exist and are in $C^k(B_R)$ for every $R > 0$.

Proof: The proof of this is simply an application of Hadamard's inequality, which asserts that

$$\|f\|_{C^s(B_R)} \leq C_{r,t} \|f\|_{C^r(B_R)}^{\mu} \|f\|_{C^t(B_R)}^{1-\mu}$$

for any function f in $C^t(B_R)$ where $0 \leq r < s < t$ and $\mu = \frac{t-s}{t-r}$. We simply take $s = k$, $r = 0$ and $t = k+1$ This inequality was originally proven by Hadamard [45] and later generalized by Kolmogoroff [58]. A more modern version of the inequality appears in [20] $\square$

Corollary 2.2.5. *For $n \geq 2$ consider the annuli $A_n = \{x \in \mathbb{R}^n : n-1 \leq |x| \leq n\}$. Suppose the estimates hold:*

$$\sup_{A_n} \|DU_\sigma^{t_0}(x)\| \leq C_n e^{\lambda(n)|\sigma - t_0|}$$

and

$$\sup_{A_n} |\mathcal{V}_\sigma - \mathcal{U}_\sigma| \leq \tilde{C}_n e^{-\mu(n)|\sigma|}$$

Where $0 < \lambda(n), \mu(n)$, $\alpha := \sup_n(\lambda(n) - \mu(n)) < 0$ and $0 < C_n \tilde{C}_n < M$ for some $M > 0$. The integrals

$$I_\pm(t_0) = \int_{t_0}^{\pm\infty} \| \left(DU_\sigma^{t_0}(\mathcal{V}_\sigma - \mathcal{U}_\sigma)\right) \circ V_{t_0}^\sigma \|_{C^0(B_R)} d\sigma$$

are finite and hence the wave maps exist and in $C^0(B_R)$ for every $R > 0$. Moreover, we also have that $\lim_{t_0 \to \infty} I_+(t_0) = \lim_{t_0 \to -\infty} I_-(t_0) = 0$

Proof: We prove the results for $\Omega_+^{t_0}$. We simply break up the integrals I_+ into parts when $V_{t_0}^\sigma$ lies in A_n for each $n \geq 2$. For example, if we let A_1 denote the ball of radius 1 then we can write I_+ as

$$\begin{aligned} I_+(t_0) &= \int_{t_0}^{\pm\infty} \| \left(DU_\sigma^{t_0}(\mathcal{V}_\sigma - \mathcal{U}_\sigma)\right) \circ V_{t_0}^\sigma \|_{C^0(B_R)} d\sigma \\ &= \sum_{n=1}^{\infty} \int_{\{\sigma > t_0 : V_{t_0}^\sigma \in A_n\}} \| \left(DU_\sigma^{t_0}(\mathcal{V}_\sigma - \mathcal{U}_\sigma)\right) \circ V_{t_0}^\sigma \|_{C^0(B_R)} d\sigma \qquad (2.10) \\ &\leq \sum_{n=1}^{\infty} \int_{\{\sigma > t_0 : V_{t_0}^\sigma \in A_n\}} M e^{-\alpha\sigma} d\sigma \leq \int_{t_0}^{\infty} M e^{-\alpha\sigma} e^{\lambda t_0} d\sigma \end{aligned}$$

It follows that $I_+(t_0) < \infty$ and $\lim_{t_0 \to \infty} I_+(t_0) = 0$.

□

The importance of this corollary is that it give conditions that guarantee the existence of the wave maps that depend only on the vector fields $\mathcal{U}_\sigma, \mathcal{V}_\sigma$ and the flow $U^t_{t_0}$, but not the flow $V^t_{t_0}$. Conditions like this are very desirable from the viewpoint of applications since the goal of scattering theory is to understand better the flow $V^t_{t_0}$. We now extend Corollary 2.2.5 to obtain conditions that guarantee higher smoothness of the wave maps, which is especially important since our proof of the invertibility of the wave maps required C^1 smoothness.

The idea behind the next proposition is straightforward to understand, though we need some terminology from differential topology (see [2] for more details). For any smooth function $f : \mathbb{R}^n \to \mathbb{R}^n$ define $Tf : \mathbb{R}^{2n} \to \mathbb{R}^{2n}$ by

$$Tf(x, v) = (x, Df(x)v)$$

The letter T refers the *tangent functor* from differential topology. We would like to say that

$$D\Omega^{t_0}_{\pm} = \lim_{T\to\infty} D\Omega^{t_0,T}_{\pm} = \lim_{T\to\infty} D(U^{t_0}_{\pm T} V^{\pm T}_{t_0})$$

exists. Consider the variational equations

$$\begin{aligned} \frac{d}{dt} DU^t_{t_0} v &= D\mathcal{U}_t(U^t_{t_0}) DU^t_{t_0} v \\ \frac{d}{dt} DV^t_{t_0} v &= D\mathcal{V}_t(V^t_{t_0}) DV^t_{t_0} v \end{aligned} \tag{2.11}$$

A convenient way of organizing the study of the variational equations (2.11) is to use the tangent functor. Indeed, consider the vector field $\mathcal{U}^1_t$ defined on $\mathbb{R}^n \times \mathbb{R}^n$ defined by

$$\mathcal{U}^1_t(x, v) = (\mathcal{U}_t(x), D\mathcal{U}_t(x)v)$$

The corresponding flow $U_t^1(t_0, x, \eta)$ is given by

$$U_t^1(t_0, x, v) = (U_{t_0}^t(x), DU_{t_0}^t(x)v)$$

and we notice that $U_t^1(t_0, x, v) = TU_{t_0}^t(x, v))$, that is, $TU_{t_0}^t$ and $TV_{t_0}^t$ correspond to flows for a vector field, and hence we can also consider the wave maps for these flows. In fact we have

$$\begin{aligned} &T\Omega_{\pm}^{t_0}(U, V)(x, v) = (\Omega_{\pm}^{t_0}(x), D\Omega_{\pm}^{t_0}(x)v) \\ &= \lim_{t\to\pm\infty} (U_t^{t_0} \circ V_{t_0}^t(x), DU_t^{t_0}(V_{t_0}^t(x))DV_{t_0}^t(x)v) = \Omega_{\pm}^{t_0}(TU, TV)(x, v) \end{aligned} \tag{2.12}$$

Thus we conclude that

$$T\Omega_{\pm}^{t_0}(U, V) = \Omega_{\pm}^{t_0}(TU, TV) \tag{2.13}$$

which is the fundamental identity. The crux of the idea for higher regularity is now simple: Corollary 2.2.5 gives conditions for the wave maps to exist and be continuous. Applying this corollary to the flows TU and TV gives us conditions on the vector fields $\mathcal{U}_t, \mathcal{V}_t$ that guarantee $\Omega_{\pm}^{t_0}(TU, TV)$ are C^0. By (2.13), these conditions this is equivalent to saying that $\Omega_{\pm}^{t_0}$ are C^1.

Proposition 2.2.6. *For $n \geq 2$ consider the annuli $A_n = \{x \in \mathbb{R}^n : n - 1 \leq |x| \leq n\}$. Suppose that for some $k \geq 1$ we have the following estimates:*

$$\sum_{i=1}^{k+1} \sup_{A_n} \|D^i U_\sigma^{t_0}(x)\| \leq C_n e^{\lambda(n)|\sigma - t_0|} \tag{2.14}$$

and

$$\sum_{i=1}^{k} \sup_{A_n} |D^i(\mathcal{V}_\sigma - \mathcal{U}_\sigma)| \leq \tilde{C}_n e^{-\mu(n)|\sigma|} \tag{2.15}$$

Where $0 < \lambda(n), \mu(n)$, $\alpha := \sup_n(\lambda(n) - \mu(n)) < 0$ and $0 < C_n\tilde{C}_n < M$ for some $M > 0$. The wave maps and their inverses exist and are in $C^k(B_R)$ for every $R > 0$.

Proof: For $k = 1$, we can say that Corollary 2.2.5 implies that $\Omega_{\pm}(TU, TV)$ exists and is in $C^0(B_R)$ for every $R > 0$. By (2.13) this implies that $\Omega_{\pm}^{t_0}(U, V)$ are $C^1(B_R)$ for every $R > 0$.

For $k > 1$, we inductively define $T^k\Omega_{\pm}^{t_0}(U, V) = T(T^{k-1}\Omega_{\pm}^{t_0}(U, V)$. By using repeatedly (2.13) we have that

$$T^k\Omega_{\pm}^{t_0}(U, V) = \Omega_{\pm}^{t_0}(T^kU, T^kV)$$

Corollary 2.2.5 implies that if conditions (2.14) and (2.15) hold, then $\Omega_{\pm}^{t_0}(T^kU, T^kV)$ exists and is $C^0(B_R)$ for every $R > 0$, which, by an inductive argument, implies that $\Omega_{\pm}^{t_0}(U, V)$ are $C^k(B_R)$ for every $R > 0$. $\square$

We would like to make a remark about the assumptions of the Proposition 2.2.6. A particular case of these assumptions occurs when one has uniform bounds on all of $\mathbb{R}^n$, that is when one has

$$\sum_{i=1}^{k+1} \sup_{\mathbb{R}^n} \|D^i U_{\sigma}^{t_0}(x)\| \leq Ce^{\lambda|\sigma - t_0|}$$

and

$$\sum_{i=1}^{k} \sup_{\mathbb{R}^n} |D^i(\mathcal{V}_{\sigma} - \mathcal{U}_{\sigma})| \leq \tilde{C}e^{-\mu|\sigma|}$$

with no mention of annuli whatsoever. However, this is not typical, and one commonly has that the growth rates of U increase as one moves further away from the origin. In this case the appropriate assumptions to consider are those given in Proposition 2.2.6.

Now, we consider the case when the vector fields depend on parameters

Corollary 2.2.7. *Suppose that $\mathcal{U}_t$ and $\mathcal{V}_t$ depend on a parameter $\lambda \in U$, an open subset of $\mathbb{R}^m$, and let $U_{t_0}^{t,\lambda}$ and $V_{t_0}^{t,\lambda}$ denote the corresponding flows. Suppose that the conditions are satisfied: The integral*

$$I_{\pm}(t_0) = \int_{t_0}^{\pm\infty} \| \left(DU_{\sigma}^{t_0} \circ (\mathcal{V}_\sigma - \mathcal{U}_\sigma) \right) \circ V_{t_0}^{\sigma} \|_{C^k(U \times B_R)} d\sigma < \infty$$

are finite and the following limits hold

$$\lim_{t_0 \to \infty} I_+(t_0) = 0 \lim_{t_0 \to -\infty} I_-(t_0) = 0$$

(note: in this case the norms include both the spatial and the parameter variables) Then, the wave maps $\Omega_{\pm}^{t_0}(\lambda)$ are C^k with respect to the parameter λ.

The proof, or course, is the same as in Theorem 2.2.1. We simply chose to treat this case separately to make the exposition of Theorem 2.2.1 clearer.

2.2.1 Scattering Theory for Classical Hamiltonian Systems

In this section we will consider the case when the vector fields $\mathcal{U}_t$ and $\mathcal{V}_t$ are Hamiltonian. Suppose that we are given Hamiltonian $H^0(Q, P, t)$ and $H = H^0(Q, P, t) + H^1(Q, P, t)$ on $\mathbb{R}^{2n}$ and let $\mathcal{U}_t = J\nabla H_t^0$ and $\mathcal{V}_t = J\nabla H_t$ be the corresponding vector fields.

The integrability condition that we use for the existence/smoothness and invertibility of the wave maps is that

$$I_{\pm}(t_0) = \int_{t_0}^{\pm\infty} \| \left(DU_{\sigma}^{t_0} \circ J\nabla H_t^1) \right) \circ V_{t_0}^{\sigma} \|_{C^k(B_r)} d\sigma$$

is finite and

$$\lim_{t_0 \to \infty} I_+(t_0) = \lim_{t_0 \to -\infty} I_-(t_0) = 0$$

Thus, if we view H^1 as a perturbation of H^0 then the integrability condition requires that the perturbation decays with time. Moreover, we proved that $\Omega_{\pm}^{t_0}$ is the limit of $\Omega_{\pm}^{t_0,T} = U_{\pm T}^{t_0} \circ V_{t_0}^{\pm T}$, which is symplectic in the case of Hamiltonian systems. It follows that as long as $\Omega_{\pm}^{t_0,T}$ converges to $\Omega_{\pm}^{t_0}$ in $C^k(B_R)$ for every $R > 0$, then the wave maps are symplectic.

We also Note that Corollary 2.2.5 gives a sufficient condition only in terms of the flow U and H_1 to guarantee that the wave maps exist and are continuous. More precisely, Corollary 3 asserts the existence of the wave maps provided that the decay rate for H_1 is stronger than the growth rate for U on every annulus. One would like to establish similar conditions on U and H_1 to guarantee that the wave maps are smooth. This is especially important since our proof of the invertibility of the wave maps required that the wave maps are at least C^1.

2.2.2 Intertwining Relations and Conjugacy

One important fact about the existence of the wave maps is that it implies that the flows of U and V are conjugate when we view them as autonomous flows in the extended phase space $\mathbb{R}^n \times \mathbb{R}$, where we add an extra variable for time. The notion that scattering theory for classical systems yields a conjugacy between two dynamics was used to study the local behavior near a hyperbolic fixed point in [61] and was used to prove that certain systems, for example the Calogero-Moser system, is integrable [44, 43, 50]. For us, we will exploit the fact that the flows are conjugate to compute invariant manifolds, which we discuss in the next section.

Let us consider two flows $U_{t_0}^t$ and $V_{t_0}^t$. If we view the flows as defining autonomous flows on the extended space $\mathbb{R}^n \times \mathbb{R}$, that is we have autonomous flows $\tilde{U}$ and $\tilde{V}$ on $\mathbb{R}^n \times \mathbb{R}$ that solve the ODE's

$$\begin{array}{ll} \dot{x} = \mathcal{U}_t(x) & \dot{x} = \mathcal{V}_t(x) \\ \dot{t}_0 = 1 & \dot{t}_0 = 1 \end{array} \tag{2.16}$$

It turns out that the dynamics of $\tilde{U}$ and $\tilde{V}$ are conjugate, as we show in the following proposition.

Proposition 2.2.8. *Suppose that U and V are flows for $\mathcal{U}_t$ and $\mathcal{V}_t$, respectively. Moreover, suppose that the wave maps $\Omega_{\pm}^s = \lim_{t\to\pm\infty} U_t^{t_0} \circ V_{t_0}^t$ exist in the sense that the limits defining them exist point-wise. Moreover assume that $\Omega_{\pm}^{t_0}$ are invertible.*

(1) We have the following intertwining relations

$$\begin{aligned} \Omega_{\pm}^t \circ V_{t_0}^t &= U_{t_0}^t \circ \Omega_{\pm}^{t_0} \\ s^{t_0} &= U_t^{t_0} \circ s^t \circ U_{t_0}^t \end{aligned} \tag{2.17}$$

(2) The extended flows $\tilde{U}$ and $\tilde{V}$ are conjugate. More precisely, define the wave maps on the extended space

$$\tilde{\Omega}_{\pm}(x,t) := \lim_{t\to\pm\infty} \tilde{U}_{-t} \circ \tilde{V}_t$$

These wave maps exist, are as smooth as the wave maps $\Omega_{\pm}^{t_0}$, are invertible, are moreover we have the following relation

$$\tilde{\Omega}_{\pm} \circ \tilde{V}_t, = \tilde{U}_t \circ \tilde{\Omega}_{\pm} \tag{2.18}$$

Proof: The proof of (1) is a consequence of the following calculation

$$\begin{aligned}\Omega_{\pm}^{t}\circ V_{t_0}^{t} &= \left(\lim_{\eta\to\infty} U_{\eta}^{t}\circ V_{t}^{\eta}\right)\circ V_{t_0}^{t} = \lim_{\eta\to\infty} U_{\eta}^{t}\circ V_{t_0}^{\eta} \\ &= U_{t_0}^{t}\circ \lim_{\eta\to\infty} U_{\eta}^{t_0}\circ V_{t_0}^{\eta} = U_{t_0}^{t}\circ\Omega_{+}^{t_0}\end{aligned} \tag{2.19}$$

and hence $\Omega_{\pm}^{t}\circ V_{t_0}^{t} = U_{t_0}^{t}\circ\Omega_{\pm}^{t_0}$ as claimed. This identity also immediately implies that

$$s^{t_0} = U_{t}^{t_0}\circ s^{t}\circ U_{t_0}^{t}$$

For the proof of (2) we first show that $\tilde{\Omega}_{\pm}(x,t_0) = (\Omega_{\pm}^{t_0}(x),t_0)$. Indeed, notice that

$$\begin{aligned}\tilde{\Omega}_{\pm}(x,t_0) &= \lim_{t\to\pm\infty}\tilde{U}_{-t}\circ\tilde{V}_{t}(x,t_0) = \lim_{t\to\pm\infty}\tilde{U}_{-t}(V_{t_0}^{t+t_0}(x),t+t_0) \\ &= \lim_{t\to\pm\infty}(U_{t+t_0}^{t_0}\circ V_{t_0}^{t+t_0}(x),t_0) = (\Omega_{\pm}^{t_0}(x),t_0)\end{aligned} \tag{2.20}$$

which proves our claim.

This shows that the wave maps $\tilde{\Omega}_{\pm}$ on the extended space exist, are smooth as smooth as $\Omega_{\pm}^{t_0}$, and are invertible. With this relation we can also deduce (2.18) as follows

$$\tilde{\Omega}_{\pm}\circ\tilde{V}_{t}(x,t_0) = \tilde{\Omega}_{\pm}(V_{t_0}^{t+t_0}(x),t+t_0) = (\Omega_{\pm}^{t+t_0}\circ V_{t_0}^{t+t_0}(x),t+t_0) \tag{2.21}$$

Now we use (2.17) to say that

$$(\Omega_{\pm}^{t+t_0} \circ V_{t_0}^{t+t_0}(x), t+t_0) = (U_{t_0}^{t+t_0} \circ \Omega_{\pm}^{t_0}, t+t_0) = \tilde{U}_t(\Omega_{\pm}^{t_0}(x), t_0) = \tilde{U}_t \circ \tilde{\Omega}_{\pm}(x, t_0) \tag{2.22}$$

and hence we conclude that $\tilde{\Omega}_{\pm} \circ \tilde{V}_t, = \tilde{U}_t \circ \tilde{\Omega}_{\pm}$ holds as claimed. $\square$

2.2.3 Time-Dependent Invariant Manifolds

Now that we have established that the existence of the wave maps implies that the flows U and V are conjugate in the extended space, we can apply this to the theory of invariant manifolds. The basic idea is that the wave maps give a way to associate invariant manifolds of U to invariant manifolds of V and vice versa.

Since the flows non-autonomous flows U and V are conjugate only in the extended space, we will need to consider an appropriate notion of an invariant manifold, which for the applications we have in mind will be a time-dependent normally hyperbolic manifold. Such manifolds appeared in [56] when studying the behavior of reacting molecules under the influence of a laser-pulse. The definitions we state are very similar to those stated in [7, 29, 47, 63], but are slightly different since we are consider time-dependent invariant manifolds. The following example motivates the definition we give. This example also appears in the applications to transition state theory that we discuss later.

Example

Let x_0 be a hyperbolic fixed point for the *autonomous* flow U_t corresponding to the vector field $\mathcal{U}$. Since the flow is autonomous, this means that all eigenvalues

of $D\mathcal{U}(x_0)$ have non-zero real part. Note that in the case of non-autonomous flows, conditions for a point to by a hyperbolic fixed point cannot be given in terms of the vector field (see chapter 3, section 7 of [46] for an example). The fact that the condition on $D\mathcal{U}(x_0)$ imply that x_0 is normally hyperbolic follows immediately from the variational equations.

Now consider the vector field $\mathcal{V}_t = \mathcal{U} + \mathcal{W}_t$, and let us suppose that the wave maps $\Omega_{\pm}^{t_0}$ corresponding to $\mathcal{U}$ and $\mathcal{V}_t$ exist. Then the flows U_t and $V_{t_0}^t$ are conjugate in the extended phase space $\mathbb{R}^n \times \mathbb{R}$. The natural question arises: what invariant objects do we have for $V_{t_0}^t$ that corresponds to the fixed point, x_0, and it's corresponding stable/unstable manifolds?

Since we are working in the extended phase space, we consider the line $\tilde{M} = \{(x_0, t) : t \in \mathbb{R}\}$. Using the fact that the wave maps on the extended phase space, $\tilde{\Omega}_{\pm}$, act trivially on the time variable, they will take $\tilde{M}$ to

$$\tilde{N}^{\pm} := \tilde{\Omega}_{\pm}(\tilde{M}) = \{(\Omega_{\pm}^{t_0}(x_0), t_0) : t_0 \in \mathbb{R}\}$$

When we project $\tilde{N}^{\pm}$ onto $\mathbb{R}^n$ we obtain the sets

$$N^{\pm} = \Pi_x \tilde{N}^{\pm} = \{\Omega_{\pm}^{t_0}(x_0) : t_0 \in \mathbb{R}\}$$

This example clarifies why we consider objects in the extended space: we started off with the zero-dimensional invariant object $\{x_0\}$ for U_t and constructed a corresponding 1-dimensional invariant objects $N^{\pm}$ for $V_{t_0}^t$ via the wave maps on the extended space. Moreover, if we define $N_{t_0}^{\pm} = \{(x_0, t_0) : (x_0, t_0) \in \tilde{N}^{\pm}\}$ then, as we show below these manifolds satisfy

$$V_{t_0}^t(N_{t_0}^{\pm}) = N_t^{\pm}$$

which is a property called time-dependent invariance. □

With this example in mind we can now define the invariant manifolds we consider.

Definition 2.2.1. Let $\mathcal{U}_t$ be a time-dependent vector field on $\mathbb{R}^n$, $U_{t_0}^t$ denote the corresponding flow map. Suppose we have a one-parameter family of manifolds, M_{t_0}, parameterized by time with the following property:

$$U_{t_0}^t(M_{t_0}) = M_t$$

The family M_t is called a time-dependent invariant manifold for U.

Moreover, we say that M_t is a time dependent normally hyperbolic invariant manifold (TDNHIM) for the flow $U_{t_0}^t$ provided that M_t is a time dependent invariant manifold and, for each $x_0 \in M_{t_0}$, we have a splitting

$$T_{x_0}\mathbb{R}^n = E^s_{(x_0,t_0)} \oplus T_{x_0}M_{t_0} \oplus E^u_{(x_0,t_0)}$$

such that the splittings are characterized by

$$\begin{aligned}
v \in E^s_{(x_0,t_0)} &\iff |DU_{t_0}^t(x_0)v| \leq Ce^{-\lambda(t-t_0)}|v| \text{ for } t - t_0 \geq 0 \\
v \in T_{x_0}M_{t_0} &\iff |DU_{t_0}^t(x_0)v| \leq Ce^{\mu(t-t_0)}|v| \text{ for all } t, t_0 \\
v \in E^u_{(x_0,t_0)} &\iff |DU_{t_0}^t(x_0)v| \leq Ce^{\beta(t-t_0)}|v| \text{ for } t - t_0 \leq 0
\end{aligned} \tag{2.23}$$

Where $0 < \beta < \lambda, \mu$. The bundles

$$E^{s,u} = \bigcup_{t_0 \in \mathbb{R}, x_0 \in M_{t_0}} E^{s,u}_{(x_0,t_0)}$$

is called the stable/unstable bundles of M_t.

For us, the main importance of these manifolds is that they possess stable and unstable manifolds, which is the content of the next proposition.

Proposition 2.2.9. *Suppose that the flow $U_{t_0}^t$ is $C^k(B_R)$ for every $R > 0$ and M_t is a time-dependent normally hyperbolic invariant manifold for$]U_{t_0}^t$. Moreover, suppose that*

$$\sup_{t\in\mathbb{R},x\in M_t} |\mathcal{U}_t(x)| < C \tag{2.24}$$

for some $C > 0$. Then for any point $x_0 \in M$ and $t_0 \in \mathbb{R}$ there exist manifolds $W^s_{x_0,t_0}$ and $W^u_{x_0,t_0}$ that have the property that

$$\begin{aligned} W^s_{x_0,t_0} &= \{(x,t_0) : d(U_{t_0}^t(x), U_{t_0}^t(x_0)) \leq C_x e^{-\lambda(t-t_0)}, t-t_0 \geq 0\} \\ W^u_{x_0,t_0} &= \{(x,t_0) : d(U_{t_0}^t(x), U_{t_0}^t(x_0)) \leq C_x e^{\beta(t-t_0)}, t-t_0 \leq 0\} \end{aligned} \tag{2.25}$$

The manifolds W^s and W^u defined by

$$W^{s,u} = \bigcup_{x_0\in M, t_0\in\mathbb{R}} W^{s,u}_{x_0,t_0} \tag{2.26}$$

are called the stable (resp. unstable) manifolds of M and $W^s_{x_0,t_0}$ (resp $W^u_{x_0,t_0}$) are called the stable (resp. unstable) fibers of the foliation of W^s (resp. W^u). If l is any number that satisfies

$$l < \min\left(r, \frac{|\log\lambda|}{\log\mu}, \frac{|\log\beta|}{\log\mu}\right)$$

then M is a C^l manifold, $W^{s,u}_{x_0,t_0}$ are C^k manifolds and the maps $(x_0,t_0) \mapsto W^{s,u}_{x_0,t_0}$ are C^{l-1-j} when $W^{s,u}_{x_0,t_0}$ are given the C^j topologies.

Proof: The idea is to show that the manifold $\tilde{M} = \{(x, t_0) : x \in M_{t_0}\}$ is a NHIM for the extended flow $\tilde{U}$. The existence of stable and unstable manifolds will then follow from the theory developed in [29, 47, 63] or see [7] for a more modern, even infinite dimensional, version. We note that some versions assume that the NHIM is compact. However, in chapter 6 of [47] and in [7] compactness is not needed.

To see that $\tilde{M}$ is a NHIM for the flow $\tilde{U}_t$ we compute

$$D\tilde{U}_t(x_0, t_0) = \begin{pmatrix} D_x U_{t_0}^{t+t_0}(x_0) & D_{t_0} U_{t_0}^{t+t_0}(x_0) \\ 0 & 1 \end{pmatrix}$$

We can compute $D_{t_0} U_{t_0}^{t+t_0}(x_0)$ using the chain rule

$$\begin{aligned} &D_{t_0} U_{t_0}^{t+t_0}(x_0) = D_t U_{t_0}^t(x)|_{t=t+t_0} + D_{t_0} U_{t_0}^t(x)|_{t=t+t_0, t_0=t_0} \\ &= \mathcal{U}_{t+t_0}(U_{t_0}^{t+t_0}(x)) + D_{t_0} U_t^{t_0}(U_{t_0}^{t+t_0}(x)) = \mathcal{U}_{t+t_0}(U_{t_0}^{t+t_0}(x)) + \mathcal{U}_{t_0}(U_{t+t_0}^{t_0} U_{t_0}^{t+t_0}(x)) \\ &= \mathcal{U}_{t+t_0}(U_{t_0}^{t+t_0}(x)) + \mathcal{U}_{t_0}(x) \end{aligned} \tag{2.27}$$

Since $U_{t_0}^t M_{t_0} = M_t$ our assumption (2.24) implies that $D_{t_0} U_{t_0}^{t+t_0}(x_0)$ remains bounded for all time, and hence this block in $D\tilde{U}_t(x_0, t_0)$ does not contribute to any sort of exponential decay/growth. It follows that, for $(x_0, t_0) \in \tilde{M}$, $T_{(x_0,t_0)}\mathbb{R}^n \times \mathbb{R}$ splits as

$$T_{(x_0,t_0)}\mathbb{R}^n \times \mathbb{R} = \tilde{E}^s_{(x_0,t_0)} \oplus \tilde{E}^u_{(x_0,t_0)} \oplus T_{(x_0,t_0)}\tilde{M}$$

where $\tilde{E}^{s,u}_{x_0} = E^{s,u}_{(x_0,t_0)}$ and $T_{(x_0,t_0)}\tilde{M} = T_{x_0} M_{t_0}$. It follows that $\tilde{E}^{s,u}_{(x_0,t_0)}$ and $T_{(x_0,t_0)}\tilde{M}$ have the same rates of exponential decay/growth as $E^{s,u}_{(x_0,t_0)}$ and $T_{x_0} M_{t_0}$, respectively. It follows that $\tilde{M}$ is NHIM for the extended flow $\tilde{U}_t$.

By the theory developed in [7, 47, 29, 63] we conclude the existence and regularity properties of $M(t_0)$ and $W^{s,u}_{(x_0,t_0)}$.

□

Using the intertwining relations, i.e. $\Omega^t_\pm \circ V^t_{t_0} = U^t_{t_0} \circ \Omega^{t_0}_\pm$, we can now use the scattering theory to relate invariant manifolds of $U^t_{t_0}$ to those of $V^t_{t_0}$ and vice versa.

Proposition 2.2.10. *Let $U^t_{t_0}$ and $V^t_{t_0}$ be flows such that the wave maps $\Omega^{t_0}_\pm$ exist , are smooth and are invertible. Furthermore, suppose that M is a time-dependent normally hyperbolic invariant manifold for $U^t_{t_0}$. Suppose that*

(1) *We have an estimate of the form*

$$\sup_{t\in\mathbb{R},x\in M_t} |\mathcal{U}_t(x)| < C$$

and (2) *the limits*

$$\lim_{t_0\to\pm\infty} (\Omega^{t_0}_\mp)^{-1} \tag{2.28}$$

exist.

Define one-parameter families of manifolds $N_\pm(t_0)$ by

$$N^\pm_{t_0} := (\Omega^{t_0}_\pm(M_{t_0}))^{-1}$$

Then $N^\pm := N_{t_0}$ are time-dependent invariant normally hyperbolic manifolds for V. Moreover, $(\tilde{\Omega}_+)^{-1}$ (resp. $(\tilde{\Omega}_-)^{-1}$) takes the stable/unstable manifolds of M_t to the stable/unstable of N^+ (resp. N^-). More precisely we have

$$(\Omega^{t_0}_\pm)^{-1}(W^{s,u}_{x_0,t_0}(M_{t_0})) = W^{s,u}_{((\Omega^{t_0}_\pm)^{-1}x_0,t_0)}(N^\pm_{t_0}) \tag{2.29}$$

Proof: We only consider N^+ since the proof for N^- is similar. We first verify that N^+ is a time-dependent invariant. The intertwining relations $\Omega_\pm^t V_{t_0}^t = U_{t_0}^t \Omega_\pm^{t_0}$ imply that

$$V_{t_0}^t(N_{t_0}^+) = N_t^+ \tag{2.30}$$

Now we compute the growth/decay rates for $DV_{t_0}^t$ on N^+. The intertwining relations imply that, for any x_0 in M_{t_0}

$$DV_{t_0}^t((\Omega_+^{t_0})^{-1}(x_0)) = D(\Omega_+^t)^{-1}(U_{t_0}^t(x_0))DU_{t_0}^t(x_0)D\Omega_+^{t_0}((\Omega_+^{t_0})^{-1}(x_0)) \tag{2.31}$$

We want to control the limit as $t \to \infty$. The third term on the right side of the equation only depends on t_0 and is thus easy to control. We are assuming that we have estimates on the second term, however the first term $D(\Omega_+^t)^{-1}(U_{t_0}^t(x_0))$ is a bit subtle to estimate. However, as we saw in the proof that $\Omega_+^{t_0}$ is invertible, we know that $\lim_{t_0\to\infty} \|\Omega_+^{t_0} - \text{ Id } \|_{C^1(B_R)} = 0$. Using this we also have that

$$\lim_{t_0\to\infty} \|(\Omega_+^{t_0})^{-1} - \text{ Id } \|_{C^1(B_R)} = 0$$

Thus, $\|D(\Omega_+^{t_0})^{-1}(x_0)\|$ is bounded as a function $t_0 > 0$. However, we are assuming that the corresponding limit

$$\lim_{t_0\to\infty} (\Omega_+^{t_0})^{-1} = \lim_{t_0\to\infty} V_t^{t_0} \circ U_{t_0}^t$$

exists, though it generally will not be the identity, and hence $\|D(\Omega_+^{t_0})^{-1}(x_0)\|$ is bounded for *all* t_0. Thus, if $v_{t_0}^s \in E_{x_0}^s$ is a vector in the stable bundle for M then we we define $\bar{v}_{t_0}^s := (D\Omega_+^{t_0}((\Omega_+^{t_0})^{-1}(x_0)))^{-1} v_{t_0}^s$ and notice that

$$
\begin{aligned}
|DV^t_{t_0}((\Omega^{t_0}_+)^{-1}(x_0))\bar{v}^s_{t_0}| &= |D(\Omega^t_+)^{-1}(U^t_{t_0}(x_0))DU^t_{t_0}(x_0)D\Omega^{t_0}_+((\Omega^{t_0}_+)^{-1}(x_0))\bar{v}^s_{t_0}| \\
&= ||D(\Omega^t_+)^{-1}(U^t_{t_0}(x_0))DU^t_{t_0}(x_0)v^s_{t_0}| \leq MCe^{-\lambda(t-t_0)}
\end{aligned}
\tag{2.32}
$$

Thus, $\bar{E}^s_{t_0} := (D\Omega^{t_0}_+((\Omega^{t_0}_+)^{-1}(x_0)))^{-1}(E^s_{t_0})$ is the stable bundle for N^+. Similarly, we define the unstable and center bundle for N^+ and show that the growth rates are the same as for M, which proves that N^+ is in fact a time-dependent normally hyperbolic invariant manifold.

The proof that the stable/unstable manifolds of M get mapped to stable/unstable manifolds of N is a similar argument using the intertwining relations and using the fact that the (four) limits

$$
\lim_{t_0\to\pm\infty}(\Omega^{t_0}_\pm)^{-1} \text{ and } \lim_{t_0\to\pm\infty}(\Omega^{t_0}_\mp)^{-1}
$$

exist.

□

Remark. In Proposition 2.2.10, we made the assumption that $\lim_{t_0\to\pm\infty}(\Omega^{t_0}_\mp)^{-1}$ exist. In the proof of Proposition 2.2.10 we saw that $\lim_{t_0\to\pm\infty}(\Omega^{t_0}_\pm)^{-1} = \mathrm{Id}$. Using this and the fact that $s^{t_0} = \Omega^{t_0}_+ \circ (\Omega^{t_0}_-)^{-1}$ we have $\lim_{t_0\to\pm\infty}(\Omega^{t_0}_\mp)^{-1} = \lim_{t_0\to\pm\infty} s^{t_0}$, which may not exist in general, and hence we make it an assumption. Without this assumption, we still have the manifolds $N^\pm$, which are time-dependent invariant. However, to check that they are normally hyperbolic and to check that $\Omega^{t_0}_\pm$ takes the stable/unstable manifolds of M to those of $N^\pm$ we needed these limits to exist.

Using only the fact that the limits

$$\lim_{t_0 \to \pm\infty} (\Omega_{\pm}^{t_0})^{-1} = \mathrm{Id} \tag{2.33}$$

hold, we can only show that $\Omega_{+}^{t_0}$ (resp. $\Omega_{-}^{t_0}$) takes the stable (resp. unstable) manifolds of M to the stable (resp. unstable) manifold of N^{+} (resp. N^{-}). We can show that we have growth/decay rates for $DV_{t_0}^{t}$ on N^{+} (resp. N^{-}) for $t - t_0 > 0$ (resp. $t - t_0 < 0$) are the same as those of $DU_{t_0}^{t}$ on M. Thus, without assuming (2.33), one can obtain interesting objects, though it is not clear that they are normally hyperbolic, nor that they have both stable and unstable manifolds. These issues are related to the notion of Lyapunov regularity appearing in hyperbolic dynamics (see [6]).

2.3 Perturbative Calculations

In this section we will study perturbations of the flows, so that our flows will depend on tow parameters t and ϵ. Let $\mathcal{U}_t^{\epsilon}$ be a time-dependent vector field that also depends on a parameter ϵ and let $U_{t_0}^{t,\epsilon}$ denotes the corresponding flow. We will compare the dynamics for $\epsilon = 0$ and $\epsilon \neq 0$ by considering the wave maps

$$\Omega_{\pm}^{\epsilon,t_0} = \lim_{t \to \pm\infty} U_t^{t_0,0} \circ U_{t_0}^{t,\epsilon}$$

and scattering map $s_{\epsilon}^{t_0} = \Omega_{+}^{\epsilon,t_0} \circ (\Omega_{-}^{t_0})^{-1}$. The main content of this section are Theorems 2 and 3 where perturbative calculations of $s_{\epsilon}^{t_0}$ are given.

Following the ideas of deformation theory (see [74] and [19]) we will write these families in terms of their generators with respect to t and ϵ. The

flow $U_{t_0}^{t,\epsilon}$ and vector field $\mathcal{U}_t$ are related by

$$\frac{d}{dt}U_{t_0}^{t,\epsilon} = \mathcal{U}_t \circ U_{t_0}^{t,\epsilon}$$

In this section we will also consider the vector field $\mathcal{F}_\epsilon$ defined by

$$\frac{d}{d\epsilon}U_{t_0}^{t,\epsilon} = \mathcal{F}_\epsilon \circ U_{t_0}^{t,\epsilon}$$

In the literature, both $\mathcal{U}_t$ and $\mathcal{F}_\epsilon$ are referred to as the generator of $U_{t_0}^{t,\epsilon}$ and to distinguish between the two usages, we will refer to $\mathcal{U}_t$ and $\mathcal{F}_\epsilon$ as the t-generator and ϵ generator, respectively.

Theorem 2.3.1. *Suppose that the following conditions hold: There exists an interval I containing zero and an integer $k \geq 1$ such that*

$$I_\pm(t_0) = \int_{t_0}^{\pm\infty} \| \left(DU_\sigma^{t_0,0}(\mathcal{U}_\sigma^\epsilon - \mathcal{U}_\sigma^0)\right) \circ U_{t_0,\epsilon}^\sigma \|_{C^k(I\times B_R)} d\sigma < \infty$$

for every $R > 0$. Here I is an interval in which the parameter ϵ lies in. Also assume that and the following hold

$$\lim_{t_0\to\infty} I_+(t_0) = \lim_{t_0\to-\infty} I_-(t_0) = 0$$

By Theorem 2.2.1 the wave and scattering maps exist, are C^k, are diffeomorphisms, depend smoothly on ϵ. If the limit

$$\mathcal{S}_\epsilon^{t_0} := \lim_{T_1,T_2\to\infty} \int_{-T_2}^{T_1} (\Omega_+^{t_0,\epsilon,T_1} \circ U_\sigma^{t_0,\epsilon})_* \left(\frac{d}{d\epsilon}\mathcal{U}_\sigma^\epsilon\right) d\sigma$$

converges in $C^1(B_R)$ for every $R > 0$, then $\mathcal{S}_\epsilon^{t_0}$ is the vector field generating $s_\epsilon^{t_0}$.

We anticipate that in the case the vector fields are Hamiltonian, the symplectic geometry will allow us to simplify Theorem 2. This is carried out in Section 3.1.

Note that an immediate corollary of Theorem 2 is that, if the conditions of Theorem 2 hold, then we have the following perturbative expansion of the scattering map

$$s_\epsilon^{t_0} = \mathrm{Id} + \epsilon \mathcal{S}_0^{t_0} + \mathcal{O}(\epsilon^2)$$

where

$$\mathcal{S}_0^{t_0} = \lim_{T_1, T_2 \to \infty} \int_{-T_1}^{T_2} (U_\sigma^{t_0,0})_* \left(\frac{d}{d\epsilon} \mathcal{U}_\sigma^\epsilon |_{\epsilon=0} \right) d\sigma$$

Proof: As in the proof of Theorem 1 we consider $\Omega_\pm^{t_0,\epsilon,T} := U_{\pm T}^{t_0,0} U_{t_0}^{\pm T,\epsilon}$. The method proof of Theorem 1 and Corollary 4 imply that $\Omega_\pm^{t_0,\epsilon,T}$ converges to $\Omega_\pm^{t_0,\epsilon}$ uniformly in $B_R \times I$ for any $R > 0$. This time, however, we will compute the vector field generating $\Omega_\pm^{t_0,\epsilon,T}$ with respect to ϵ not T. That is, we want to compute the vector fields $\mathcal{X}_{\pm,\epsilon}^{t_0,T}$ that satisfy

$$\frac{d}{d\epsilon} \Omega_\pm^{t_0,\epsilon,T} = \mathcal{X}_{\pm,\epsilon}^{t_0,T} \circ \Omega_\pm^{t_0,\epsilon,T}$$

To do this, we use Proposition A.0.8 (c.f. Appendix A), which tells us how to compute generators of compositions of diffeomorphisms. If $\mathcal{F}_{t_0}^{t,\epsilon}$ is the ϵ-generator of $U_{t_0}^{t,\epsilon}$ then Proposition A.0.6 implies that

$$\mathcal{X}_{\pm,\epsilon}^{t_0,T} = (U_{\pm t}^{t_0,0})_* \left(\mathcal{F}_{t_0}^{\pm t,\epsilon} \right)$$

The next proposition explains how to compute $\mathcal{F}_{t_0}^{t,\epsilon}$

Proposition 2.3.2. *If $U_{t_0}^{t,\epsilon}$ denotes the time-t flow for $\mathfrak{U}_t^\epsilon$, then the ϵ generator $\mathcal{F}_{t_0}^{t,\epsilon}$ is given by*

$$\mathcal{F}_{t_0}^{t,\epsilon} = \int_{t_0}^{t} (U_\sigma^{t,\epsilon})_* \left(\frac{d}{d\epsilon} \mathfrak{U}_\sigma^\epsilon \right) d\sigma$$

Proof: First note that we have the following variational equations (in what follows $\cdot$ and D refer to differentiation with respect to ϵ and x respectively)

$$\begin{aligned} \frac{d}{dt} \dot{U}_{t_0}^{t,\epsilon} &= D\mathfrak{U}_t^\epsilon \circ U_{t_0}^{t,\epsilon} \circ \dot{U}_{t_0}^{t,\epsilon} + \dot{\mathfrak{U}}_t^\epsilon \circ U_{t_0}^{t,\epsilon} \\ \frac{d}{dt} DU_{t_0}^{t,\epsilon} &= D\mathfrak{U}_t^\epsilon \circ U_{t_0}^{t,\epsilon} \circ DU_{t_0}^{t,\epsilon} \end{aligned} \tag{2.34}$$

We consider (2.34) as equations for $\dot{U}_{t_0}^{t,\epsilon}$ and $DU_{t_0}^{t,\epsilon}$. These are supplemented with the initial conditions $\dot{U}_{t_0}^{t_0,\epsilon} = 0$ and $DU_{t_0}^{t_0,\epsilon} =$ Id, which come from taking derivatives of the equation $U_{t_0}^{t_0,\epsilon} = x$ with respect to ϵ and x.

We see that the first equation of (2.34) is linear nonhomogeneous, while the second is the corresponding homogeneous equation. Thus, using the fact that $(DU_{t_0}^{t,\epsilon})^{-1} = DU_t^{t_0,\epsilon} U_{t_0}^{t,\epsilon}$ we can use the variation of parameters formula to say that

$$\begin{aligned} \dot{U}_{t_0}^{t,\epsilon} &= \int_{t_0}^{t} DU_{t_0}^{t,\epsilon} DU_\sigma^{t_0,\epsilon} \circ U_{t_0}^{\sigma,\epsilon} \dot{\mathfrak{U}}_\sigma^\epsilon \circ U_{t_0}^{\sigma,\epsilon} d\sigma = \int_{t_0}^{t} DU_{t_0}^{t,\epsilon} (Ut_0, {}^\epsilon{}_\sigma)_* \dot{\mathfrak{U}}_\sigma^\epsilon d\sigma \\ &= \left(\int_{t_0}^{t} (U_{t_0}^{t,\epsilon})_* ((U_\sigma^{t_0,\epsilon})_* \dot{\mathfrak{U}}_\sigma^\epsilon) d\sigma \right) \circ U_{t_0}^{t,\epsilon} = \left(\int_{t_0}^{t} (U_{t_0}^{t,\epsilon} \circ U_\sigma^{t_0,\epsilon})_* \dot{\mathfrak{U}}_\sigma^\epsilon d\sigma \right) \circ U_{t_0}^{t,\epsilon} \end{aligned} \tag{2.35}$$

It follows that the ϵ-generator of $U_{t_0}^{t,\epsilon}$ is $\int_{t_0}^{t} (U_\sigma^{t,\epsilon})_* \dot{\mathfrak{U}}_\sigma^\epsilon d\sigma$.

□

Thus, we obtain that

$$\begin{aligned}\mathcal{X}^{t_0,T}_{\pm,\epsilon} &= (U^{t_0,0}_{\pm T})_*\left(\int_{t_0}^{\pm T}(U^{\pm T,\epsilon}_{t_0}\circ U^{t_0,\epsilon}_{\sigma})_*\dot{\mathcal{U}}^{\epsilon}_{\sigma}d\sigma\right)\\ &= \int_{t_0}^{\pm T}(U^{t_0,0}_{\pm T}\circ U^{\pm T,\epsilon}_{t_0}\circ U^{t_0,\epsilon}_{\sigma})_*\dot{\mathcal{U}}^{\epsilon}_{\sigma}d\sigma = \int_{t_0}^{\pm T}(\Omega^{t_0,\epsilon,T}_{\pm}\circ U^{t_0,\epsilon}_{\sigma})_*\dot{\mathcal{U}}^{\epsilon}_{\sigma}d\sigma\end{aligned} \tag{2.36}$$

Thus, the ϵ-generator $\mathcal{S}^{t_0,T}_{\epsilon}$ of $s^{t_0,T}_{\epsilon}$ is given by

$$\begin{aligned}\mathcal{S}^{t_0,T}_{\epsilon} &= \mathcal{X}^{t_0,T}_{+,\epsilon} - (\Omega^{t_0,\epsilon,T}_{+})_*((\Omega^{t_0,\epsilon,T}_{-})^{-1})_*\mathcal{X}^{t_0,T}_{-,\epsilon} = \mathcal{X}^{t_0,T}_{+,\epsilon} - (\Omega^{t_0,\epsilon,T}_{+}\circ(\Omega^{t_0,\epsilon,T}_{-})^{-1})_*\mathcal{X}^{t_0,T}_{-,\epsilon}\\ &= \int_{t_0}^{T}(\Omega^{t_0,\epsilon,T}_{+}\circ U^{t_0,\epsilon}_{\sigma})_*\dot{\mathcal{U}}^{\epsilon}_{\sigma}d\sigma - (\Omega^{t_0,\epsilon,T}_{+}\circ(\Omega^{t_0,\epsilon,T}_{-})^{-1})_*\left(\int_{t_0}^{-T}(\Omega^{t_0,\epsilon,T}_{-}\circ U^{t_0,\epsilon}_{\sigma})_*\dot{\mathcal{U}}^{\epsilon}_{\sigma}d\sigma\right)\\ &= \int_{t_0}^{T}(\Omega^{t_0,\epsilon,T}_{+}\circ U^{t_0,\epsilon}_{\sigma})_*\dot{\mathcal{U}}^{\epsilon}_{\sigma}d\sigma + \int_{-T}^{t_0}(\Omega^{t_0,\epsilon,T}_{+}\circ U^{t_0,\epsilon}_{\sigma})_*\dot{\mathcal{U}}^{\epsilon}_{\sigma}d\sigma = \int_{-T}^{T}(\Omega^{t_0,\epsilon,T}_{+}\circ U^{t_0,\epsilon}_{\sigma})_*\dot{\mathcal{U}}^{\epsilon}_{\sigma}d\sigma\end{aligned} \tag{2.37}$$

Our assumptions in Theorem 2 are that $\mathcal{S}^{t_0,T}_{\epsilon}$ converges, as $T\to\infty$, to a function that is in $C^k(B_R)$ for every $R>0$. Let us call the limiting function $S^{t_0,\infty}_{\epsilon}$.

Now we will show show that $S^{t_0,\infty}_{\epsilon}$ is in fact the vector field generating $s^{t_0}_{\epsilon}$, that is, we need to show that

$$\frac{d}{d\epsilon}s^{t_0}_{\epsilon} = \mathcal{S}^{t_0,\infty}_{\epsilon}\circ s^{t_0}_{\epsilon}$$

Since we know that $s^{t_0,T}_{\epsilon}\to s^{t_0}_{\epsilon}$ uniformly in ϵ we can say that

$$\begin{aligned}\frac{d}{d\epsilon}s^{t_0}_{\epsilon} &= \frac{d}{d\epsilon}\lim_{T\to\infty}s^{t_0,T}_{\epsilon} = \lim_{T\to\infty}\frac{d}{d\epsilon}s^{t_0,T}_{\epsilon}\\ &= \lim_{T\to\infty}\mathcal{S}^{t_0,T}_{\epsilon}\circ s^{t_0,T}_{\epsilon} = \mathcal{S}^{t_0,\infty}_{\epsilon}\circ s^{t_0}_{\epsilon}\end{aligned} \tag{2.38}$$

It follows that

$$\mathcal{S}^{t_0}_{\epsilon} = \lim_{T_1,T_2\to\infty}\int_{-T_2}^{T_1}(\Omega^{t_0,\epsilon,T_1}_{+}\circ U^{t_0,\epsilon}_{\sigma})_*\dot{\mathcal{U}}^{\epsilon}_{\sigma}d\sigma \tag{2.39}$$

□

2.3.1 The Hamiltonian case

In the case that the flow $U_{t_0}^{t,\epsilon}$ corresponds to the time-t evolution of a Hamiltonian system with Hamiltonian $H_\epsilon(Q,P,t)$ we show that the scattering map $s_\epsilon^{t_0}$ also has a Hamiltonian structure. To be more precise, we refine the results of the previous section to show that $s_\epsilon^{t_0}$ is the time-ϵ map of a Hamiltonian $S_\epsilon^{t_0}$, which we now compute. Before we state the next theorem, let us introduce some terminology. If f_ϵ^t is a 2 parameter of exact symplectic diffeomorphisms, then as is shown in Appendix A, the ϵ-generator of f_ϵ^t satisfies

$$\mathcal{F}_\epsilon^t = J\nabla F_\epsilon^t$$

for some function F_ϵ^t, which we call the *Hamiltonian ϵ-generating* f_ϵ^t.

Theorem 2.3.3. *Suppose that the following condition holds: There exists an interval I containing zero and an integer $k \geq 1$ such that*

$$I_\pm(t_0) = \int_{t_0}^{\pm\infty} \|(DU_\sigma^{t_0,0} J\nabla H_\sigma^1)(U_{t_0}^{\sigma,\epsilon})\|_{C^k(I\times B_r)} d\sigma < \infty$$

for every $R > 0$. Here I is an interval in which the parameter ϵ lies in. Also assume that and the following limits hold

$$\lim_{t_0\to\infty} I_+(t_0) = \lim_{t_0\to-\infty} I_-(t_0) = 0$$

By Theorem 2.2.1 the wave and scattering maps exist, are C^k, are diffeomorphisms, depend smoothly on ϵ. If the limit

$$S_\epsilon^{t_0} = \lim_{T_1,T_2\to\infty} \int_{-T_1}^{T_2} \frac{d}{d\epsilon} H_\epsilon \circ U_T^{\sigma,\epsilon} \circ U_{t_0}^{T,0} d\sigma \tag{2.40}$$

converges in $C^1(B_R)$ for every $R > 0$, then $S_\epsilon^{t_0}$ is the Hamiltonian ϵ-generating $s_\epsilon^{t_0}$

The significance of Theorem 3 is that it allows us to compute $s_\epsilon^{t_0}$. More precisely, Theorem 3 implies that $s_\epsilon^{t_0}$ is the time-ϵ map of the Hamiltonian S_ϵ given in (2.40). Hence, if F is any observable, it follows that

$$F \circ s_\epsilon^{t_0} = F + \epsilon\{S_0, F\} + \mathcal{O}(\epsilon^2)$$

where

$$S_0^{t_0} = \lim_{T_1, T_2 \to \infty} \int_{-T_1}^{T_2} \left(\frac{d}{d\epsilon} H_\epsilon|_{\epsilon=0} \right) \circ U_{t_0}^{\sigma,0} d\sigma$$

In particular, one can take F to be a coordinate function q_i or p_i, and hence we see that the above formula allows us to compute s_ϵ^t up to first order in ϵ knowing only the unperturbed flow and the Hamiltonian.

These first order calculations are often called Melnikov theory. We note that many expositions require extra assumptions such as the limiting behavior of the orbits [48]

The fact that Theorem 2.3.3 allows us to compute any observable is quite significant. Indeed, one can use averaging [5] to understand how the action, a slow variable, of a nearly integrable system changes in time. However, averaging does not yield estimates on how the fast variables, i.e. the angle variables, change. Theorem 2.3.3 gives a way to compute the effect of an external force that decays rapidly with time has on *any* quantity.

Proof: We first compute the Hamiltonian for $s_\epsilon^{t_0,T} = U_T^{t_0,0} \circ U_{t_0}^{T,\epsilon} \circ U_{-T}^{t_0,\epsilon} \circ U_{t_0}^{-T,0}$ and take the limit as $T \to \infty$. Since $s_\epsilon^{t_0,T}$ is exact symplectic, we can use deformation theory to construct the Hamiltonian $S_\epsilon^{t_0,T}$ ϵ-generating $s_\epsilon^{t_0,T}$ (c.f. Appendix A), i.e. $S_\epsilon^{t_0,T}$ satisfies

$$\frac{d}{d\epsilon} s_\epsilon^{t_0,T} = J\nabla S_\epsilon^{t_0,T} \circ s_\epsilon^{t_0,T}$$

Using Proposition A.0.8 from Appendix A, we have that

$$S_\epsilon^{t_0,T} = F_{-T}^{T,\epsilon} \circ U_{t_0}^{T,0}$$

where $F_{-T}^{T,\epsilon}$ is the Hamiltonian generating $U_{-T}^{T,\epsilon}$, which we can compute via the following Proposition.

Proposition 2.3.4. *If $U_{t_0}^{t,\epsilon}$ denotes the time-t flow for $\mathfrak{U}_t^\epsilon$, then the Hamiltonian $F_{t_0}^{t,\epsilon}$ ϵ-generating $U_{t_0}^{t,\epsilon}$ is given by*

$$F_{t_0}^{\epsilon,t} = \int_{t_0}^t \frac{d}{d\epsilon} H_\epsilon \circ U_t^{\sigma,\epsilon} d\sigma$$

Proof: We computed the vector field $\mathcal{F}_{t_0}^{T,\epsilon}$ generating $U_{t_0}^{T,\epsilon}$, and hence we only need to compute the contraction of this vector field with the symplectic form ω, which need not be the canonical symplectic form, and obtain

$$\begin{aligned} i_{\mathcal{F}_{t_0}^{t,\epsilon}}\omega &= \int_{t_0}^t i_{(U_\sigma^{t,\epsilon})_* \mathfrak{U}_\sigma^\epsilon} \omega d\sigma = \int_{t_0}^t (U_\sigma^{t,\epsilon})_* i_{\mathfrak{U}_\sigma^\epsilon} \omega d\sigma \\ &= \int_{t_0}^t (U_\sigma^{t,\epsilon})_* d\dot{H}_\sigma^\epsilon d\sigma = d\int_{t_0}^t \dot{H}_\sigma^\epsilon \circ U_t^{\sigma,\epsilon} d\sigma \end{aligned} \tag{2.41}$$

□

It follows that

$$S_\epsilon^{t_0,T} = \int_{-T}^T \frac{d}{d\epsilon} H_\sigma^\epsilon \circ U_T^{\sigma,\epsilon} \circ U_{t_0}^{T,0} d\sigma \tag{2.42}$$

Our assumptions guarantee that $S_\epsilon^{t_0,T}$ converges, as $T \to \infty$ to a function $S_\epsilon^{t_0,\infty}$ in $C^k(B_R)$ for every $R > 0$. The proof that $S_\epsilon^{t_0,\infty}$ is the Hamiltonian generating $s_\epsilon^{t_0}$ is similar the proof that $\mathcal{S}_\epsilon^{t_0,\infty}$ is the vector field generating $s_\epsilon^{t_0}$ in Theorem 2.3.1

□

Comparison to Fermi's Golden Rule in quantum mechanics

In this section we relate the perturbative calculations given in Theorems 2.3.1 and 2.3.3 to Fermi's Golden Rule in quantum mechanics [62, 72] . For a given Hamiltonian H, i.e. a self-adjoint operator in this context, we can consider the corresponding Schrödinger equation

$$\begin{aligned} i\partial_t U(t) &= H(t)U(t) \\ U(0) &= U_0 \end{aligned} \tag{2.43}$$

Suppose that we have a Hamiltonians H_0 and $H = H_0 + H_1$ and let U and V denote their respective solution operators. We can also define the wave operators in this setting in the exact same manner as before

$$\Omega_{\pm}^{t_0} = \lim_{t_0 \to \pm\infty} U_{\pm t}^{t_0} V_{t_0}^{t}$$

And the scattering operator is defined as

$$s^{t_0} = \Omega_+ \circ (\Omega_-)^{-1} = \lim_{T_1, T_2 \to \infty} U_{T_1}^{t_0} V_{-T_2}^{T_1} U_{t_0}^{-T_2} \tag{2.44}$$

In the classical setting, the physical interpretation of s^{t_0} is that its input is the asymptotic past of an orbit, and the output is the asymptotic future. The analogy in quantum mechanics is that the quantity

$$\left\langle u_+ | s^{t_0} | u_- \right\rangle = \int u_+(x) \overline{s^{t_0} u_-(x)} dx$$

Is the probability that the system is asymptotically in state x_+ in the future if it was asymptotically in state x_- in the past.

In similar spirit as in [62], we can now formulate Fermi's Golden Rule and see that it is very similar to the perturbative calculations. Let us suppose

that $H = H_0 + \epsilon H_1 + \mathcal{O}(\epsilon^2)$ and consider the scattering operator

$$s_\epsilon^{t_0} = \lim_{T_1, T_2 \to \infty} U_{T_1}^{t_0} V_{-T_2}^{T_1} U_{t_0}^{-T_2} \tag{2.45}$$

The variation of parameters formula says that

$$V_{t_0}^t = U_{t_0}^t - \epsilon U_{t_0}^t \int_{t_0}^t U_s^{t_0} i H_1(s) U_{t_0}^s ds + \mathcal{O}(\epsilon^2)$$

and hence substituting this expression for $V_{t_0}^t$ into (2.45)we can compute the scattering operator as

$$s_\epsilon^{t_0} = s_0^{t_0} + \epsilon \lim_{T_1, T_2 \to \infty} U_{T_1}^{t_0} \left(\int_{-T_2}^{T_1} i H_1 U_{t_0}^t ds \right) U_{T_2}^{t_0} + \mathcal{O}(\epsilon^2)$$

This formula is Fermi's Golden Rule. This formula gives us a perturbative way to compute the probability of a system having a certain asymptotic past and future. As in Theorems 2.3.1 and 2.3.3, the result is that we integrate the perturbation along the unperturbed trajectory.

2.4 Application to transition state theory

In this section we show how to use scattering theory to understand better a problem arising in transition state theory [76]. This theory was developed to determine the rate of chemical reactions. The theory has also been useful in understanding qualitatively and quantitatively how chemical reactions take place. For example, invariant manifold theory has been used to separate regions consisting of initial conditions resulting in a reaction.

In [56], they consider two reactant molecules, R_1 and R_2 that collide with each other to form a meta-stable complex. After some time, the meta-stable complex can dissolve either back to original state $R_1 + R_2$ or to one of

two products $P_1 + P_2$ and $P_1' + P_2'$. The goal is to understand how exposing the molecules to a laser shortly before and after the collision affects the outcome of the reaction.

The system they consider is the laser driven Henon-Heiles system given by the Hamiltonian

$$H = \frac{1}{2}(p_x^2 + p_y^2) + \frac{1}{2}(x^2 + y^2) + x^2 y - \frac{1}{3}y^3 + \mathcal{E}_1(t)\exp(-\alpha x^2 - \beta y^2) \quad (2.46)$$

where $\mathcal{E}_1 = -\frac{\partial}{\partial t}A(t)$ where $A(t)$ is given by

$$A(t) = \begin{cases} -A_0 \cos^2\left(\frac{\omega t}{2N}\right), & \text{if } |t| < \frac{N\pi}{\omega} \\ 0, & \text{otherwise} \end{cases}$$

The key features of the the Hamiltonian $H_0 = \frac{1}{2}(p_x^2 + p_x^2) + \frac{1}{2}(x^2 + y^2) + x^2 y - \frac{1}{3}y^3$ is that the Henon-Heiles potential $U(x, y) = \frac{1}{2}(x^2 + y^2) + x^2 y - \frac{1}{3}y^3$ has three saddle points which give rise to three asymptotic channels in phase space. These channels correspond to each of the three possible outcomes of the reaction. The driving term, $H_1 = \mathcal{E}_1(t)\exp(-\alpha x^2 - \beta y^2)$ corresponds to adding a laser to the system, which in practice can be used to manipulate the result of the interaction of the two molecules.

In [56], they use time-dependent normal-form theory to carry out numerical computations of invariant manifolds for the system. These invariant manifolds separate the reactive and non-reactive regions of phase space.

We now explain how to use the scattering theory developed in Section 2 to construct the invariant manifolds computed in their paper. Moreover, we suggest an alternative method to compute numerically the invariant manifolds.

First let us have a closer look at the system without the presence of a laser field, that is the system given by $H_0 = \frac{1}{2}(p_x^2+p_x^2)+\frac{1}{2}(x^2+y^2)+x^2y-\frac{1}{3}y^3$. This system has three saddle points, $x_1 = (\sqrt{3}/2, -1/2), x_2 = (-\sqrt{3}/2, -1/2)$, and $x_3 = (0, 1)$. These points define three asymptotic channels, one of which is interpreted as defining a reactant region, while the other two are interpreted as defining two distinct product regions.

These saddle points have stable (resp. unstable) invariant manifolds $W^s_{x_i}$ (resp. $W^u_{x_i}$). These manifolds are characterized by having the following asymptotic properties

$$W^s_{x_i} = \{x | d(U^0_t(x), x_i) \leq C_x e^{-\lambda t}, t \geq 0\} \tag{2.47}$$

$$W^u_{x_i} = \{x | d(U^0_t(x), x_i) \leq C_x e^{\mu t}, t \leq 0\} \tag{2.48}$$

Here λ and μ is the expansion/contraction rate of the saddle points. In the presence of a laser field, these manifolds become time-dependent normally hyperbolic invariant manifolds. Indeed, even though the system without the laser term is autonomous, we can still view the fixed points as being time dependent normally hyperbolic manifolds.

The next proposition allows us to compute an associated TDNHIM and the associated stable/unstable manifolds for the full system.

Proposition 2.4.1. *Let x_0 be a fixed point of the system without the laser-driving term and consider $\tilde{M} = \{(x_0, t_0) : t_0 \in \mathbb{R}\}$ then $N^{\pm} := \Pi_x(\tilde{\Omega}^{t_0}_{\pm}(\tilde{M})$ are time-dependent normally hyperbolic invariant manifolds for the system with*

the presence of a laser-pulse. Moreover, we have that

$$(\Omega_{\pm}^{t_0})^{-1}(W^{s,u}_{(x_0,t_0)}(M) = W^{s,u}_{((\Omega_{\pm}^{t_0})^{-1}x_0,t_0)}(N^{\pm})$$

Note that this follows immediately from Proposition 2.2.10. The conditions that the limits

$$\lim_{t_0\to\pm\infty}(\Omega_{\mp}^{t_0})^{-1}$$

exist follows from the fact that the laser-pulse term is compactly supported in time. Indeed in this case

$$\lim_{t_0\to\pm\infty}(\Omega_{\mp}^{t_0})^{-1} = V_{\pm T}^{t_0}\circ U_{t_0}^{\pm T}$$

where the support of H_1 lies in $[-T, T]$.

Proposition 2.4.1 could be used as a basis as an alternate approach to computing the stable/unstable manifolds computed in [56]. All that is necessary is to compute the stable/unstable manifolds of the system in the absence of a laser field, numerically compute $\Omega_{\pm}$, and finally compute the images of the original stable/unstable manifolds under $(\Omega_{\pm})^{-1}$.

2.4.1 The branching ratio

An important quantity in transition state theory is the *branching ratio*, also commonly called the *branching fraction* (see [1]). Recall that for the Henon-Heiles system, there are two possible products, $P_1 + P_2$ and $P_1' + P_2'$, that the meta-stable complex can dissolve into. Informally speaking, the branching ratio is the ratio of the probabilities that the outcome of the reaction is one product versus another.

For the Henon-Heiles system without the laser term, the measure of the asymptotic channels for each of the two products is infinite. However, it is common to consider only a subset of the phase space. Indeed, in [56] restrict themselves to a energy surface and then take a surface of section and obtain a two-dimensional planar subset of phase space. Since the region is planar, the probability that a given reaction takes place can be computed by taking the Lebesgue measure of the corresponding asymptotic channel intersected with the planar region, which is finite. In [56] it is noticed that there is a change in the branching ratio when the laser-term is included.

We now give perturbative calculations of the change in the branching ratio that sheds light on the calculations given in [56]. The calculations we give can be thought of as a version of Fermi's Golden Rule for the branching ratio. Indeed, the results and techniques are similar to the perturbative calculations for the scattering map.

We will consider general Hamiltonian systems. Thus we let $H_\epsilon(Q, P, t)$ be a Hamiltonian and let c_1^0 and c_2^0 be two asymptotic channels for H_0, that is c_0^1 and c_0^2 are regions of phase space that are invariant for the unperturbed system. Since the asymptotic channels will generally have infinite measure, we take a sample space U of initial data, which we take to be an open subset of phase space. Using the intertwining relations, we deduce that

$$c_{i,\pm}^{t_0,\epsilon} := (\Omega_\pm^{t_0})^{-1}(c_i^0)$$

are asymptotic channels for the full system. As expected, the asymptotic channel depends on the starting time t_0. For example, for the laser-driven

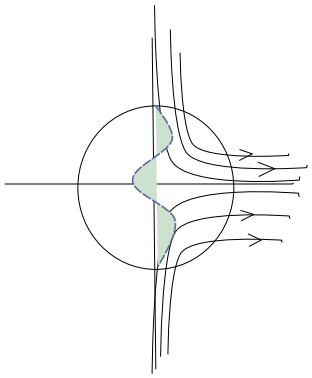

Figure 2.2: The unperturbed asymptotic channel c^0 is the right-half plane, the blue (color may not appear on the printed version) dashed line is the boundary of the perturbed asymptotic channel c^ϵ, the sample space U is the unit ball, the net volume of the green (or the shaded region in the printed version) region is $|c^\epsilon \cap U| - |c^0 \cap U|$ and is given by integrating the flux of $J\nabla X^+$ over $\partial(U \cap c^0) \cap U$

Henon-Heiles system the asymptotic channels are different for starting times t_0 before, during, or after the laser-pulse. The *branching ratio* is defined as

$$b_\pm^{t_0,}(c_1^\epsilon, c_2^\epsilon, U) = \frac{|c_{1,\pm}^\epsilon \cap U|}{|c_{2,\pm}^\epsilon \cap U|}$$

We now give perturbative calculations for $|c_{i,\pm}^{t_0,\epsilon} \cap U|$.

Figure 2.2 helps to understand the computation. In this case the channel c_i^0 is the right-half plane and the sample space U is the unit ball and the blue (color may not show up on the printed version) dashed line is the boundary of the perturbed asymptotic channel c^ϵ. The following formula computes the change in the in the volume due to the presence of a laser-field

$$|c_{i,\pm}^{t_0,\epsilon} \cap U| = |c_i^0 \cap U| + \epsilon \int_{\partial(U \cap c_i^0) \cap U} J\nabla X_{t_0}^{0,\pm}(x) \cdot n(x) dA + \mathcal{O}(\epsilon^2)$$

Here $X_{t_0}^{\epsilon,\pm}$ is the Hamiltonian ϵ-generating $(\Omega_\pm^{t_0,\epsilon})^{-1}$ with respect to ϵ and n is the outward pointing normal. Thus the change in volume is computed by integrating the flux of $J\nabla X_{t_0}^{\epsilon,\pm}$ over $\partial(U \cap c_i^0) \cap U$. In a similar fashion as the perturbative calculations given in Theorem 2.3.3 we can compute $X_{t_0}^{\epsilon,\pm}$ by first computing $X_{t_0,T}^{\epsilon,+}$, the Hamiltonian ϵ-generating

$$(\Omega_\pm^{t_0,T})^{-1} = U_{\pm T}^{t_0,\epsilon} U_{t_0}^{\pm T,0}$$

and taking the limit as $T \to \infty$. Using Proposition A.0.8 we have that

$$X_{t_0,T}^{\epsilon,\pm} = -F_{t_0}^{\epsilon,\pm T} \circ U_{t_0}^{\pm T,\epsilon}$$

Where $F_{t_0}^{\epsilon T}$ is the Hamiltonian ϵ-generating $U_{t_0}^T$, and by Proposition 2.3.4 is given by $F_{t_0}^{\epsilon,T} = \int_{t_0}^t \dot{H}_\epsilon \circ U_t^{\sigma,\epsilon} d\sigma$, and hence we conclude that $X_{t_0}^{\epsilon,\pm} = \int_{t_0}^{\pm\infty} \frac{d}{d\epsilon} H_\epsilon \circ U_{t_0}^{\sigma,\epsilon}$ and hence,

$$X_{t_0}^{0,\pm} = \int_{t_0}^{\pm\infty} \frac{d}{d\epsilon} (H_\epsilon) \mid_{\epsilon=0} \circ U_{t_0}^{\sigma,0}$$

We summarize this in the following Proposition.

Proposition 2.4.2. *Let $H_\epsilon(Q,P,t)$ be a Hamiltonian with corresponding flow $U_{t_0}^t$ and suppose that the wave maps $\Omega_\pm^{\epsilon,t_0}$ exist, are smooth and invertible. Let c_1^0, c_2^0 be two asymptotic channels for H_0 and U an open subset of phase space. Then $c_{i,\pm}^{t_0,\epsilon} := (\Omega_\pm^{t_0})^{-1}(c_i^0)$ are asymptotic channels for H_ϵ and*

$$|c_{i,\pm}^{t_0,\epsilon} \cap U| = |c_i^0 \cap U| + \epsilon \int_{\partial(U \cap c_i^0) \cap U} J\nabla X_{t_0}^{0,\pm}(x) \cdot n(x) dA + \mathcal{O}(\epsilon^2)$$

where

$$X_{t_0}^{0,\pm} = \int_{t_0}^{\pm\infty} \frac{d}{d\epsilon} \left(H_\epsilon\right)|_{\epsilon=0} \circ U_{t_0}^{\sigma,0}$$

2.5 Computational Results

In this section we will give computational results for the laser-driven Henon-Heiles system.

The dynamic objects of the Henon-Heiles system considered in this paper include fixed points and invariant manifolds, both stable and unstable. The fixed points for $e = \frac{1}{12}$ are hyperbolic and considered with respect to the Poincare map. As for $e = \frac{1}{6}$, there is one fixed point that is calculated and it is with respect to the flow of the entire system. The invariant manifolds are considered with respect to the Poincare map for both energies and are computed for both the unperturbed and perturbed systems.

Each fixed point $(y_i^\star, p_{y_i}^\star), i = 1, 2, 3$, for $e = \frac{1}{12}$ was computed using Newton's method on the function

$$F(y, p_y) = P(y, p_y) - \mathrm{Id}(y, p_y), \tag{2.49}$$

where $P(y, p_y)$ is the Poincare map at $x = 0$ and Id is the identity map. Initial guesses were gathered from approximations using the Poincare map.

Calculation of the stable and unstable manifolds of the unperturbed system required a combination of linearization and the use of the Poincare map. First, the Jacobian matrix $DP(y^\star, {p_y}^\star)$ was computed for each fixed point.

The eigenvector $(x_y^s, x_{p_y}^s)$ of this matrix corresponding to the eigenvalue with a value less than one is used in the computation of the stable manifold. Without loss of generality, the other eigenvector $(x_y^u, x_{p_y}^u)$, which has a corresponding eigenvalue with a value greater than one, is used to compute the unstable manifold. A small perturbation

$$(s_y, s_{p_y}) = (hx_y^s, hx_{p_y}^s) \tag{2.50}$$

or

$$(u_y, u_{p_y}) = (hx_y^u, hx_{p_y}^u) \tag{2.51}$$

is then added to each fixed point in the respective stable or unstable direction, where $h = \pm 10^{-9}$. The eigenvectors are scaled in both the positive and negative directions to account for the fact that hyperbolic fixed points have two incoming stable manifolds and two outgoing unstable manifolds. The manifolds are then calculated by iterating $P(y^\star + u_y, {p_y}^\star + u_{p_y})$ for the unstable manifold and $P^{-1}(y^\star + s_y, {p_y}^\star + s_{p_y})$ for the stable manifold.

Objects of the perturbed system corresponding to the Poincare map were computed by applying the inverse wave map

$$(\Omega_+^{t_0})^{-1} = V_{t_f}^{t_0} \circ U_{t_0}^{t_f}, \tag{2.52}$$

where $t_0 = -4.2$ and $t_f = 4.2$, to every point of the Poincare map. Similarly, the invariant manifolds of this system were computed by applying the same

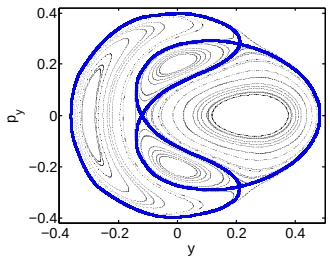

Figure 2.3: For the $e = \frac{1}{12}$ case, the manifolds of the Poincare map for the unperturbed system shown in (a) were computed via Newton's method, linearization, and iterations of the Poincare map

inverse wave map to every point of the respective manifolds from the unperturbed system. Comparison between the unperturbed and perturbed systems can be seen in Figures 2.3 and 2.4 for $e = \frac{1}{12}$ and $e = \frac{1}{6}$, respectively.

In addition to computing the dynamic objects of the perturbed system, scattering theory provides a way to compute the change in energy

$$\triangle e = |H_u \circ (\Omega_+^{t_0})^{-1}(y, p_y) - H_u(y, p_y)| \tag{2.53}$$

between the unperturbed and perturbed systems, where $H_u(y, p_y)$ represents $H(0, y, p_x(y, p_y), p_y)$ under the unperturbed system,. Figure 2.8 shows that the energy differences were increased within the same order of magnitude for both cases.

The differences in position between corresponding objects of the unperturbed and perturbed systems were also computed via wave maps. This was done by discretizing y and p_y within the domain of the Poincare maps and

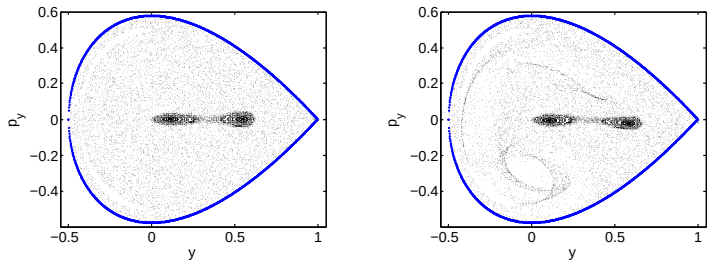

(a) (b)

Figure 2.4: For the $e = \frac{1}{6}$ case, the manifolds of the Poincare map for the unperturbed system shown in (a) were computed explicitly by making use of the invariant plane $(0, y, 0, p_y)$ to solve $p_y(y)$ with a discretized y. Objects of the perturbed system shown in (b) were calculated by applying $(\Omega_+^{t_0})^{-1}$ to the corresponding objects the unperturbed system.

applying the difference function

$$D = ||(\Omega_+^{t_0})^{-1}(y, p_y) - \mathrm{Id}(y, p_y)|| \tag{2.54}$$

to each node. Plots of this data can be seen in Figures 2.5 and 2.6. Note that for $e = \frac{1}{12}$ the maximum difference is around 0.2. Whereas the maximum difference for $e = \frac{1}{6}$ is around 3, an entire order of magnitude higher. This is due to the fact that $\frac{1}{6}$ is a critical value of the Henon-Heiles system and orbits with $e > \frac{1}{6}$ escape to infinity due to bifurcation (see Figure 2.7). Since the laser causes an increase in energy, the $e = \frac{1}{6}$ case of the perturbed system has an energy that is greater than the critical value. As a result, the orbits travel farther under the perturbed system for $e = \frac{1}{6}$ than for $e = \frac{1}{12}$, causing a greater maximum difference for $e = \frac{1}{6}$.

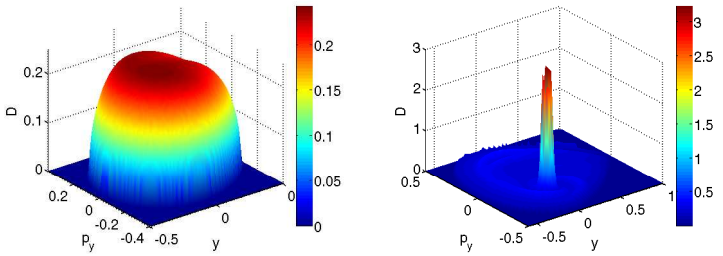

(a) (b)

Figure 2.5: y and p_y are discretized within the domain of the Poincare map and the difference function D is applied to each node in order to compute the difference in position between the unperturbed and perturbed systems for both cases. Note that D is an entire order of magnitude greater for $e = \frac{1}{6}$ in (a) than for $e = \frac{1}{12}$ in (b). Figure 2.7 and Figure 2.8 help to explain the cause of this.

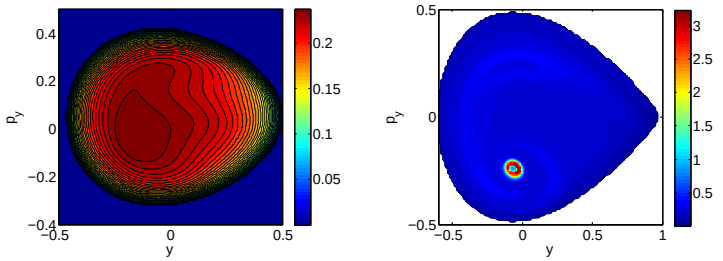

(a) (b)

Figure 2.6: Contour plots of the differences calculated in Figure 2.5 were also rendered for $e = \frac{1}{12}$ in (a) and $e = \frac{1}{6}$ in (b).

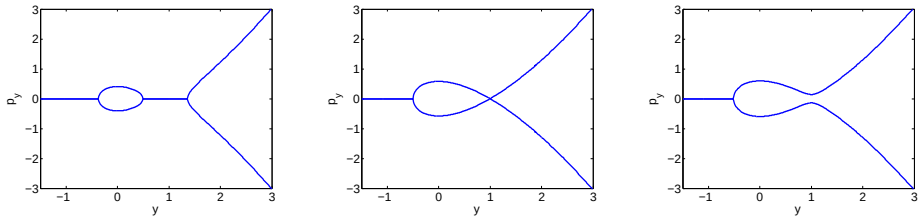

(a) (b) (c)

Figure 2.7: Bifurcation of the regions where the Poincare map is defined for energies (a) $e = 1/12$, (b) $e = 1/6$, (c) $e = 1/6 + 0.001$. The energy value $e = 1/6$ is a critical value of energy since orbits for $e = 1/6 + 0.001$ escape to infinity, which is why there are orbits some orbits in Figure 2.5 that have a relatively larger change in phase space under the inverse wave map $\left(\Omega_+^{t_0}\right)^{-1}$. However, Figure 2.8 shows that the change in energy is on the same order of magnitude for both $e = 1/12$ and $e = 1/6$.

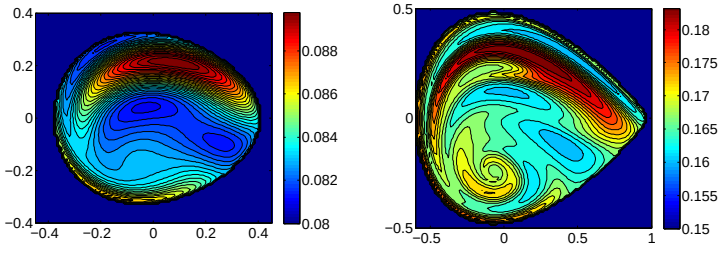

(a) (b)

Figure 2.8: A change in energy between the unperturbed and perturbed systems was computed for $e = \frac{1}{12}$ in (a) and for $e = \frac{1}{6}$ in (b). This was done by discretizing y and p_y within the domain of the Poincare map and calculating $\triangle e$ for each node.

For $e = \frac{1}{12}$ the Poincare map of the unperturbed system is symmetric about the y-axis. This brings about the question as to whether or not the corresponding objects of the perturbed system are also symmetric about the y-axis. In order to test this, a single orbit

$$B = \{P^n(y, p_y)\} \tag{2.55}$$

of the unperturbed system was considered. Points in this set were first reflected across the y-axis and then the inverse wave map was applied, resulting in the set

$$W_1 = \{((\Omega_+^{t_0})^{-1} \circ R)(y, p_y) \mid (y, p_y) \in B\}, \tag{2.56}$$

where $R(y, p_y) = (y, -p_y)$. W_1 represents the orbit of the perturbed system that corresponds to $\hat{B}$, where $\hat{B}$ is the reflection of B across the y-axis. A second set

$$W_2 = \{(R \circ (\Omega_+^{t_0})^{-1})(y, p_y) \mid (y, p_y) \in B\} \tag{2.57}$$

was also computed by reversing the order of function composition used to compute W_1. In other words, W_2 is a reflection of the orbit of the perturbed system that corresponds to B. Thus, symmetry about the y-axis for the perturbed case would imply that $W_1 = W_2$. Comparing the two sets shows that dynamic objects of the perturbed system are not necessarily symmetric about the y-axis for $e = \frac{1}{12}$, which is shown in Figure 2.9.

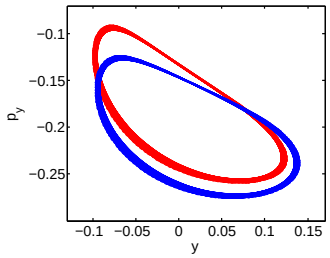

Figure 2.9: A symmetry test about the y-axis for the perturbed case is performed by comparing $(\Omega_+^{t_0})^{-1} \circ R$ (blue) and $R \circ (\Omega_+^{t_0})^{-1}$ (red) of each point in a periodic orbit B of the unperturbed system. The significant difference between the two results implies a lack of symmetry about the y-axis for the perturbed system.

Finally, using the language of scattering theory, one can understand what happens to fixed points and periodic orbits for the perturbed system. Suppose that we have a periodic orbit of the unperturbed system with initial conditions $\mathbf{x} = (x_0, y_0, p_{x_0}, p_{y_0})$ and with period T_p. Then the corresponding object for the perturbed system $\mathbf{x}_+ := \left(\Omega_+^{t_0}\right)^{-1}(\mathbf{x})$ is an *eventually periodic* orbit for the laser-driven system. That is, $V_{t_0}^T(\mathbf{x}_+)$ will have irregular behavior, but after time T the orbit becomes periodic since the perturbation vanishes after time T, and $V_{t_0}^T(\mathbf{x}_+)$ lies on the unperturbed periodic orbit by the definition of the wave maps. This is illustrated in Figure 2.10.

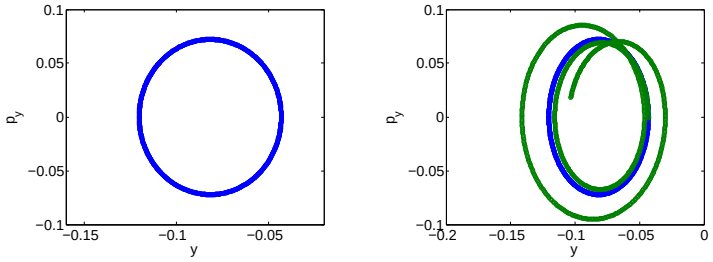

(a) (b)

Figure 2.10: Periodic unperturbed orbit in (a) and eventually periodic orbit in (b). If $\mathbf{x}$ is an initial condition for the unperturbed orbit, then $\mathbf{x}_+ := \left(\Omega_+^{t_0}\right)^{-1}(\mathbf{x})$ is an initial condition for an eventually periodic orbit. In (b), in green shows the evolution of $\mathbf{x}_+$ while the perturbation is on, and in blue show the evolution after the perturbation is turned off

Chapter 3

Periodic orbits in the concentric circular restricted four-body problem and their invariant manifolds

3.1 Introduction

That there are periodic orbits in the circular restricted three-body problem (CRTBP) has been known for a long time. Such orbits are of great practical importance, for instance the Lyapunov orbits near the collinear libration points have been used in the Earth-Sun-spacecraft system to place satellites to observe the Sun. Moreover, computing the stable manifolds of the Lyapunov orbits has proved to be a useful method in constructing low-energy transfers between orbits [17, 8, 41, 59].

In this paper, we give calculations of periodic orbits and stable/unstable manifolds under the presence of another massive celestial body. We consider the motion of a massless object, which we refer to as a spacecraft, in the presence of three massive celestial bodies m_1, m_2, m_3 with $m_1 >> m_2, m_3$ and in an m_1-centered inertial reference frame m_1 is fixed while m_2 and m_3 orbit around m_1 in different circles. It should be noted that the assumed motion of bodies m_1, m_2 and m_3 does not satisfy the Newton's equations of motion, but

is merely an approximation.

The two main goals of the paper are to find periodic orbits in the four-body systems we consider and develop a better understating of the stable/unstable manifolds that appear. What makes the periodic orbits that we construct new and interesting is that they are periodic in the full-four body system, not a patched system as has been considered before [59]. In the patched system, one uses well-known methods to compute Lyapunov orbits and their stable/unstable manifolds under the assumption that one of the relatively smaller masses m_2 or m_3 is turned off. However, in our work, the periodic orbits we compute are periodic for the full four-body system, i.e. one always takes the masses m_1, m_2, and m_3 into account.

Periodic orbits and their stable/unstable manifolds in the restricted four-body problem have been considered before in [49, 54, 57, 69]. However, in [49] the parameters values for m_1, m_2 and m_3 are dramatically different than the parameters for the Jupiter-Europa-Ganymede system and it not clear that their method works for the parameters we consider. Also, in [54, 57, 69] they assume that m_2 and m_3 have equal masses and lie on the same circle, which simplifies the situation since in such a scenario the equations of motion are autonomous in a rotating frame.

Finding periodic orbits in the full four-body system is a delicate task for several reasons, the most difficult obstacle unique to the system we consider is that one needs to find periodic orbits with a prescribed period. We were able to find many stable retrograde orbits by experimentation using Newton's

method with different initial guesses. What is more subtle is to find unstable orbits, i.e. the analogy of Lyapunov orbits in the four-body system. We give an algorithm in Section 3.3 to construct unstable orbits in the full four-body system that is based off of the Laplace resonance. This algorithm is then successfully implemented in Section 3.5 using the parameters for the Jupiter-Europa-Ganymede system.

Another significant new result of this paper is that we observe that the stable manifold of a periodic orbit near m_2 does not intersect the unstable manifold of a periodic orbit near m_3, but the manifolds get stuck in the region between m_2 and m_3. This is in stark contrast to the results in [59] where they find intersections that lead to low-energy transfers, though the intersections found in [59] are for the patched system. The method we use to compute the stable/unstable manifolds is the same as in the CRTBP or the patched system. What is new is the observed lack of intersection for the particular orbits we construct.

3.2 Equations of motion

The system we consider is the motion of a massless object, e.g. a spacecraft, in the presence of three massive celestial objects with masses m_1, m_2 and m_3. We will assume that $m_1 >> m_2, m_3$, as in the case of the Jupiter-Europa-Ganymede-spacecraft system.

In our model we impose that, in an m_1-centered inertial reference frame, m_2 and m_3 rotate about m_1 in circles of radii r_{12} and r_{13}, respectively. In such

a model, the motion of m_1, m_2 and m_3 do not satisfy Newton's equations of motion, but is merely an approximation. The frequencies ω_2 and ω_3 of motion of m_2 and m_3 about m_1 are governed by the relation for circular orbits in the two-body problem [60]

$$\omega_i = \sqrt{\frac{Gm_1 + Gm_i}{r_{1i}^3}} \tag{3.1}$$

We will normalize units of mass and distance so that

$$\begin{aligned} Gm_1 &= 1 \\ r_{13} &= 1 \end{aligned} \tag{3.2}$$

Let (x, y) denote the planar coordinates of the spacecraft, (x_i, y_i) denote the coordinates of $m_i, i = 1, 2, 3$. The equations of motion for the spacecraft in an m_1 centered inertial frame are given by

$$\begin{aligned} \ddot{x} &= -m_1\frac{x}{r_1^3} - m_2\frac{x - x_2}{r_2^3} - m_3\frac{x - x_3}{r_3^3} - m_2\frac{x_2}{r_{12}^3} - m_3\frac{x_3}{r_{13}^3} \\ \ddot{y} &= -m_1\frac{y}{r_1^3} - m_2\frac{y - y_2}{r_2^3} - m_3\frac{y - y_3}{r_3^3} - m_2\frac{y_2}{r_{12}^3} - m_3\frac{y_3}{r_{13}^3} \end{aligned} \tag{3.3}$$

where r_i is the distance from m_i to the spacecraft. We will assume that (x_2, y_2) and (x_3, y_3) coordinates of the point masses m_2 and m_3 , which we assume to take the form

$$\begin{aligned} (x_2(t), y_2(t)) &= r_{12}(\cos(\omega_2 t), \sin(\omega_2 t)) \\ (x_3(t), y_3(t)) &= r_{13}(\cos(\omega_3 t), \sin(\omega_3 t)) \end{aligned} \tag{3.4}$$

Whenever ω_2 and ω_3 are not commensurate, that is $\frac{\omega_2}{\omega_3}$ is irrational, Equations (3.3) are quasi-periodic in time. Thus, in general, we do not expect periodic solutions to (3.3).

The periodic orbits we consider are periodic in either an m_1-m_2 or an m_1-m_3 rotating frame centered at m_1. If we let (ξ, η) denote the planar coordinates of the spacecraft in an m_1-m_2 rotating frame, then using a similar technique in deriving the equations for the CRTBP as done in [60, 71], one can derive the equations of motion in an m_1-m_2 rotating frame centered at m_1

$$\begin{aligned}
\ddot{\xi} &= 2\omega_2\dot{\eta} + \omega_2^2\xi - m_1\frac{\xi}{r_1^3} - m_2\frac{\xi - r_{12}}{r_2^3} - m_3\frac{\xi - \xi_3}{r_3^3} - m_2\frac{1}{r_{12}^2} - m_3\frac{\xi_3}{r_{13}^3} \\
\ddot{\eta} &= -2\omega_2\dot{\xi} + \omega_2^2\eta - m_1\frac{\eta}{r_1^3} - m_2\frac{\eta}{r_2^3} - m_3\frac{\eta - \eta_3}{r_3^3} - m_3\frac{\eta_3}{r_{13}^3}
\end{aligned} \tag{3.5}$$

Where (ξ_3, η_3) are coordinates for m_3, which are given by

$$(\xi_3(t), \eta_3(t)) = r_{13}(\cos[(\omega_3 - \omega_2)t], \sin[(\omega_3 - \omega_2)t]) \tag{3.6}$$

Thus we see that Equations (3.5) are periodic in time with period $T_p = \frac{2\pi}{|\omega_3 - \omega_2|}$. For completeness, the equations in an m_1-m_3 frame are

$$\begin{aligned}
\ddot{\xi} &= 2\omega_3\dot{\eta} + \omega_3^2\xi - m_1\frac{\xi}{r_1^3} - m_2\frac{\xi - \xi_2}{r_2^3} - m_3\frac{\xi - 1}{r_3^3} - m_2\frac{\xi_2}{r_{12}^3} - m_3\frac{1}{r_{13}^2} \\
\ddot{\eta} &= -2\omega_3\dot{\xi} + \omega_3^2\eta - m_1\frac{\eta}{r_1^3} - m_2\frac{\eta - \eta_2}{r_2^3} - m_3\frac{\eta - 1}{r_3^3} - m_3\frac{\eta_2}{r_{12}^3}
\end{aligned} \tag{3.7}$$

Where (ξ_2, η_2) are coordinates for m_2, which are given by

$$(\xi_2(t), \eta_2(t)) = r_{12}(\cos[(\omega_2 - \omega_3)t], \sin[(\omega_2 - \omega_3)t]) \tag{3.8}$$

Thus, the Equation (3.7) are also periodic with period $T_p = \frac{2\pi}{|\omega_3 - \omega_2|}$.

Remark 1: The librations points in our model

Due to the non-autonomous nature of the equations of motion, there are no fixed points to either (3.5) nor (3.7). Thus, one should be careful when one mentions libration points in our model. Consider, for example, the case

of $L1$ of m_2: If one turns off m_3, then one has the usual libration point $L1$ of m_2. Although this point is not fixed in the full four-body system, *we will still refer to* $L1$ *of* m_2 *as the point on the* x*- axis that is in between* m_1 *and* m_2 *and is fixed in an* m_1-m_2 *rotating frame when one turns off* m_3. Similar remarks hold for the other libration points in the system.

3.3 Method of finding Lyapunov-like periodic orbits in the full four-body system

In this section we will describe how one can find periodic orbits about the collinear libration points near m_2 and m_3 assuming that the frequencies of ω_2 and ω_3 are resonant frequencies. We adopt the conventions in Remark 1 in Section 3.2 when referring to the libration points for our system, even though such points are not fixed. The algorithm yields orbits which are periodic in the full four-body system, that is, we assume that the spacecraft is governed by the gravitational forces of all the bodies m_1, m_2 and m_3. As mentioned in Section 3.2, the equations of motion are not periodic in an inertial frame centered at m_1 provided that $\frac{\omega_3}{\omega_2}$ is irrational. However, the equations of motion are periodic in either an m_1-m_2 or an m_1-m_3 rotating frame with period $T_p = \frac{2\pi}{|\omega_3 - \omega_2|}$, and hence it is possible to have periodic orbits in these frames.

Periodic orbits that rotate around one or more of the primaries in a rotating frame are stable and are therefore easier to find than Lyapunov-like orbits that stay near $L1$ or $L2$. Some of these stable orbits are computed in Section 3.5, though in this section we focus on describing an algorithm for finding unstable Lyapunov-like orbits.

The m_1-m_2-spacecraft and the m_1-m_3-spacecraft systems are instances of the circular restricted three-body problem (CRTBP) and are much better understood than the full four-body system. Indeed, let us consider the m_1-m_2-spacecraft system. In an m_1-m_2 rotating frame we have the unstable collinear fixed points $L1$ and $L2$ near m_2. Near each of these fixed points are the Lyapunov orbits, that is a family of unstable periodic orbits about the fixed points.

One may hope that in the full-four body system, there are corresponding periodic orbits since the mass of $m_3 << m_1$. However, there are two difficulties one needs to consider when trying to find analogous orbits in the full system: First, since the equations of the four-body system in the m_1-m_2 rotating frame are periodic with period T_p, any periodic orbit must have period nT_p where n is positive integer [42]. Thus we need to find periodic orbits with a prescribed period, which is not the case in the CRTBP.

Secondly, in the CRTBP the Lyapunov orbits are unstable, and hence a small change in initial conditions of a Lyapunov orbit will result in a non-periodic trajectory. Thus, initial conditions for a Lyapunov orbit in an embedded CRTBP does not serve as a good initial guess for using Newton's method to find a periodic orbit in the full four-body system. Indeed, in the Jupiter-Europa-Ganymede-spacecraft system, this phenomena was observed.

Nevertheless, we propose a new technique based off of linearizing the full four-body system near the libration points that exist in the embedded CRTBPs we can find periodic orbits in the full four-body system. We now ex-

plain a crucial property about the linearized dynamics of the Jupiter-Europa-Ganymede-spacecraft system that motivates the method. Consider $L2$ of the m_1-m_2 CRTBP and the linearization of the dynamics at $L2$. As is well known, in the linearized system, there is a linear subspace of periodic orbits, all with a fixed period that we call $T_{L2,m_2,lin}(m_3 = 0)$. Moreover, for CRTBPs such as the ones embedded in our problem, we have the approximate relations [71, 60]

$$\begin{aligned} T_{m_2} &\approx 2T_{L2,m_2,lin}(m_3 = 0) \\ T_{L2,m_2,lin} &\approx T_{L1,m_2,lin}(m_3 = 0) \end{aligned} \tag{3.9}$$

where $T_{m_2} = \frac{2\pi}{\omega_2}$ is the orbital period of m_2 about m_1. Equation (3.10) is a known fact about the CRTBP. What we observed for the parameters of the Jupiter-Europa-Ganymede-spacecraft system is that

$$\begin{aligned} T_{L2,m_2,lin}(m_3 = 0) &\approx T_{L2,m_2,lin}(m_3 \neq 0) \\ T_{L2,m_2,lin}(m_3 = 0) &\approx T_{L1,m_2,lin}(m_3 \neq 0) \end{aligned} \tag{3.10}$$

where, on the right we linearize the full system at the same point $L2$ or $L1$, which are not fixed for the full system. Since all the computations done in this paper are for the full system *from now on* $T_{L2,m_2,lin}$ *will refer to the linearization in the full system, that is* $T_{L2,m_2,lin}(m_3 \neq 0)$, and similarly for the other libration points.

In the Jupiter-Europa-Ganymede system, there is the well-known Europa-Ganymede resonance, namely $\omega_2 \approx 2\omega_3$ [60]. Thus applying Equations (3.10) and using the fact that $T_p = \frac{2\pi}{|\omega_2 - \omega_3|}$ we obtain

$$\begin{aligned} T_{L1,m_2,lin} &\approx \frac{\pi}{\omega_2} \approx \frac{\pi}{2\omega_3} \approx \frac{1}{4}\frac{2\pi}{\omega_2 - \omega_3} = \frac{1}{4}T_p \\ T_{L1,m_3,lin} &\approx \frac{\pi}{\omega_3} = \frac{1}{2}\frac{2\pi}{2\omega_3 - \omega_3} \approx \frac{1}{2}\frac{2\pi}{\omega_2 - \omega_3} = \frac{1}{2}T_p \end{aligned} \tag{3.11}$$

Because of (3.10), we see that (3.11) holds if we replace $L1$ with $L2$ as well. A more general situation that we will consider is to suppose that

$$\begin{aligned} T_{L1,m_2,lin} &\approx \frac{q_2}{p_2} T_p \\ T_{L1,m_3,lin} &\approx \frac{q_3}{p_3} T_p \end{aligned} \tag{3.12}$$

where q_i, p_i are integers and $\frac{q_i}{p_i} < 1$. Finding a good initial guess for using Newton's method to find a periodic orbit of the full system is more difficult than in the CRTBP since (1) we need to find a periodic orbit with a prescribed period that can be much larger than $T_{L2,m_2,lin}$ and (2) symmetry about the x-axis does not hold in the full system (c.f. Remark 2 in Section 3.5 for details about symmetry in the full system). However, we give an algorithm for finding a good initial guess if we assume that Equation (3.12) holds.

The algorithm is as follows: Since the linearized dynamics at $L2$ mimics the full dynamics in a neighborhood of $L2$, we expect there to exist a solution of the full system that starts on the x-axis and $\dot{x} = 0$ initially and has a perpendicular crossing of the x-axis at time $\frac{q_2}{2p_2} T_p \approx \frac{1}{2} T_{L2,m_2,lin}$. By assumption $\frac{q_2}{p_2} < 1$, and hence finding a good initial guess for a perpendicular crossing at time $\frac{q_2}{2p_2} T_p$ is much easier than finding a good initial guess for a periodic orbit with period T_p.

One can then use the initial condition of that has a perpendicular crossing at $\frac{q_2}{2p_2} T_p \approx \frac{1}{2} T_{L2,m_2,lin}$ as an initial guess for a solution of finding a perpendicular crossing at $\frac{q_2}{p_2} T_p \approx T_{L2,m_2,lin}$. Of course, once can repeat this procedure of finding more and more crossings until one has $2p_2$ perpendicular crossings which may then serve as a good initial guess of using Newton's method of

finding a periodic orbit with period $q_2 T_p$. This method was successful in finding periodic orbits of the Jupiter-Europa-Ganymede-spacecraft system, and is expected to be a robust algorithm provided that one has that p_3 is small. Note that since Equation (3.12) is an approximation one may be able to choose p_3 small provided that it is still a reasonable approximation. What a reasonable approximation is for this method is still not clear. The problem that one has for large p_3 is that the more crossings one has to find, the more unstable the orbit becomes, i.e. the eigenvalues of the state transition matrix $\Phi(t_f, t_0)$ (STM) the more crossing one has to find, which may make things difficult in carrying out the algorithm.

3.4 Computing the stable/unstable manifolds of the unstable periodic orbits

As in the CRTBP, an integration of the monodromy matrix $\Phi(T_p, 0)$ tells us that the periodic orbits are linearly unstable. More specifically, $\Phi(T_p, 0)$ has eigenvalues λ_s, and λ_u, with $|\lambda_s| < 1$, $|\lambda_u| > 1$. It follows that these periodic orbits have stable/unstable manifolds.

The interesting phenomena we notice is that although the unstable/stable manifolds wander off a bit from the periodic orbits, orbits on the stable/unstable manifold either result in retrograde orbits about either m_2 or m_3, or get stuck in the region between m_2 and m_3 where the forces of m_2 and m_3 balance each other out and motion is essentially governed solely by m_1. We find that the stable/unstable manifolds of the periodic orbits near $L2$ of m_2 does not intersect the unstable/stable manifolds of the periodic orbit near $L1$ of m_3.

The method we use to compute the stable/unstable manifolds of the periodic orbits is described in [67]. For the stable (resp. unstable) manifold, this method starts by fixing a point $P_0 = (x(0), y(0), v_x(0), v_y(0))$ on the periodic orbit, computing $\Phi(T_p, 0)$ and the stable (resp. unstable) eigenvector v_s (resp. v_u) for the stable (resp. unstable) eigenvalue λ_s (resp. λ_u). With this one can compute the corresponding stable and unstable vectors $v_{s,u}(\tau)$ at the point $P(\tau) = (x(\tau), y(\tau), v_x(\tau), v_y(\tau))$ for $0 \leq \tau \leq T_p$ using the relation

$$v_{s,u}(\tau) = \Phi(\tau, 0) v_{s,u} \tag{3.13}$$

The stable/unstable fibers over the point $P(\tau)$ are tangent to the periodic orbit at $P(\tau)$, and hence the points

$$x^{\pm}_{s,u} := P(\tau) \pm \epsilon \frac{v_{s,u}(\tau)}{|v_{s,u}(\tau)|} \tag{3.14}$$

are, for $\epsilon > 0$ small, close to points on the actual stable/unstable fibers at $P(\tau)$. Since the fibers are one-dimensional invariant curves, it follows that integrating the points $x^{\pm}_s(\tau)$ (resp. $x^{\pm}_u(\tau)$) backward (resp. forward) yields stable (resp. unstable) fibers at $P(\tau)$. For numerical purposes it is important to add $\frac{v_{s,u}(\tau)}{|v_{s,u}(\tau)|}$ not simply $v_{s,u}(\tau)$ since, by definition, $v_s(\tau)$ (resp $v_u(\tau)$) decays (resp. increases) exponentially fast and it may be difficult to choose an ϵ that is uniform in τ if one uses merely uses $v_{s,u}(\tau)$. For our purposes, choosing $\epsilon = 10^{-6}$ is sufficient.

3.5 Results for the Jupiter-Europa-Ganymede-spacecraft system

In this section we present the results of finding the periodic orbits and computing their stable manifolds described in Sections 3.3 and 3.4. Using our normalization conventions in Equation (3.2) the relevant parameters are:

$$\begin{array}{ll} m_1 = 1 & \omega_1 = 1.000038 \\ m_2 = 7.79850e-05 & \omega_2 = 2.01416 \\ m_3 = 2.52805e-05 & T_p = 6.19568 \\ r_{12} = .627009 & T_{L2,m_2,lin} = 1.52734531 \\ r_{13} = 1 & T_{L1,m_3,lin} = 3.0298153 \end{array} \tag{3.15}$$

The integration of the system was carried out using the explicit embedded Runge-Kutta-Fehlberg $(4, 5)$ method available in the GNU Scientific Library (GSL). The absolute and relative error tolerances were set to $1e-11$ for all integrations. The root-finding algorithms and computations of eigenvalues/eigenvectors were also carried out using the GSL.

Figure 3.1 shows trajectories that, in a rotating frame, orbit about a primary. Such orbits are stable, and hence are not too difficult to find numerically. We were able to find a few such orbits using Newton's method, though giving a classification of these stable orbits seems difficult since, contrary to the case of the CRTBP, we need to find orbits with a prescribed period. We do not attempt to classify all such orbits in this chapter, but the orbits we found are interesting and worth mentioning.

Figure 3.2 shows the progression of the algorithm in finding a periodic orbit near $L2$ of m_2. Since $T_{L2,m_2,lin} \approx \frac{1}{4}T_p$ we expect the periodic orbit near $L2$ of m_2 to loop around $L2$ four times, which is indeed what we observe. Figure

3.3 shows periodic orbits about the other collinear libration points near m_2 and m_3. The orbits in Figure 3.3 either loop around four times in the case of m_2 and two times for m_3, which is expected from the algorithm.

Notice that, in Figure 3.2, the size of the orbit decreases dramatically as the algorithm progresses. This seems to be due to the fact that the orbits closer to the libration points mimic their linearized counterparts much better for much longer times. It would very interesting if there are different periodic orbits near the orbits constructed in the beginning of the algorithm. For example, the orbit in Figure 3.2 (b) is about twice as large as the true periodic orbit constructed in Figure 3.2 (d), and perhaps there is another periodic orbit near the orbit of Figure 3.2 (b), though finding such an orbit seems difficult. The initial conditions for all the orbits are in Table (1).

The results for the computation of the stable/unstable manifolds of the periodic orbits computed in Figures 3.2 (d) and 3.3 (d) are shown in Figures 3.5 and 3.6. Figure 3.5 shows the invariant manifolds in the respective rotating frame and only in a small vicinity of the periodic orbit. Figure 3.6 shows both the stable and unstable manifolds plotted in an inertial frame centered at m_1. It is observed that the manifolds do not intersect, but get trapped in the region in between m_2 and m_3 where the gravitational forces of m_2 and m_3 balance each other out.

Remark about the symmetry of the periodic orbits

Some of the periodic orbits we construct are symmetric about the y-axis, though not all of them. It is important to note that symmetry with respect

to the y-axis does not, in general, hold for solutions for the four-body system we consider. In the CRTBP, if an orbit satisfies $y(t_0), v_x(t_0) = 0$ and $y(t_0+T), v_x(t_0+T) = 0$ then the orbit is periodic with period $2T$. However, this need not be the case in four- body system we consider. Indeed, in Figure 3.4 (a) shows an orbit such that $y(t_0), v_x(t_0) = 0$ and $|y\left(t_0 + \frac{T_p}{2}\right), v_x\left(t_0 + \frac{T_p}{2}\right)| < 1e-13$. Yet if we run this orbit for an additional $\frac{T_p}{2}$ units of time, we see that the orbit is not periodic, as seen in 3.4 (b). This phenomena is due to the fact that m_2 is rotating in a circle in the m_1-m_3 rotating frame and hence the only way an orbit that returns to itself at a later time t to be periodic is for m_2 to be in the same position at the start time and at time t. For the sake of comparison we run the orbit in 3.3 (c) for an extra $\frac{T_p}{2}$ and T_p units of time and we notice the orbit stays put. $\square$

Table 3.1: Initial conditions for the periodic orbits

Figure	x	y	v_x	v_y	t_0
1 (a)	0.6323257626	-0.0046941290	0.0400377803	-0.0005372854	0.0
1 (c)	0.5413991355	0.0	0.0	0.3593389644	
1 (d)	0.6178086512	-0.0030339801	0.0130224917	0.0181830389	0.0
1 (e)	0.9948176294	0.0	0.0	-0.1182192534	0.0
1 (g)	0.9883935350	0.0	0.0	0.0977950038	0.0
1 (h)	0.9785090753	0.0	0.0	0.0166235833	0.0
2 (d)	0.6399118669	0.0	0.0	-0.0008513990	0.0
3 (a)	0.6143474403	0.0000000088	0.0000000045	-0.0002327567	0.0
3 (b)	1.0312064038	0.0	0.0	-0.0084591055	0.0
3 (d)	0.9706653133	0.0	0.0	0.0001805997	0.0
4 (a)	1.0282069010	0.0	0.0	0.0104665145	1.43967

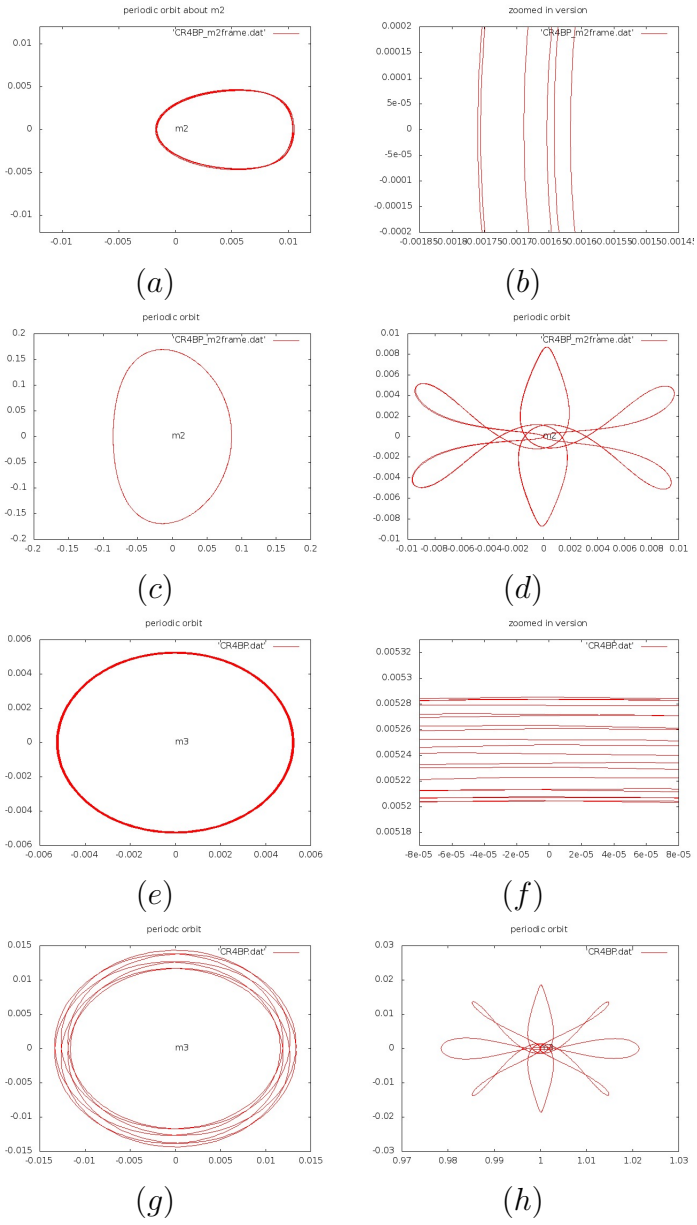

Figure 3.1: Periodic orbits that, in a rotating frame, orbit around one or more of the primaries. We found orbits that (a), (c), (d) rotate around m_2 in an m_1-m_2 rotating frame and $(d), (g), (h)$ rotate around m_3 in an m_1-m_3 rotating frame. (b) and (e) are zoomed in versions of (a) and (d), respectively, and it is noticed that the orbits loop around several times. All orbits have period T_p.

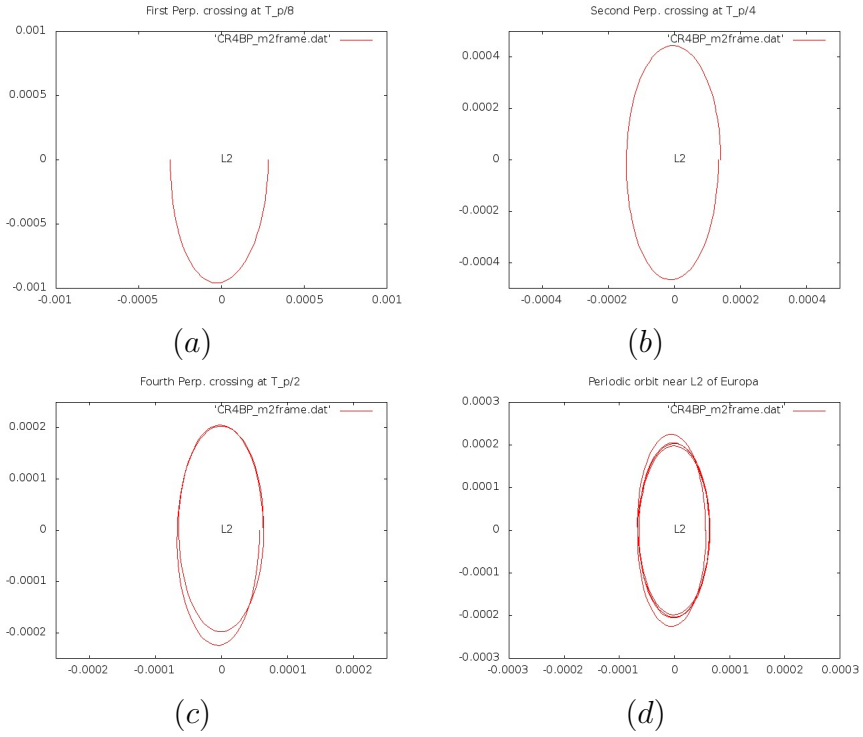

Figure 3.2: Progression of finding a periodic orbit near $L2$ of m_2. We first find a perpendicular crossing at $\frac{T_p}{8} \approx \frac{1}{2}T_{L2,m_2,lin}$, which is depicted in (a). This is used as an initial guess for finding a perpendicular crossing at $\frac{T_p}{4} \approx T_{L2,m_2,lin}$, as in (b). This procedure is repeated until eight perpendicular crossings are found. (c) is shows the fourth crossing, and (d) is the periodic orbit for the full four-body system.

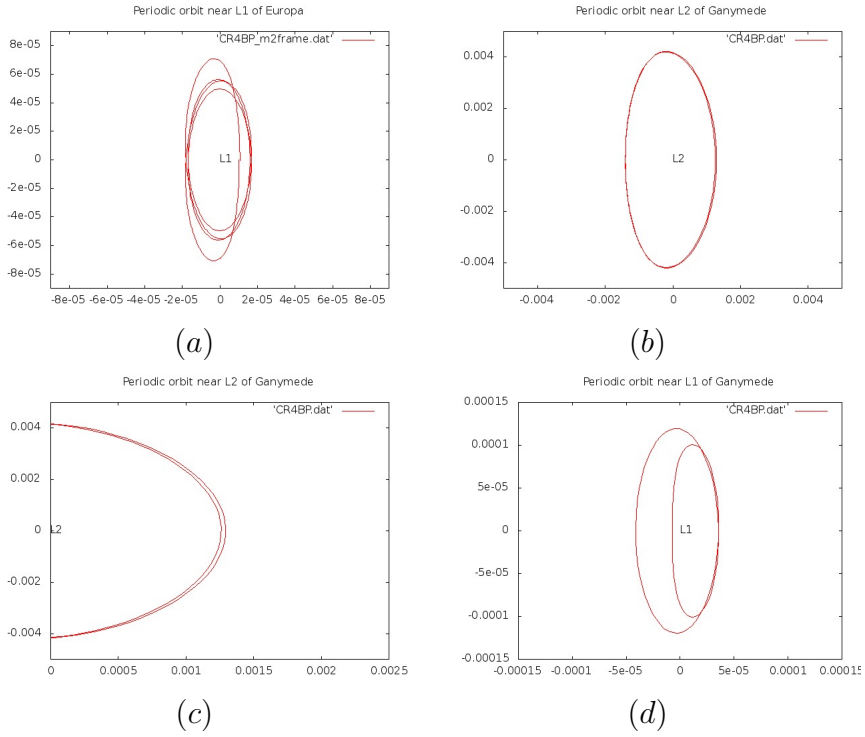

Figure 3.3: Periodic orbits near other collinear libration points. A periodic orbit near (a) $L1$ of Europa (b) $L1$ of Ganymede and (d) $L2$ of Ganymede. (c) is a zoomed in view of part of the periodic orbit in (b). As expected, the orbit in (a) loops around four times and the orbits in $(b), (c), (d)$ each loop around two times.

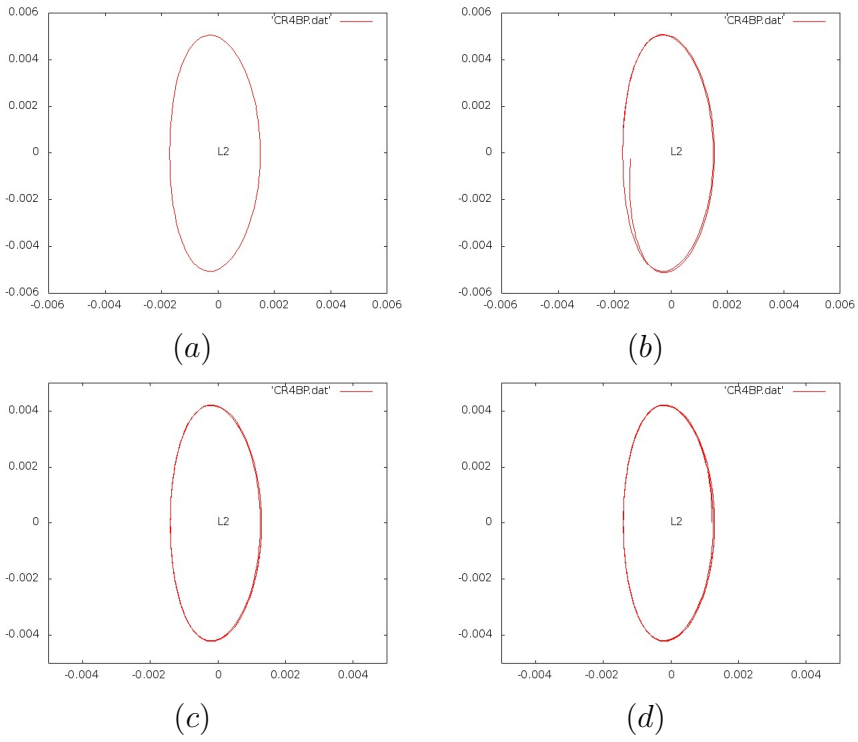

Figure 3.4: Illustration of the lack of symmetry. (a) shows an orbit for which $y(0), v_x(0) = 0$ and $y(\frac{T_p}{2}), v_x(\frac{T_p}{2}) = 0$ yet is not periodic as shown in (b) which is the same orbit run for and additional $\frac{T_p}{2}$ units of time. To compare, we ran the orbit computed in Figure 3.3 (c) for extra $\frac{T_p}{2}$ units of time which is shown in (c). For good measure, we also (d) run the orbit of 3.3 (c) an extra T_p units of time. This shows that the orbit in (a) is not truly periodic but the one in (c) is.

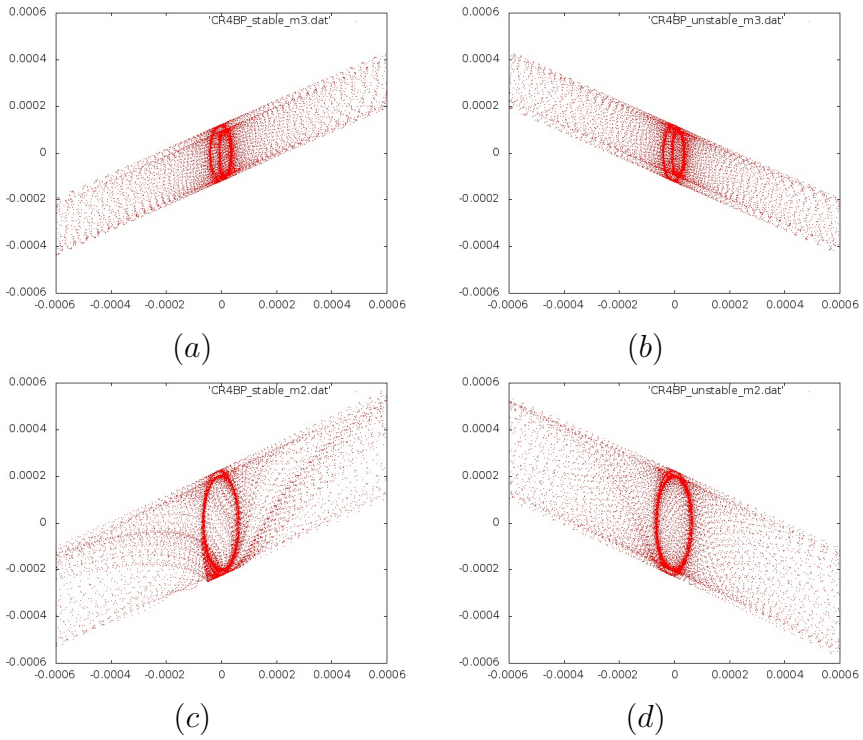

Figure 3.5: Computation of the stable/unstable manifolds of the periodic orbits in rotating frames. The stable (a) and unstable (b) manifolds of the periodic orbit near $L1$ of m_3 shown in Figure 3.3 (d) and the stable (c) and unstable (d) manifolds of the periodic orbit near $L1$ of m_2 shown in Figure 3.2 (d).

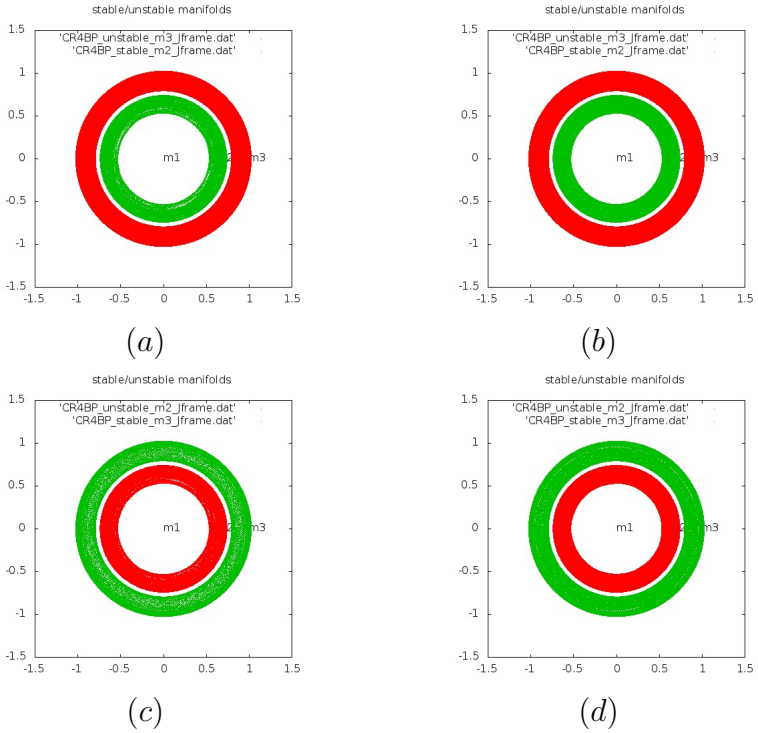

Figure 3.6: The stable/unstable manifolds of the periodic orbits from Figures 3.2 (d) and 3.3 (d) in an $m1$-centered inertial frame. The unstable manifolds appear in red, the stable manifolds appear in green. The unstable manifolds of the orbit near $L2$ of m_2 and the stable manifold of the orbit near $L1$ of m_3 were ran for (a) $2T_p$ units of time and (b) $4T_p$ units of time. Similarly, the stable manifolds of the orbit near $L2$ of m_2 and the unstable manifold of the orbit near $L1$ of m_3 were ran for (c) $2T_p$ units of time and (d) $4T_p$ units of time.

3.6 Conclusions

We presented a method to compute periodic orbits in the restricted four-body problem under the assumption (3.12) that the linearized periods of motion is approximately commensurate with the period T_p of the equations of motion in a rotating frame. Physically T_p is the period of m_2 (resp. m_3) in an m_1-m_3 (resp. m_1-$m-2$) rotating frame. This assumption was merely a generalization of the Europa-Ganymede resonance.

We also computed the stable/unstable manifolds of these orbits and showed that they do not in fact intersect. It is interesting to compare this with the work of [59], where they use invariant manifold theory to come up with a low-energy transfer from Ganymede to Europa. In [59] the invariant objects (i.e. periodic orbits and stable/unstable manifolds) are computed in a patched system where either Ganymede or Europa is turned off in the computation of Lyapunov orbits and their stable/unstable manifolds and it is observed that the unstable manifold of a Lyapunov orbit near $L1$ of Ganymede intersects the stable manifold of a Lyapunov orbit near $L2$ of Europa. The corresponding intersection point has a corresponding Δv which is much smaller than the Δv's needed for a Hohman transfer. This orbit is then chosen as an initial guess for the implementation of a differential correction procedure to obtain a transfer in the full system with a similarly small Δv.

In the present work, all the invariant objects are computed in the full-four body system. Figure 3.6 suggests that the final transfer computed in [59] may not arise from finding intersections of stable/unstable manifolds of peri-

odic orbits, where both the periodic orbits and their stable/unstable manifolds are computed in the full four-body system.

A related issues is that, in the CRTBP, there is a one-parameter family of Lyapunov orbits near $L1$ and $L2$. The mathematical theory tells us that for *sufficiently small* values of a perturbing mass, some of these orbits will persist in the presence of another massive body. However, for realistic parameters as the ones used in this chapter, it is not clear whether or not there are any other periodic orbits near $L1$ and $L2$. Any insight in this issue would be interesting. Also, if there are in fact other unstable periodic orbits, it would be interesting to see if their stable/unstable manifolds intersect.

Moreover, all the results in the paper are for the planar restricted four-body problem. Halo orbits for the spatial problem and an analysis of their invariant manifolds would also be an interesting problem to investigate in the future.

Finally, we exploited the Europa-Ganymede resonance to obtain the periodic orbits in this chapter. As is well-known, this resonance is part of an even more interesting resonance, namely the Laplace resonance involving Io-Europa-Ganymede [60]. In this case $\omega_I \approx 2\omega_E \approx 4\omega_G$. If one assumes, for instance, that $\omega_I = 2\omega_E$ then the five body Jupiter-Io-Europa-Ganymede-Spacecraft system will still be periodic in rotating frames and their may be periodic orbits, though if we use the exact value of ω_I then the equations will be quasi-periodic in any rotating frame and hence there are be no periodic orbits. It would be interesting to see if their are periodic orbits in the five-body

system under the assumption that $\omega_I = 2\omega_E$.

Chapter 4

Anisotropic heat transport in reversed shear magnetic field configurations

4.1 Introduction

In this chapter, we consider the problem of understanding how heat is transported in confined plasma. In fusion plasmas, the transport of heat is strongly anisotropic. Indeed, the conductivity along a magnetic field line, $\chi_{\|}$ is roughly 10 orders of magnitude larger than the conductivity perpendicular to a field line, $\chi_{\perp}$. In this chapter, we adopt the Lagrangian Green's function (LG) method used in [22] to compute purely parallel heat transport, that is we assume that $\chi_{\perp} = 0$.

As is well-known, reversed shear magnetic field configurations are known to have robust transport barriers [25, 23, 24, 15] where the safety factor q has a critical point. In this paper, we study how the features unique to reversed shear magnetic fields (e.g separatrix reconnection, banded chaos, the shearless curve) relate to heat transport in the presence of the underlying field.

Of particular interest is the case of leaky barriers. In the field line structure, we observe strong partial barriers arising from shearless Cantori in

what otherwise seem like stochastic magnetic fields. In this regime where the magnetic field is fully chaotic with the exception for Cantor-like remnants of the shearless curve, we observe that the Cantori slow down the transport of heat. We find phenomena that is indicative of non-locality of the effective radial heat transport, i.e. the evolution of the temperature averaged over the toroidal and poloidal directions. We find regions of zero gradient but non-zero flux, in violation of the Fourier-Fick law, and we also find that the flux decays algebraically in contrast to Fourier-Fick diffusion on a $1 - D$ interval that predicts an exponential decay.

4.2 Lagrangian method of solving parallel heat transport

In this section we review the method to compute heat transport along magnetic field lines developed in [22]. We adopt the assumption in [22] that diffusion occurs only in the direction of the magnetic field lines, that is the diffusivity rate $\chi_\perp$ in the direction perpendicular to the magnetic field is zero. We consider local and nonlocal heat transport, and the basic structure of either local and nonlocal heat flow is

$$\partial_t T = -\nabla \cdot \mathbf{q} \tag{4.1}$$

where $\mathbf{q}$ is the heat flux. There are several ways to close (4.1) by expressing the heat flux q in terms of T. In the local setting we have

$$\mathbf{q} = -\chi_\parallel (\partial_s T)\hat{\mathbf{b}} \tag{4.2}$$

where $\partial_s T = \hat{\mathbf{b}} \cdot (\nabla T)$ is the derivative along the magnetic field and $\hat{\mathbf{b}} = \frac{\mathbf{B}}{B}$ is the corresponding unitary magnetic field. Thus in the local heat transport we obtain the equation

$$\begin{aligned} \partial_t T =& \nabla \cdot \mathbf{q} = \nabla \cdot \left[\chi_{\|} (\partial_s T) \hat{\mathbf{b}} \right] \\ &= \chi_{\|} \partial_s^2 T + \chi_{\|} (\partial_s T) \nabla \cdot \hat{\mathbf{b}} \end{aligned} \tag{4.3}$$

We assume that $\nabla \cdot \mathbf{B} = 0$, but that does not imply that $\nabla \cdot \hat{\mathbf{b}} = 0$. However, in this chapter we will assume the tokamak ordering $\partial_s(\ln B) \approx 0$, and therefore ignore the second term in (4.3) in which case (4.3) becomes

$$\partial_t T = \chi_{\|} \partial_s^2 T \tag{4.4}$$

In the magnetic fields considered in this chapter, the size of $\partial_s(\ln B)$ was on the order of 10^{-3}.

A more general model we consider is nonlocal heat transport with the closure

$$q_{\|} = \frac{\chi_{\|}}{\pi} \int_0^{\infty} \frac{T(s+z) - T(s-z)}{z^{\alpha}} dz \tag{4.5}$$

and the corresponding heat transport equation becomes

$$\partial_t T = -\partial_s q_{\|} \tag{4.6}$$

In the limit as $\alpha \to 2$ we obtain the local heat flux (4.2), and we will also consider non-local transport by choosing $\alpha \in [1, 2)$. Another way of writing (4.6) is

$$\partial_t T = -\chi_{\|} (-\partial_s^2)^{\alpha/2} T \tag{4.7}$$

Where the operator $(-\partial_s)^{\alpha/2}$ is defined on Fourier space by

$$\widehat{(-\partial_s^2)^{\alpha/2} T} = |k|^{\alpha} \hat{T} \tag{4.8}$$

where k is an integer since we are implicitly restricting T to a 1-D field line. In [22], they take a Lagrangian approach to solving (4.7) that is based off of using the Green's function. We parameterize the field lines $\mathbf{r}$ by finding trajectories of the ODE

$$\begin{aligned} \frac{d\mathbf{r}}{ds} &= \hat{\mathbf{b}} \\ \mathbf{r}(0) &= \mathbf{r}_0 \end{aligned} \tag{4.9}$$

The solution of (4.7) is then given by

$$T(\mathbf{r}_0, t) = \int_{-\infty}^{\infty} T_0(\mathbf{r}(s)) G_\alpha(s,t) ds \tag{4.10}$$

where G_α is the Green's function and T_0 is the initial temperature. Explicit formulas are only known for $\alpha = 1, 2$. For the local case G_2 takes the form

$$G_2(s,t) = \frac{1}{\sqrt{2}\pi} (\chi_\parallel t)^{-1/2} \exp\left(-\frac{s^2}{4\chi_\parallel t}\right) \tag{4.11}$$

When $\alpha = 1$ (4.7) is non-local and the Green's function takes the form

$$G_1(s,t) = \frac{(\chi_\parallel t)^{-1}}{\pi} \frac{1}{1 + (s/\chi_\parallel t)^2} \tag{4.12}$$

For $1 < \alpha < 2$, G_α takes the form

$$G_\alpha = \frac{1}{(\chi_\parallel t)^{\frac{1}{\alpha}}} K_{\alpha,0}\left[\frac{1}{(\chi_\parallel t)^{\frac{1}{\alpha}} s}\right] \tag{4.13}$$

where $K_{\alpha,0}$ is the symmetric α-stable Levy distribution. Notice that G_2 has exponential decay in s whereas G_1 has algebraic decay. This agrees with our intuition that non-local equations allow for longer range interactions on a shorter time interval. We give computations highlighting the difference between local and non-local diffusion in chaotic magnetic fields in Section 4.6. We observed

that the asymptotic temperature is the same for both local and nonlocal, but how the asymptotic temperature is reached is dramatically different. The main difference is that the relaxation time for in the nonlocal setting is much smaller in the nonlocal setting.

4.3 B-field model

Now we discuss the magnetic field configurations used in this chapter. We consider a cylindrical magnetic field that is periodic in the z direction. The perturbed reverse shear magnetic fields we consider are of the form

$$\mathbf{B}(r,\theta,z) = \mathbf{B}_0(r) + \mathbf{B}_1(r,\theta,z) \tag{4.14}$$

Where $\mathbf{B}(r)$ is an integrable magnetic field with a non-monotonic q-profile, which we take to be

$$\mathbf{B}_0 = \frac{r}{q_0 R\left(1+\lambda^2\left(r-\frac{1}{\sqrt{2}}\right)^2\right)}\hat{\mathbf{e}}_\theta + B_0\hat{\mathbf{e}}_z \tag{4.15}$$

where $2\pi R$ is the height of the cylinder in the z-direction and we take $R = 5$, B_0 =1, q_0 =0.64 is the minimum value of the q-profile and λ is a constant chosen to make the maximum value of the q-profile to be 3.5 . The q-profile for the unperturbed integrable magnetic field $\mathbf{B}_0$ is given by $q(r) = \frac{r}{R}\frac{B_0}{B_\theta(r)}$, and in our case is

$$q(r) = q_0\left(1+\lambda^2\left(r-\frac{1}{\sqrt{2}}\right)^2\right) \tag{4.16}$$

which is non-monotonic in r and has a minimum at $r = \frac{1}{\sqrt{2}}$.

We assume that the perturbation $\mathbf{B}_1$has no z-component and hence looks like

$$\mathbf{B}_1 = \nabla \times A_z \hat{\mathbf{e}}_z \tag{4.17}$$

where $A_z(r, \theta, z)$ is a superposition of modes, which we assume to take the form

$$\sum_{m,n} A_{mn}(r) \cos\left(m\theta - \frac{nz}{R} + \zeta_{mn}\right) \tag{4.18}$$

Before describing the intricate structure of A_{mn} let us recall some facts from the Hamiltonian description of magnetic field lines. Since $\nabla \cdot \mathbf{B} = 0$ and the z component of $\mathbf{B}$ is a constant, the magnetic field lines have a Hamiltonian structure to them. More precisely, if we introduce the radial flux coordinate $\psi = \frac{r^2}{2R^2}$ and the toroidal angle $\phi = \frac{z}{R}$ then it can be shown that

$$\begin{aligned} \frac{d\psi}{d\phi} &= \frac{1}{B_0 R} \frac{\partial A_z}{\partial \theta} \\ \frac{d\theta}{d\phi} &= \frac{B_\theta(r)}{\sqrt{2\psi}} - \frac{1}{R} \frac{\partial A_z}{\partial \psi} \end{aligned} \tag{4.19}$$

which are Hamiltonian's equations of motion where we view ϕ as the time variable and the non-autonomous Hamiltonian is given by $H(\psi, \theta) = H_0(\psi) + H_1(\psi, \theta)$, where

$$\begin{aligned} H_0(\psi) &= \int \frac{B_\theta(\psi)}{\sqrt{2\psi} R} d\psi = \int \frac{1}{q(\psi)} d\psi \\ H_1(\psi, \theta) &= \frac{-1}{R} A_z(\psi, \theta, z) \end{aligned} \tag{4.20}$$

Now we explain the structure of the terms A_{mn} in (4.18). We take

$$\begin{aligned} A_{mn}(r) =& \epsilon_{mn} a(r) \Bigg\{ C_{mn,1} r^m \exp\left[-\left(\frac{r - r_{01}}{\sqrt{2}\sigma} \right)^2 \right] \\ &+ C_{mn,2} r^m \exp\left[-\left(\frac{r - r_{02}}{\sqrt{2}\sigma} \right)^2 \right] \Bigg\} \\ &= \epsilon_{mn} a(r) \left(A_{mn,1} + A_{mn,2} \right) \end{aligned} \tag{4.21}$$

where ϵ_{mn} is a small parameter that we will vary, σ =0.05, and for brevity we write, for $i = 1, 2$

$$A_{mn,i} = C_{mn,i} r^m \exp\left[-\left(\frac{r - r_{0i}}{\sqrt{2}\sigma} \right)^2 \right] \tag{4.22}$$

We take $a(r)$= $\{1 - \tanh[(r-1)/0.05]\}/2$, which quickly dies of near $r = 1$, which guarantees that the magnetic field lines have a well-defined boundary. We want the perturbations to be localized near the resonance sites, i.e. the values of r for which the q-profile takes the value m/n (see Figure 4.1, which shows the q as a function of the radial flux coordinate $R^2\psi$). The factor of r^m is introduced to ensure that the $A_{mn}(r)$ is differentiable at $r = 0$.

Since the q-profile is non-monotonic, there can be two resonance sites for each value of m/n. In the case that q is monotonic, there can be at most one resonance site. We refer to the two possible resonance sites as r_{1*} and r_{2*}, and they are characterized by $q(r_{i*}) = m/n$. Note that there are no resonance sites if m/n is not in the range of q. In our case, as Figure 4.1 indicates because it is possible to have two, one, or no resonance sites depending on the value of m/n.

The other constants $C_{mn,1}, C_{mn,2}, r_{01}, r_{02}$ are chosen to satisfy the following two conditions: We want to have that (1) $\frac{dA_{mn,i}}{d\psi}(\psi_{i*}) = 0$ for $i = 1, 2$

to guarantee that $A_{mn,i}$ has maximum at ψ_{i*} and (2) $A_{mn,i}(\psi_{i*}) = 1$ to control of amplitude perturbation. These two conditions yield

$$\begin{aligned} r_{0i} &= r_{i*} - \frac{m\sigma^2}{r_{i*}} \\ C_{mn,i} &= \left(\frac{1}{r_{*i}}\right)^m \exp\left[\left(\frac{r_{i*} - r_{0i}}{\sqrt{2}\sigma}\right)\right] \end{aligned} \tag{4.23}$$

We choose the width σ of the Guassians to be small enough to guarantee that the two Guassians have little overlap. The overlap naturally increases near the minimum of the q-profile, but for the modes we chose, it was observed that choosing $\sigma = 0.05$ was sufficient.

4.4 Single mode perturbations

We restrict our attention to a single mode perturbation with $(m, n) = (2, 3)$. Based on the resonance condition, we expect to see $m = 2$ islands whenever the unperturbed magnetic field has q-factor of $m/n = 2/3$. Since the minimum of the q-profile was chosen to be $q_0 = 0.64$ and $q(0) = 3.5$, $q(\psi = 0.5) = 1.13$, we expect there to be two sets of islands, one on each side of the "shearless" curve.

For different values of the amplitude of the perturbation, we obtain qualitatively different magnetic fields, though there are no chaotic regions. Three dynamically distinct behaviors of the field lines are given in Figure 4.2. If the perturbation amplitude is small, as in Figure 4.2 (a) we observe the so-called hetereoclinic topology of the field lines. In this case there are two sets of islands, each set having $m = 2$ islands. These islands are separated by

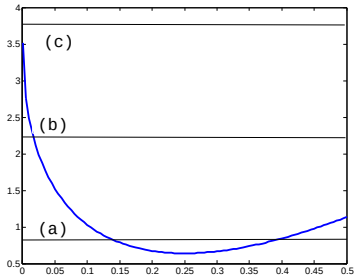

Figure 4.1: The q-profile as a function of the radial flux coordinate $R^2\psi$. If we fix a value of m/n in the range of q, then the resonance site occur at the values of $R^2\psi$ for which $q(R^2\psi) = m/n$. In $(a), (b)$, and (c) there are two, one and zero resonance sites for the corresponding value of m/n.

KAM curves and the unstable fixed points in each set of islands are connected with separatrices, and hence the name hetereoclinic topology.

In (b) the two islands connect if we increase the amplitude of the perturbation. At this threshold the hetereoclinic arcs connecting the unstable fixed points of each set of islands coincide. In this case there are no KAM curves separating the two islands

If we further increase the perturbation amplitude, we obtain the homoclinic topology of the field lines in Figure 4.2 (c). In this case the unstable fixed points have both homoclinic and heteroclinic arcs, that is the separatrices of the unstable fixed points will not always connect to a different unstable fixed point. We see that there are KAM curves separate the islands, but in contrast to Figure 4.2 (a) the curves wrap around the islands.

4.4.1 Heat transport in single mode perturbations

Now we consider heat transport for the different field configurations discussed in Section 4.4. In this section, we will assume that heat is initially concentrated in the center of the cylinder and decreases linearly in the radial flux coordinates , that is we take

$$T_0 = 1 - 2R^2\psi \tag{4.24}$$

Using the Green's function method outlined Section 4.2 we integrated the evolution of the temperature until the steady state is reached. Figure 4.3 shows the asymptotic state of the temperature for two fixed angles $\theta_1 = 2, 14$ and $\theta_2 = 2.96$, that is we compute the steady state temperature for points of the form $(\psi, \theta_i, z = 0)$.

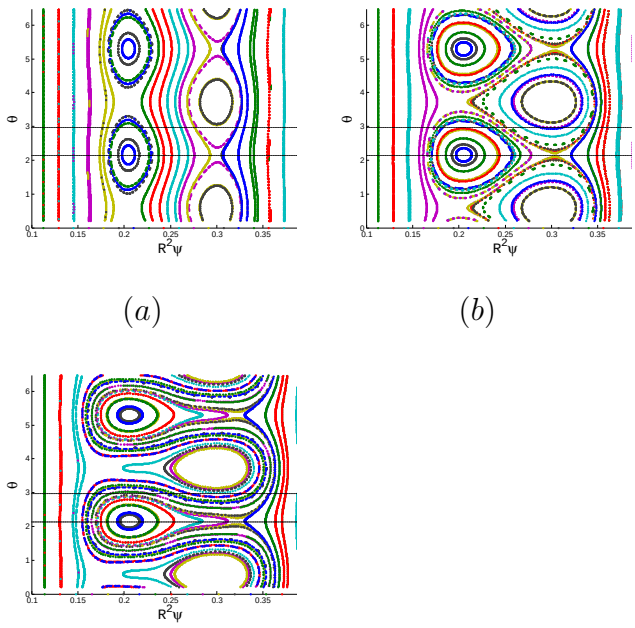

Figure 4.2: Poincarè plots for a single-mode perturbation. The mode was chosen to be $(m, n) = (2, 3)$, which places the resonance near the minimum of the q-profile. The values of ϵ in the plots are (a) $\epsilon = 10^{-4}$, (b) $\epsilon = 3.95 \times 10^{-4}$ and (c) $\epsilon = 9 \times 10^{-4}$, respectively.

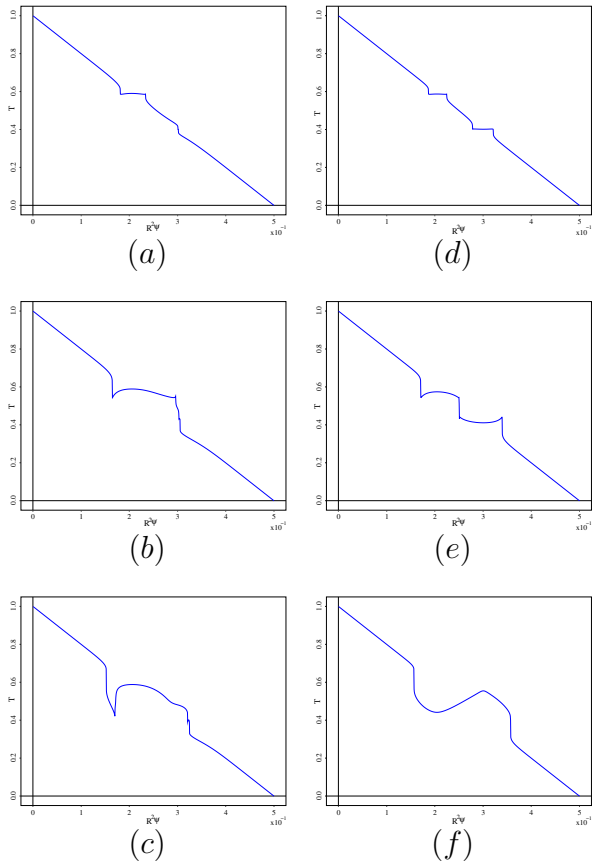

Figure 4.3: Radial temperature profiles with a single-mode perturbation. The initial temperature was chosen to be $T_0 = 1 - 2R^2\psi$. (a) - (c) correspond to taking a cut at $\theta = 2.14$ in the Poincarè plot in Figures 4.2 (a) - (c) , which is the value of θ that cuts through the fixed points. Similarly (d) - (f) correspond to $\theta = 2.96$, which goes in between the two islands.

In Figures 4.3 (a) - (c) correspond to taking a angular cut for $\theta = 2.14$, which cuts through the stable fixed point for the left resonance site of Figure 4.2 (a) and the unstable fixed point on the right resonance site. Figure 4.3 (d) - (f) correspond the magnetic fields depicted in Figures 4.2 (a)-(c), respectively with an angular cut of $\theta = 2.96$. It was noticed that the temperature in the islands homogenizes, which leads to gradients in the asymptotic temperature. Also, we notice a gradient at the unstable fixed points as well.

Similarly in Figures 4.3 (d)-(f) we notice the same phenomena. In this case, we chose $\theta = 2.96$ since that angle cuts through in the middle of both islands. Again we notice gradients in the asymptotic temperature profiles which lead to a certain level of homogenization in the temperature within the islands.

In all the cases in Figure 4.3, it was noticed that the temperature does not completely flatten out in the islands., but has extrema in the center of the islands. There are two factors that explain this: One is that we are considering *parallel* heat transport and hence there is not any sort of local averaging of the temperature among neighboring field lines. Also, because the orbits in an island are somewhat elliptical, the magnetic field lines have a biased temperature corresponding to the shape of the orbits and explains why the extrema lie in the center of the islands.

An especially intriguing feature of Figure 4.3 (f) is that there is the middle region where $0.2 \leq R^2\psi \leq 0.3$ and the temperature profile looks linear, but has a positive gradient while the initial temperature was linear and had a

negative gradient. The reason for this is that based on Figure 4.2 (c) field lines passing near $(R^2\psi, \theta, z) = (0.2, 2.14, 0)$ have a larger average radius than field lines passing near $(R^2\psi, \theta, z) = (0.3, 2.14, 0)$. Thus, the average of the initial temperature for the field lines near $(R^2\psi, \theta, z) = (0.2, 2.14, 0)$ is greater than the than the average of the initial temperature for field lines near $(R^2\psi, \theta, z) = (0.3, 2.14, 0)$.

4.5 Two-mode perturbations

In Section 4.4 we saw that, although intricate, there were no chaotic magnetic field lines. However, if we add another mode, we start to see chaotic regions in the Poincarè plots of the magnetic fields which give rise to different phenomena both at the level of the field lines and the asymptotic temperature states.

In this section we will consider how the effect to adding a $(m, n) = (7, 10)$ mode to the system in each of the three qualitatively distinct magnetic field configurations in Figure 4.2. We also analyze heat flow in each for each configuration.

4.5.1 Chaos in the hetereoclinic topology

In Figure 4.2 (a) we added a $(m, n) = (2, 3)$ mode to an integrable magnetic field with amplitude $\epsilon = 10^{-4}$. Now we add another $(m, n) = (7, 10)$ mode to the magnetic field. We suppose that each of the two modes has the same amplitude, which we vary and obtain qualitatively distinct fields. Figure 4.4 shows the results. For perturbations with small amplitudes we notice the so-called banded chaos phenomena in Figure 4.4 (a). In this case the dominant

mode is the $(7, 10)$ mode and the islands from the $(2, 3)$ have almost disappeared. In between the two chaotic regions are KAM flux surfaces. As the perturbation amplitude is increased the chaotic regions grow and eventually we reach a threshold where there are still two chaotic regions separated by a transport barrier as in Figure 4.4 (b), but for slightly larger values of the perturbation amplitude the transport barrier breaks down as in Figure 4.4. We do not attempt to give a very precise account of when the central transport barrier breaks down as such computations have been done in [23, 66, 15] before.

The results for heat flow corresponding to the Poincarè plot of Figure 4.4 are shown in Figure 4.4 (d) - (f). The overall picture is that the temperature, to some extent, homogenizes in the chaotic regions and within the islands. Moreover, we notice a sharp gradient in the temperature at the threshold as in Figure 4.4 (e). Indeed in Figure 4.4 (d) we notice that the temperature is almost unchanged on the flux surfaces, but the temperature in the two chaotic regions is almost constant, though with small fluctuations. In Figure 4.4 (e) we slightly more intricate phenomena: Since there is no longer a range of flux surfaces in between the chaotic regions, there is a sharp gradient between the two chaotic regions instead of a smooth curve. Also, the influence the islands have on the temperature is more apparent since there are visible flat spots within the chaotic fluctuations, that give rise to other gradients in the temperature profile. The flat spots are larger in this case since the a larger perturbation amplitude corresponds to larger islands. In Figure 4.4 (f) we see that since the transport central transport barrier is broken, there is no longer

a gradient in the temperature profile other than the gradients from the islands and the outer flux surfaces.

Remark: It was interesting to explore the chaotic fluctuations in the temperature profiles in Figure 4.4 that correspond to the chaotic regions in the Poincarè plots. This seems to be a general phenomena and was noticed in all the temperature plots that correspond to magnetic fields with some chaotic regions. One natural question to ask is whether the actual asymptotic temperature profile has these chaotic fluctuations or whether the temperature eventually completely flattens out. A definitive answer to this question is difficult, especially because of the lack of ergodicity of the field lines in the chaotic regions.

We did notice that solving the temperature for longer times for non-chaotic regions did not lead to any difference in the temperature. However, in the chaotic regions the magnetic fields explore a much larger portion of the cylinder, and hence we expect the temperature to take longer to reach its true asymptotic state. In the chaotic regions we noticed that the temperature did not fully settle into a single state for fairly long integration times ($\chi_{\|}t = 10^7$). However, we did notice that if we compute the temperature for different field lines in a given chaotic region, the fluctuations in time for a given field line are similar to the ensemble fluctuations for a fixed time.

4.5.2 Chaos in the homoclinic topology

The last class of two mode perturbations for the magnetic field we consider is to add a mode after the separatrix reconnection has taken place. More

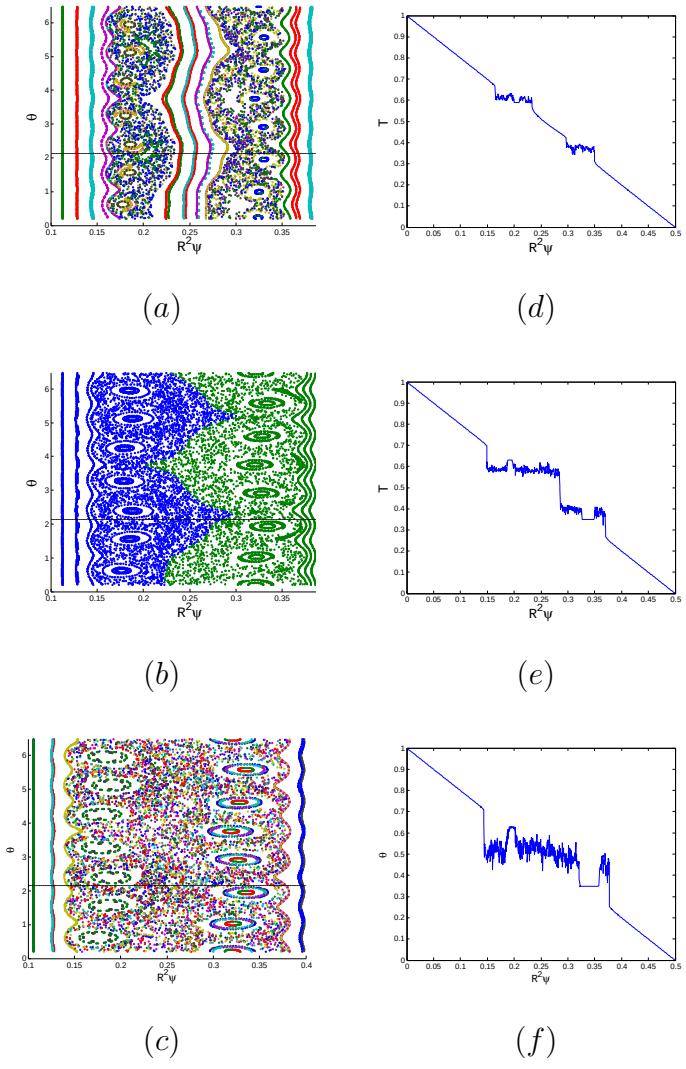

Figure 4.4: Poincarè plots for a two-mode perturbation. The modes was chosen to be $(m, n) = (2, 3), (7, 10)$. The amplitudes, ϵ_{mn}, of the two modes were chosen to be equal. The amplitude is chosen to be (a)$\epsilon = 10^{-4}$, (b) $\epsilon = 3.38 \times 10^{-4}$, and (c) $\epsilon = 5 \times 10^{-4}$, respectively. (d) - (f) are the asymptotic temperature profiles corresponding to (a) - (c)

precisely, we start with the magnetic field in Figure 4.2 (c) and add a $(7, 10)$ mode of varying amplitude.

With small amplitude of the $(7, 10)$ mode small chaotic regions begin to develop near the separatrices of the islands as seen in Figure 4.5 (a). As the amplitude increase the chaotic regions get larger, and eventually a these chaotic regions get close and there is a threshold for when exactly when the chaotic regions meet, yet do not start to mix. The barriers preventing the mixing of the chaotic regions is again due to the existence of the central transport barrier unique to reverse-shear magnetic fields and is shown in Figure 4.5 (b).

4.6 Chaotic magnetic fields and non-local heat transport

We now consider the case of fully chaotic magnetic fields. In this case, we consider 18 different modes (m, n) of equal amplitude, which eliminates as many flux surfaces as possible. Even in this scenario, because we have a non-monotonic q-profile we can still observe a central transport barrier, even though essentially all other flux surfaces have been destroyed. Because of this strong transport barrier that exists amidst an otherwise chaotic magnetic field, this turns out to be a convenient regime to study the existence of leaky barriers. Moreover, as we will see in this section heat flow for chaotic field configurations is also a good way to illustrate the difference between the local and non-local heat flow.

Figure 4.6 shows a magnetic field configuration consisted of adding 18 modes of equal amplitude $\epsilon = 3.75 \times 10^{-4}$. The modes and the amplitudes were

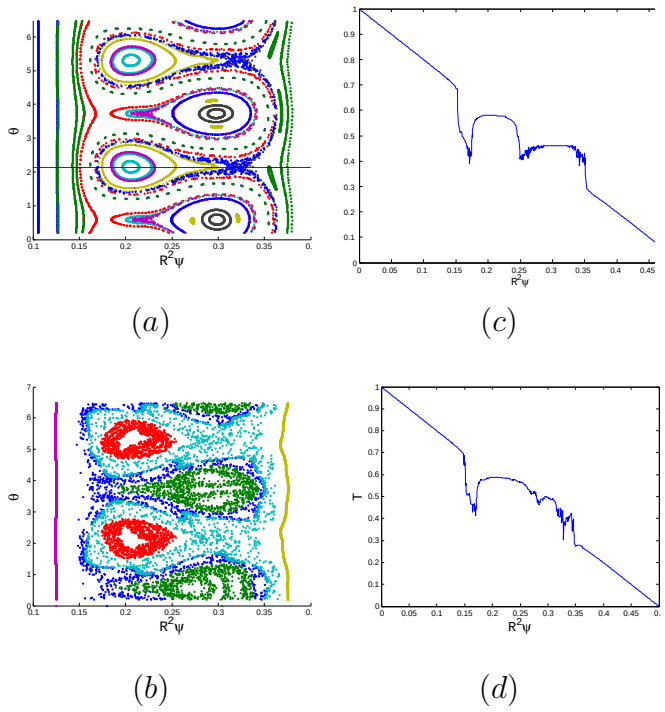

(a) (c)

(b) (d)

Figure 4.5: Poincarè plots obtained by adding a $(7, 10)$ mode to the plot in Figure 4.2. The amplitude of the first mode was fixed to be $\epsilon_1 = 9 \times 10^{-4}$, which is after the separatrix reconnection, while we let the amplitude of the second mode vary from (a) $\epsilon_2 = 5 \times 10^{-6}$ and (b) $\epsilon = 4.3 \times 10^{-5}$. (c) and (d) are the corresponding asymptotic radial temperature profiles.

carefully chosen so that one can have the "two-sided chaos" picture in Figure 4.6, which was obtained by iterating only two initial conditions for a large number of crossings ($100,000$). Although the Poincarè plot looks chaotic, there is still a clear transport barrier located in the middle of the plot.

This transport barrier again leads to gradients in the asymptotic temperature profiles for heat flow along the field lines, as indicated in Figures 4.7 and 4.8. In both cases the initial temperature was the difference of two Gaussians, one peaked on the left chaotic region of 4.6 the other on the right, i.e.

$$T_0 = \exp\left(-\left(\frac{R^2(\psi-\psi_1)}{\sigma}\right)^2\right) - \exp\left(-\left(\frac{R^2(\psi-\psi_2)}{\sigma}\right)^2\right) \tag{4.25}$$

Where $\psi_1 = 0.15$ and $\psi_2 = 0.37$. In Figure 4.7 we considered local heat flow (i.e. $\alpha = 2$) and in Figure 4.8 we considered the non-local heat flow for $\alpha = 1$. We notice that the final asymptotic temperature profiles are identical in the $\alpha = 2$ and $\alpha = 1$ case, but transient behavior is dramatically different and the time it takes to reach the asymptotic steady state is much longer in the local versus the non-local case. This is due to the fact that the Greens function in the local case G_2 exhibits exponential decay, whereas in the non-local case G_1 has algebraic decay. This difference in algebraic/exponential decay means that G_1 sees more of the magnetic field lines for a given fixed time $\chi_{\|}t$ than G_2.

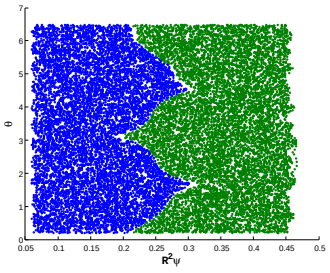

Figure 4.6: Poincarè plot for a chaotic magnetic field. Eighteen different modes were chosen, all of which had amplitude $\epsilon = 3.75 \times 10^{-4}$. Only two initial conditions were chosen for this plot, and it is observed that there is a transport barrier. Adding more initial conditions did not change the structure of the plot.

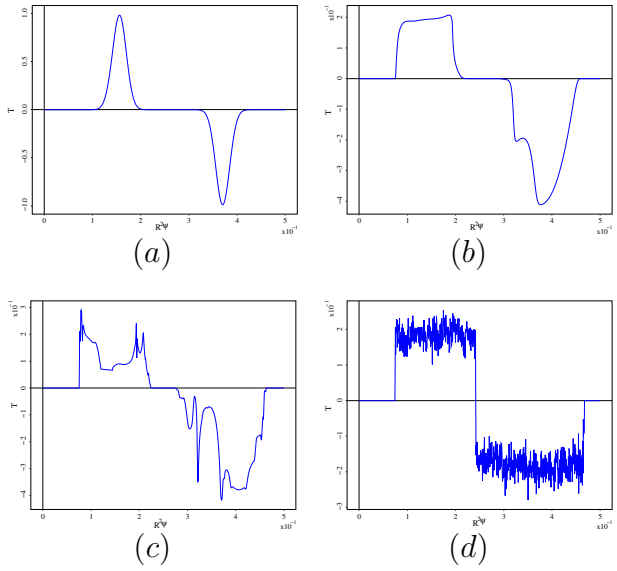

Figure 4.7: We chose an initial temperature profile to be the sum of two Gaussians $T_0 = \exp^{-\left(\frac{\psi-\psi_{01}}{\sigma}\right)^2} - \exp^{-\left(\frac{\psi-\psi_{02}}{\sigma}\right)^2}$, where $\sigma = 0.02$ and ψ_{01}, ψ_{02} are chosen on the left and right side of the barrier in Figure 4.6, respectively. (a)-(d) correspond to temperature profiles using the local model with $\alpha = 2$ with $\chi_{\|}t = 10^{-2}, 10, 10^2, 10^6$, respectively. We choose an angular cut of $\theta = 0$.

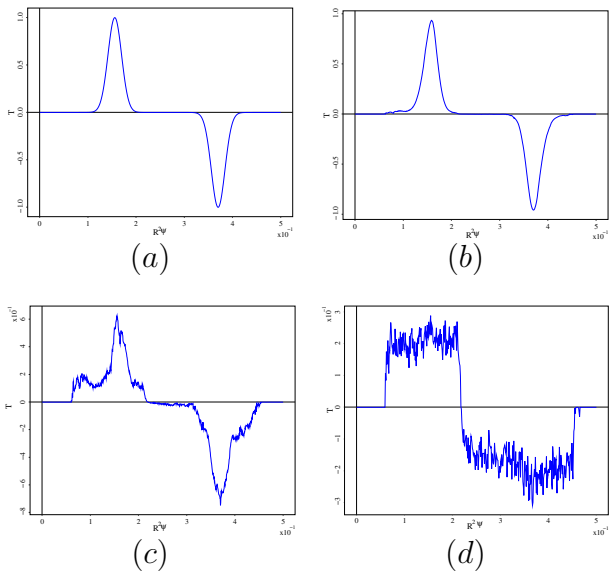

Figure 4.8: The same initial temperature profile as in Figure 4.7 was considered, but the non-local model with $\alpha = 1$ was considered. (a) - (d) correspond to evolution of the profiles at $\chi_{\|}t = 0.01, 1, 10, 150$. $\theta = 0$

4.6.1 Leaky barriers

In this section we will investigate the issue of leaky barriers. It turns out slightly adjusting the perturbation amplitude for the B-field configuration in Figure 4.6 and looking the corresponding heat flow is a convenient way to give computational evidence of leaky barriers. If the amplitude of the perturbation is increased by a small amount ($\Delta\epsilon = 1 \times 10^{-5}$) for the configuration in Figure 4.6 then the transport barrier is broken, though as Figure 4.9 indicates there is still some sort of partial barrier, given by the so-called Cantori. In Figure 4.9 we took a single initial condition for the field line and computed the orbit for the Poincarè map for a different number of crossings. As seen in Figure 4.9 (a) for $2,500$ crossings the field line stays in the left region of the Poincarè plot, though in Figure 4.9 (b) we see that after $3,000$ crossing we notice the filed line starts to move over to the other side of the Poincarè plot. Eventually the Poincarè plot homogenizes a bit as in Figure 4.9 (c). The breaking of the leaky barrier does not appear to be an issue of numerical error since we noticed a strong barrier in Figure 4.6 for $100,000$ crossings and the perturbation amplitude was changed from $\epsilon = 3.75 \times 10^{-4}$ to $\epsilon = 3.85 \times 10^{-4}$.

It was also interesting to see the leakage from the viewpoint of heat flow. A natural way to study this was to consider a Gaussian peaked on the right side of the Poincarè plot. This way, the temperature on the right should remain zero until a field line on the left of the leaky barrier crosses over to the right. Figure 4.9 shows that diffusion of heat across the Cantori does occur, but diffusivity rate is much longer than diffusion away from the Cantori.

To estimate the time of leakage we used Equations (4.10) and (4.11). The Green's function for local heat flow is a Gaussian whose width is given by $\sqrt{4\chi_{\|}t} = 2\sqrt{\chi_{\|}t}$. This gives an estimate on how much arc-length the Green's function computes when computing the temperature at time $\chi_{\|}t$. Also, if N is the number of crossings of a Poincarè plot, then the arc length of the field integrated during those N crossings is given by $2\pi RN$, where $2\pi R = 10\pi$ is the height of the cylinder. Thus, a heuristic relation to relate the number of crossings N to the time $\chi_{\|}t$ of the heat flow is given by $2\sqrt{\chi_{\|}t} = 2\pi RN$, which is to say that

$$\chi_{\|}t \approx (\pi R)^2 N^2 \tag{4.26}$$

Recall that in Figure 4.9 the field line crossed the partial barrier at around $N = 3,000$ crossings. Using Equation (4.26) we estimated that the time needed to see the leakage in the temperature profile is roughly $\chi_{\|}t \approx 25\pi^2 9 \times 10^6 \approx 2.2 \times 10^9$.

The leaky barriers noticed in Figure 4.9 were noticed to be fairly robust, that is, the Cantori were observed to persist for relatively large values of the perturbation amplitude. For instance, if we increase the perturbation amplitude to $\epsilon = 4.1 \times 10^{-4}$ then we still observe a leaky barrier, but the barrier seems to become "more leaky" since it only takes less than 500 crossings for a field line on the left to pierce to the right. This is shown in Figure 4.10 (a) and (b). Plotted in 4.10 (c) and (d) is the evolution of $\langle T \rangle$, the average of T over the z and θ variables. We chose T_0 to be a Gaussian peaked at $\psi = .25$, the center of the barrier. In Figure 4.11 we show the evolution of a linear profile averaged in only the θ variable. In both Figure 4.10 and 4.11 we see

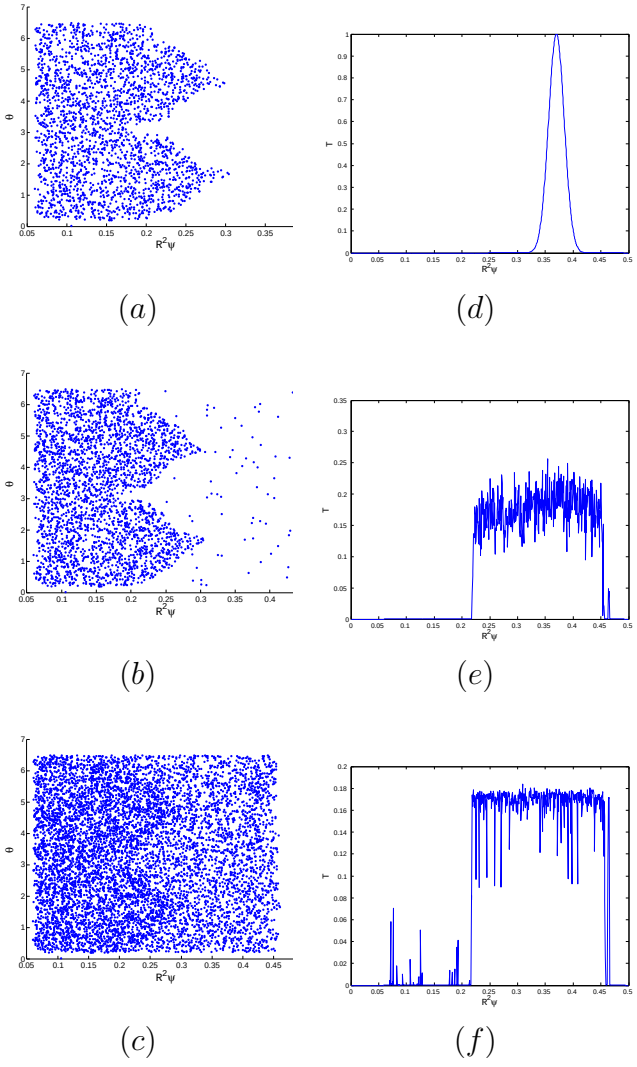

Figure 4.9: Poincarè plots for $(a) - (d)$ a leaky barrier. Here we chose $\epsilon = 3.85 \times 10^{-4}$ and considered a single initial condition for the Poincarè plot. The number of crossings were (a) $2,500$, (b) $3,000$, (c) $7,500$. (d)-(f) are the t-profiles: $\chi_{\|}t = 10^{-2}, 10^{6}, 10^{10}$.

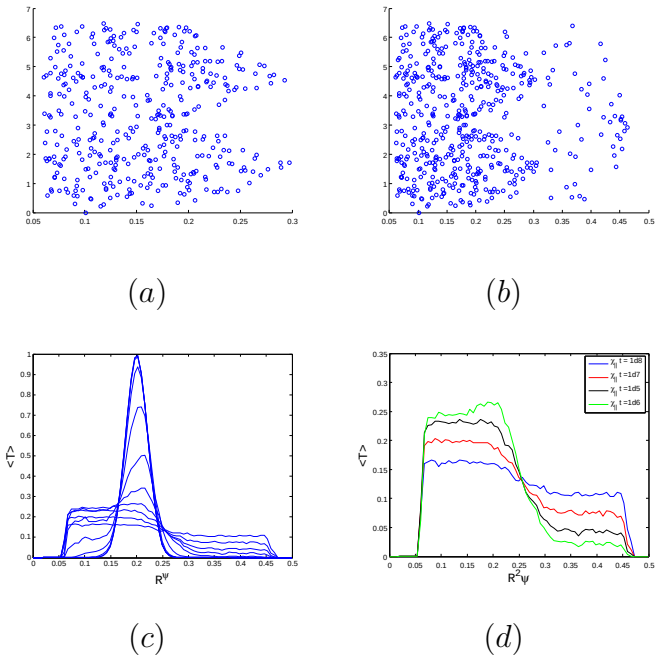

Figure 4.10: Poincarè plots for $(a) - (b)$ a "very leaky" barrier. Here we chose $\epsilon = 4.1 \times 10^{-4}$ and considered a single initial condition for the Poincarè plot. The number of crossings were (a) 400, (b) 500. (c),(d) show the $\langle T \rangle$, the temperature averaged over the z and θ variables for times (c) $\chi_{\|} t = 10^{-2}, \ldots 10^{8}$ and (d) $\chi \parallel t = 10^{5}, \ldots, 10^{8}$.

that diffusion across the partial barriers given the Cantori is much slower than diffusion away from the leaky barrier.

Moreover, we also saw a bifurcation in the concentration of the flux, which is what is shown in Figure 4.12. It is also interesting to see flat spots in the temperature profile in Figure 4.11, yet Figure 4.12 shows regions where the heat flux is nonzero, in violation of the Fourier-Fick law.

This violation of the Fourier-Fick law for the evolution of the averaged temperature $< T >$ is even more pronounced if we take T_0 to be a Gaussian.

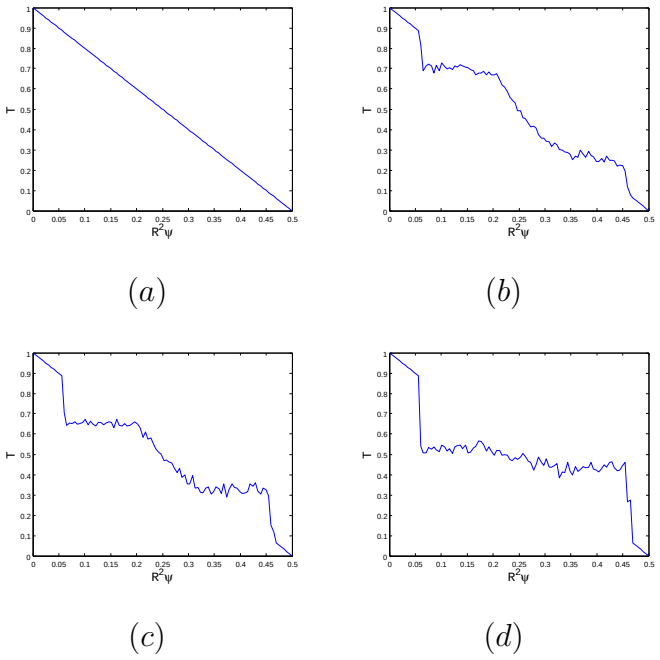

Figure 4.11: The evolution of a linear profile averaged over the θ variable. (a) shows the initial temperature profile, (b), (c) and (d) show the temperature profile at $\chi_{\|}t = 10^4, 10^6, 10^8$, respectively.

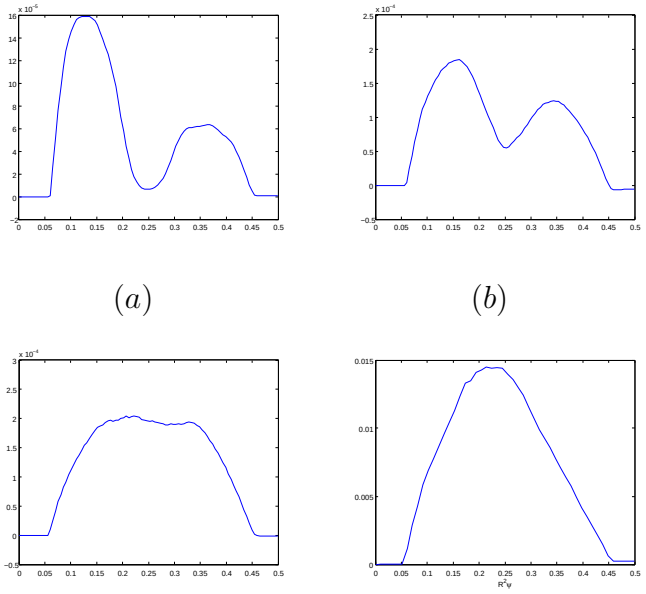

Figure 4.12: This show the flux averaged over time intervals (a) $[10^2, 10^2+10^1]$, (b), $[10^3, 10^3+10^2]$, (c), $[10^3, 10^3+10^2]$ and (d) $[10^6, 10^7]$. We see that there is a bifurcation in the regions where the flux is concentrated

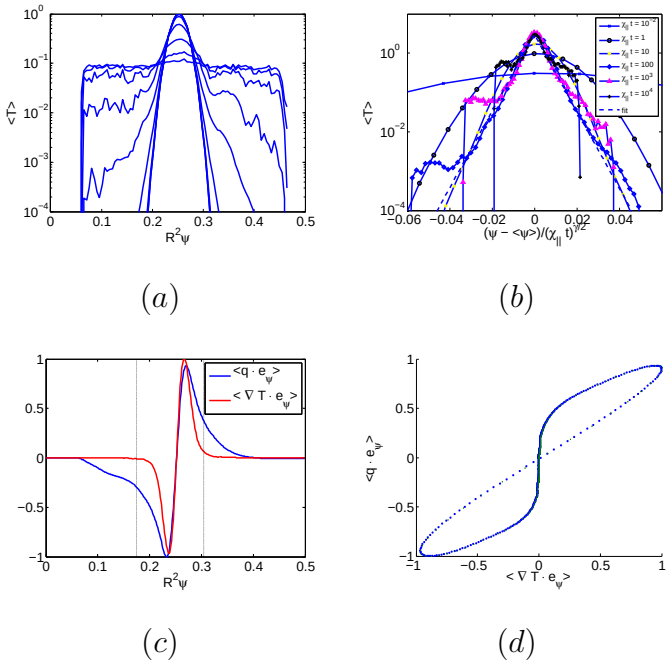

Figure 4.13: This shows (a) the evolution of a Gaussian, (b) the evolution in self-similar coordinates, (c), the computation of the flux and gradient for $\chi_{\|}t = 200$ and (d) the flux-gradient parametric curve

In Figure 4.13 we see the evolution of a Gaussian. The evolution behave self-similarly for some time as indicated in Figure 4.13 (b), which plots the evolution in the self similar sub-diffusive scaling $\gamma = 0.5$. (c) shows the flux and the gradient normalized to their max values at time $\chi_{\|}t = 200$, and shows the flux-gradient parametric curve. In (c) and (d) we clearly see regions of zero gradient and non-zero flux.

Chapter 5

Localized stable manifolds for whiskered tori in coupled map lattices with decaying interaction

5.1 Introduction

In this chapter we study stable manifold theorems in coupled map lattices. We recall that coupled map lattices are copies of a dynamical system at each point in the lattice coupled by some local interaction. They have been extensively studied as models in neuroscience, chemistry and other disciplines.

The goal of this paper is to prove invariant manifold theorems for localized whiskered tori. We recall that whiskered tori are quasi-periodic solutions such that the linearized dynamics around them have exponentially expanding (or contracting) directions. In this paper we refer to quasi-periodic as solutions whose frequency vector is infinite dimensional (Sometimes in the literature they are called almost periodic solutions). See Definition 5.3.1 for a precise definition of a whiskered torus.

We say that the whiskered tori are "localized" when the oscillations are concentrated near a specific collection of sites (which we allow to be finite or infinite) The existence of localized whiskered tori has been proved (under

some hypotheses) for symplectic maps and flows in [33] (e.g. for coupled pendula or Fermi-Pasta-Ulam systems [30], see Example 1). We note, however, that in this paper we do not need the assumption that the dynamics is symplectic. Localized quasi-periodic solutions happen also in coupled dissipative systems with limit cycles. Such localized excitations have been considered in neuroscience ([51, 28]), and our results also apply in this dissipative context.

We prove an invariant manifold theorem for such localized whiskered tori. We show that corresponding to some spectral subspaces in the linearization, once can find smooth manifolds of initial conditions which converge to the quasi-periodic solutions. The invariant manifold theorem we prove includes as particular cases the classical stable and unstable manifold theorems or the strong (un) stable manifolds theorems. We just need some non-resonance conditions in the spectrum. This allows us to make sense of the slow manifold in some cases.

It is also important to remark that the invariant manifolds we construct are essentially localized. That is, the manifold is parameterized by a function W such that

$$\left|\frac{\partial W_i}{\partial x_j}\right| \tag{5.1}$$

decays as the lattice site $i \in \mathbb{Z}^N$ gets further away from the excited sites, or if i is very different from j. See Section 5.2.2 for precise definitions of localized embeddings.

One motivation for this study is that whiskered tori separate asymptotic dynamics. Transverse intersections of stable and unstable manifolds of

whiskered tori were constructed for specific examples in [4] and conjectured to be a generic mechanism proven to be a robust mechanism of transport in phase space and global instability (see, for example, [26] for a review with references to the original literature in recent developments). One can hope that similar effects happen in lattice systems and this paper is a step towards the implementation of the [4] program in coupled map lattices.

In the applied literature there are quite a number of phenomena (e.g. bursting [18], spiking [40], transfer of energy [70, 27]) which indeed are reminiscent of homoclinic chaos in infinite dimensions. We think it would be interesting to clarify mathematically these issues.

5.2 Preliminaries: the phase space and functions with decay

In this section we introduce several technical definitions that follow the setup in [33, 31, 32]. This section can be used a reference. The central idea is to make precise the notion that objects are localized by imposing that the derivatives of a component with respect to a variable are small if the distance between index of the component and the variable is large.

We need two sets of definitions of localized objects: diffeomorphisms and the embeddings giving the parameterization of the invariant manifolds. An important technical notion introduced in [53] is that of a "decay function".

With these technical definitions, we will see that some (but not all) of the techniques from finite dimensional systems generalize to the infinite

dimensional setting of coupled map lattices. Of course, some features have to be significantly different (e.g. coupled map lattices may have uncountably many periodic points which are uniformly hyperbolic, as well as other features that are impossible in finite dimensional systems in a compact manifold).

5.2.1 The phase space

In this section we will define the phase space of the system we will be considering.

The phase space for each lattice site will be $M = \mathbb{T}^l \times \mathbb{R}^{2d-l}$, where $\mathbb{T} = \mathbb{R}/\mathbb{Z}$. This choice of M is done for convenience since $\mathbb{T}$ has straightforward complex extensions and, since we are considering neighborhoods of quasi-periodic solutions, it entails no loss of generality. The full phase space $\mathcal{M}$ for the entire lattice system is a subset of

$$M^{\mathbb{Z}^N} = \prod_{j \in \mathbb{Z}^N} M \tag{5.2}$$

consisting of bounded sequences of points in M. That is,

$$\mathcal{M} = \ell^\infty(\mathbb{Z}^N) = \{x \in M^{\mathbb{Z}^N} : \sup_{i \in \mathbb{Z}^N} |x_i| < \infty\} \tag{5.3}$$

unless $l = 0$ (i.e. unless $M = \mathbb{R}^{2d}$) $\mathcal{M}$ will not be a Banach space, but will be a Banach manifold. Moreover, $\mathcal{M}$ has a natural notion of distance, which is given by

$$d(x, y) = \sup_{i \in \mathbb{Z}^N} d(x_i, y_i) \tag{5.4}$$

Although $\mathcal{M}$ is a manifold, since $\mathbb{T}^l$ is a Euclidean space (i.e. we can identify the tangent space at each point with $\mathbb{R}^l$) the tangent space of $\mathcal{M}$ can be identified with ℓ^∞.

Since we want to consider analytic functions defined on $\mathcal{M}$ it is natural to consider the complexification of $\mathcal{M}$, which is given by

$$\mathcal{M}^{\mathbb{C}} = \{z \in \prod_{j \in \mathbb{Z}^N} M^{\mathbb{C}} : \sup_{i \in \mathbb{Z}^N} |z_i| < \infty\} \tag{5.5}$$

Unless otherwise specified, we will be working with $\mathcal{M}^{\mathbb{C}}$ and omit the superscript $\mathbb{C}$. We use the ℓ^∞ norm to allow for components of the tori to be uniform in size irrespective of the lattice site. Using, for example, the ℓ^2 norm would require that the components of the tori vanish at infinity. The ℓ^∞ norm is also a convenient for the notion of decaying interaction we use in the following sections.

5.2.2 Decay functions and the corresponding functions spaces

We will now discuss suitable notions of decaying interactions, and the appropriate function spaces that are used throughout the paper. As mentioned before, we will assume that the coupling of the lattice sites is localized. To make this notion more precise, we will use the notion of a decay function as done in [53, 31, 32, 33].

Definition 5.2.1. A function $\Gamma : \mathbb{Z}^N \to \mathbb{R}_+$ is a decay function provided that

$$\begin{aligned} &\sum_{j \in \mathbb{Z}^N} \Gamma(j) \leq 1 \\ &\sum_{j \in \mathbb{Z}^N} \Gamma(i-j)\Gamma(j-k) \leq \Gamma(i-k) \ , i, k \in \mathbb{Z}^N \end{aligned} \tag{5.6}$$

Given a decay function Γ we consider several spaces of functions that decay like Γ.

Function spaces for the dynamics

In this section we will discuss the function spaces relevant for the map F that governs the dynamics of the lattice. This is similar to the setup in [33], though we will need to consider analytic functions of infinitely many variables and some notions that we consider were either only mentioned briefly or not considered at all in [33].

In the following section we will consider function spaces for embeddings of tori and their stable and unstable manifolds.

First, we consider the Banach space of decay linear operators that are represented by their matrix elements

$$\mathcal{L}_\Gamma(\ell^\infty(\mathbb{Z}^N)) = \left\{ \begin{array}{c} A \in \mathcal{L}(\ell^\infty(\mathbb{Z}^N)) : \text{ for every } i,j \in \mathbb{Z}^N \exists A_{ij} \in \mathcal{L}(M), \\ (Au)_i = \sum_{j\in\mathbb{Z}^N} A_{ij} u_j, \\ \sup_{i,j\in\mathbb{Z}^N} \Gamma(i-j)^{-1}|A_{ij}| < \infty \end{array} \right\} \tag{5.7}$$

where $\mathcal{L}(\ell^\infty(\mathbb{Z}^N))$ denotes the usual space of continuous linear maps from $\ell^\infty(\mathbb{Z}^N)$ to itself. A norm on $\mathcal{L}_\Gamma(\ell^\infty(\mathbb{Z}^N))$ is given by

$$\|A\|_\Gamma = \sup_{i,j\in\mathbb{Z}^N} \Gamma(i-j)^{-1}|A_{ij}|$$

Remark 5.2.1. As emphasized in [31], not all bounded linear operators from $\ell^\infty(\mathbb{Z}^N)$ can be represented by their matrix elements. For example consider the linear closed subspace $E_0 = \{v \in \ell^\infty(\mathbb{Z}) | \lim_{|j|\to\infty} v_j \text{ exists } \}$ of $\ell^\infty(\mathbb{R})$ and the bounded linear functional $f : E_0 \to \mathbb{Z}$ defined by

$$f(v) = \lim_{|j|\to\infty} v_j \tag{5.8}$$

The linear operator f is bounded, having operator norm equal to 1. By the Hahn-Banach theorem we can extend f to a bounded linear functional L on all of $\ell^\infty(\mathbb{Z})$ which also has norm 1. The matrix elements of L are zero, yet certainly L is a non-zero functional.

□

The space of C^1 functions on a open set $\mathcal{B} \subset \mathcal{M}$ that decay like Γ is

$$C^1_\Gamma(\mathcal{B}) = \left\{ \begin{array}{c} F : \mathcal{B} \to \mathcal{M} : F \in C^1(\mathcal{B}), DF(x) \in C^0(\mathcal{B}, \mathcal{L}_\Gamma(\ell^\infty(\mathbb{Z}^N))) \\ \sup_{x\in\mathcal{B}} \|F(x)\| < \infty, \sup_{x\in\mathcal{B}} \|DF(x)\|_\Gamma < \infty \end{array} \right\} \quad (5.9)$$

The space $C^1_\Gamma(\mathcal{B})$ is a Banach space with the norm

$$\|F\|_{C^1_\Gamma} = \max\left(\sup_{x\in\mathcal{B}} \|F(x)\|, \sup_{x\in\mathcal{B}} \|DF(x)\|_\Gamma\right)$$

Definition 5.2.2. Let $\mathcal{B}$ be an open set of $\mathcal{M}$. We say that $F : \mathcal{B} \to \mathcal{M}$ is analytic if it is in $C^1_\Gamma(U_r)$, where U_r is a complex neighborhood of $\mathcal{B}$.

We will also need to consider the space $\mathcal{L}^k(\ell^\infty(\mathbb{Z}^N))$ of k-multilinear maps that are represented by their matrix elements, that is $B \in \mathcal{L}^k(\ell^\infty(\mathbb{Z}^N))$ if and only if we can write

$$(B(x^1, \ldots, x^n))_i = \sum_{(i_1,\ldots,i_k)\in(\mathbb{Z}^N)^k} B_{i,i_1,\ldots,i_k} x^1_{i_1} \cdots x^k_{i_k} \quad (5.10)$$

where $i, i_1, \ldots, i_k \in \mathbb{Z}^N, (x^1, \ldots, x^k) \in (\ell^\infty(\mathbb{Z}^N))^k$ and $B_{i,i_1,\ldots,i_k} \in \mathcal{L}^k(M, M)$. Given a decay function Γ, we will consider the space $\mathcal{L}^k_\Gamma(\ell^\infty(\mathbb{Z}^N))$ of k-multilinear maps that decay like Γ, that is all maps $B \in \mathcal{L}^k(\ell^\infty(\mathbb{Z}^N))$ such that

$$|B_{i,i_1,\ldots,i_k}| \leq C \min(\Gamma(i - i_1), \ldots, \Gamma(i - i_k)) \quad (5.11)$$

for some $C > 0$. A norm on $\mathcal{L}^k_\Gamma(\ell^\infty(\mathbb{Z}^N))$ is given by

$$\|B\|_\Gamma = \sup_{i,i_1,\ldots,i_k \in \mathbb{Z}^N} |B_{i,i_1,\ldots,i_k}| \max(\Gamma^{-1}(i-i_1),\ldots,\Gamma^{-1}(i-i_k)). \tag{5.12}$$

We will now consider the space $S^k_{\underline{\rho},\Gamma}$ of k-multilinear maps that depend analytically on θ. To this end, we let $\underline{\rho} = \{\rho_n : n \in \mathbb{N}, \rho_n > 0\}$ be a sequence of radii and let $D_{\underline{\rho}} = \{\theta \in (\mathbb{C}^l)^{\mathbb{N}}/(\mathbb{Z}^l)^{\mathbb{N}} : |\operatorname{Im}(\theta_n)| < \rho_n\}$.

We will assume that elements in $S^k_{\underline{\rho},\Gamma}$ have the form

$$M(\theta) = \sum_{n \geq 0} M^{(n)}(\theta_1,\ldots,\theta_n) \tag{5.13}$$

where each $M^{(n)}$ is complex differentiable in the strip D_{ρ_n} and we can define a norm on M by

$$\|M\|_{\underline{\rho},\Gamma} = \sum_{n \geq 0} \|M^{(n)}\|_{\rho_n,\Gamma} \tag{5.14}$$

where

$$\|M^{(n)}\|_{\rho_n,\Gamma} = \sup_{\theta \in D_{\rho_n}} \|M^{(n)}(\theta)\|_\Gamma \tag{5.15}$$

We now define the space $S^k_{\underline{\rho},\Gamma}$ by

$$S^k_{\underline{\rho},\Gamma} = \{M : D_{\underline{\rho}} \to \mathcal{L}^k_\Gamma \ : \ M \in C^1_\Gamma, \|M(\theta)\|_{\underline{\rho},\Gamma} < \infty\} \tag{5.16}$$

$$S^k_{\underline{\rho},\Gamma} := \{M : D_{\underline{\rho}} \to \mathcal{L}^k_\Gamma(\ell^\infty(\mathbb{Z}^N)) \mid M \in C^1_\Gamma, \sup_{\theta \in D_{\underline{\rho}}} \|M(\theta)\|_\Gamma < \infty\} \tag{5.17}$$

And we equip $S^k_{\underline{\rho},\Gamma}$ with the norm

$$\|M\|_{\Gamma,\underline{\rho}} = \sup_{\theta \in D_{\underline{\rho}}} \|M(\theta)\|_\Gamma$$

The following basic lemma will be useful for us later.

Lemma 5.2.1. *(1) If $A, B \in \mathcal{L}_\Gamma(\ell^\infty(\mathbb{Z}^N))$ then $AB \in \mathcal{L}_\Gamma(\ell^\infty(\mathbb{Z}^N))$ and*

$$\|AB\|_\Gamma \leq \|A\|_\Gamma \|B\|_\Gamma$$

(2) More generally, if $A \in \mathcal{L}^k_\Gamma(\ell^\infty(\mathbb{Z}^N))$ and $B_j \in \mathcal{L}^{n_j}_\Gamma(\ell^\infty(\mathbb{Z}^N))$ for $1 \leq j \leq k$. Then the composition $AB_1 \cdots B_k \in \mathcal{L}^{n_1+\cdots+n_k}_\Gamma(\ell^\infty(\mathbb{Z}^N))$ and

$$\|AB_1 \cdots B_k\|_\Gamma \leq \|A\|_\Gamma \|B_1\|_\Gamma \cdots \|B_k\|_\Gamma$$

(3)if $A \in S^k_{\underline{\rho},\Gamma}(\ell^\infty(\mathbb{Z}^N))$ and $B_j \in S^{n_j}_{\underline{\rho},\Gamma}(\ell^\infty(\mathbb{Z}^N))$ for $1 \leq j \leq k$. Then the composition $AB_1 \cdots B_k \in S^{n_1+\cdots+n_k}_{\underline{\rho},\Gamma}(\ell^\infty(\mathbb{Z}^N))$ and

$$\|AB_1 \cdots B_k\|_{\underline{\rho},\Gamma} \leq \|A\|_{\underline{\rho},\Gamma} \|B_1\|_{\underline{\rho},\Gamma} \cdots \|B_k\|_{\underline{\rho},\Gamma}$$

Proof: Parts (1) and (2) have already been proven in [31]. As for part (3), the fact that $AB_1 \cdots B_k(\theta)$ is in $\mathcal{L}^k_\Gamma$ for each θ is a consequence of (2), and analyticity in θ follows from the chain and product rule. Finally the estimate $\|AB_1 \cdots B_k\|_{\underline{\rho},\Gamma} \leq \|A\|_{\underline{\rho},\Gamma} \|B_1\|_{\underline{\rho},\Gamma} \cdots \|B_k\|_{\underline{\rho},\Gamma}$ is also a consequence of (2). □

Function spaces for embeddings of manifolds

In this section we will consider spaces of localized vectors and embeddings of invariant manifolds that are used in the paper. We start by discussing the notion of localized vectors and associated multilinear maps. In [33], they primary work with finite dimensional tori and eventually take limits to obtain infinite dimensional tori. We however, work with infinite dimensional tori from the start and therefore start carefully notions of analytic embedding for infinite dimensional tori and their stable manifolds.

Definition 5.2.3. Given a decay function and a collection of sites $\underline{c} = \{c_k\}_{k\in\mathcal{K}} \subset \mathbb{Z}^N$ we define

$$\|v\|_{\underline{c},\Gamma} = \sup_{i\in\mathbb{Z}^N} \inf_{k\in\mathcal{K}} |v_i|\Gamma^{-1}(i-c_k) \tag{5.18}$$

we denote

$$\ell^\infty_{\underline{c},\Gamma} = \{v \in \ell^\infty(\mathbb{Z}^N) | \|v\|_{\underline{c},\Gamma} \leq \infty\} \tag{5.19}$$

That, is, $\ell^\infty_{\underline{c},\Gamma}$ is the space of vectors localized at the lattice sites $c_k, k \in \mathcal{K}$. Note that $\mathcal{K}$ can be infinite of finite.

We denote by $\mathcal{L}_{\underline{c},\Gamma}$ to be the space of linear operators on $\ell^\infty_{\underline{c},\Gamma}$ such that

$$\begin{aligned} (Av)_i &= \sum_{j\in\mathbb{Z}^N} A_{ij}v_j \\ |A_{ij}| &\leq C \min(\sup_{k\in\mathcal{K}} \Gamma(i-c_k), \Gamma(i-j)) \end{aligned} \tag{5.20}$$

We denote by $\|A\|_{\underline{c},\Gamma}$ the best constant C above, i.e.

$$\|A\|_{\underline{c},\Gamma} = \max(\sup_{i,j\in\mathbb{Z}^N} |A_{ij}|\Gamma^{-1}(i-j), \sup_{i,j\in\mathbb{Z}^N} \inf_{k\in\mathcal{K}} |A_{ij}|\Gamma^{-1}(i-c_k)) \tag{5.21}$$

Finally, we denote by $\mathcal{L}^k_{\underline{c},\Gamma}$ the space of k-multilinear operators B on $\ell^\infty_{\underline{c},\Gamma}$ such that

$$|B_{i,i_1,\ldots,i_k}| \leq C \min(\sup_{k\in\mathcal{K}} \Gamma(i-c_k), \Gamma(i-i_1), \ldots, \Gamma(i-i_k)) \tag{5.22}$$

for some $C > 0$. A norm on $\mathcal{L}^k_{\underline{c},\Gamma}(\ell^\infty(\mathbb{Z}^N))$ is given by the best constant C above, that is,

$$\|B\|_{\underline{c},\Gamma} = \sup_{i,i_1,\ldots,i_k\in\mathbb{Z}^N} |B_{i,i_1,\ldots,i_k}| \max(\Gamma^{-1}(i-i_1), \ldots, \Gamma^{-1}(i-i_k), \inf_{k\in\mathcal{K}} \Gamma^{-1}(i-c_k)) \tag{5.23}$$

In similar spirit to the space $S^k_{\underline{\rho},\Gamma}$ will consider the space $S^k_{\underline{\rho},\underline{c},\Gamma}$ of "localized" multilinear maps parameterized by θ in $D_{\underline{\rho}}$. Recall that from Section 5.2.2 $D_{\underline{\rho}} = \{\theta \in (\mathbb{C}^l)^{\mathbb{N}}/(\mathbb{Z}^l)^{\mathbb{N}} : |\operatorname{Im}(\theta_n)| < \rho_n\}$ where $\underline{\rho} = \{\rho_n : n \in \mathbb{N}, \rho_n > 0\}$ is a sequence of radii. The elements $M(\theta)$ in the space $S^k_{\underline{\rho},\underline{c},\Gamma}$ are multilinear maps on the space of localized vectors $\ell^\infty_{\underline{c},\Gamma}$ that depend analytically by $\theta \in D_{\underline{\rho}}$, which we assume to take the form

$$M(\theta) = \sum_{n\geq 0} M^{(n)}(\theta_1, \ldots, \theta_n) \tag{5.24}$$

We will assume that each $M^{(n)}$ is complex differentiable in the strip D_{ρ_n} and we can define a norm on M by

$$\|M\|_{\underline{\rho},\underline{c},\Gamma} = \sum_{n\geq 0} \|M^{(n)}\|_{\rho_n,\underline{c},\Gamma} \tag{5.25}$$

where

$$\|M^{(n)}\|_{\rho_n,\underline{c},\Gamma} = \sup_{\theta\in D_{\rho_n}} \|M^{(n)}(\theta)\|_{\underline{c},\Gamma} \tag{5.26}$$

We now define the space $S^k_{\underline{\rho},\underline{c},\Gamma}$ by

$$S^k_{\underline{\rho},\underline{c},\Gamma} = \{M : D_{\underline{\rho}} \to \mathcal{L}^k_{\underline{c},\Gamma} \ : \ M \in C^1_\Gamma, \|M(\theta)\|_{\underline{\rho},\underline{c},\Gamma} < \infty\} \tag{5.27}$$

In similar spirit to Lemma 5.2.1, we have the following result for compositions of multilinear functions acting on the space of localized vectors.

Lemma 5.2.2. *(1) If $A, B \in \mathcal{L}_{\underline{c},\Gamma}(\ell^\infty(\mathbb{Z}^N))$ then $AB \in \mathcal{L}_{\underline{c},\Gamma}(\ell^\infty(\mathbb{Z}^N))$ and*

$$\|AB\|_{\underline{c},\Gamma} \leq \|A\|_{\underline{c},\Gamma}\|B\|_{\underline{c},\Gamma}$$

(2) More generally, if $A \in \mathcal{L}^k_{\underline{c},\Gamma}(\ell^\infty(\mathbb{Z}^N))$ and $B_j \in \mathcal{L}^{n_j}_{\underline{c},\Gamma}(\ell^\infty(\mathbb{Z}^N))$ for $1 \leq j \leq k$. Then the composition $AB_1\cdots B_k \in \mathcal{L}^{n_1+\cdots+n_k}_{\underline{c},\Gamma}(\ell^\infty(\mathbb{Z}^N))$ and

$$\|AB_1\cdots B_k\|_{\underline{c},\Gamma} \leq \|A\|_{\underline{c},\Gamma}\|B_1\|_{\underline{c},\Gamma}\cdots\|B_k\|_{\underline{c},\Gamma}$$

(3)if $A \in S^k_{\underline{\rho},\underline{c},\Gamma}(\ell^\infty(\mathbb{Z}^N))$ *and* $B_j \in S^{n_j}_{\underline{\rho},\underline{c},\Gamma}(\ell^\infty(\mathbb{Z}^N))$ *for* $1 \le j \le k$. *Then the composition* $AB_1 \cdots B_k \in S^{n_1+\cdots+n_k}_{\underline{\rho},\underline{c},\Gamma}(\ell^\infty(\mathbb{Z}^N))$ *and*

$$\|AB_1 \cdots B_k\|_{\underline{\rho},\underline{c},\Gamma} \le \|A\|_{\underline{\rho},\underline{c},\Gamma}\|B_1\|_{\underline{\rho},\underline{c},\Gamma} \cdots \|B_k\|_{\underline{\rho},\underline{c}\Gamma}$$

□

Now we consider the space of analytic embeddings $K : D_{\underline{\rho}} \to \mathcal{M}$ and $W : D_{\underline{\rho}_1} \times U_{\rho_2} \to \mathcal{M}$ that are localized near infinitely many lattice sites. The reader should think of the function K as giving the parameterization of the torus, and W as giving the parameterization of its stable manifold. We will assume that each component $(K)_i$ of K takes the form

$$(K)_i(\theta) = \sum_{n \ge 0} (K^{(n)})_i(\theta_1, \ldots, \theta_n) \tag{5.28}$$

where $(K^{(n)})_i$ is a finite dimensional analytic function and we give a norm to $(K)_i$ by

$$\|(K)_i\|_{\underline{\rho}} = \sum_{n \ge 0} \|(K^{(n)})_i\|_{\rho_n} \tag{5.29}$$

$$\|K\|_{\underline{\rho},\underline{c},\Gamma} = \sup_{i \in \mathbb{Z}^N} \min_{k \in \mathcal{K}} \Gamma^{-1}(i - c_k)\|K_i\|_{\underline{\rho}} \tag{5.30}$$

We now come to the definition of the space of analytic localized embeddings of a torus, namely the space

$$\mathcal{A}_{\underline{\rho},\underline{c},\Gamma}((\mathbb{T}^l)^{\mathbb{N}}) = \{K : D_{\underline{\rho}} \to \mathcal{M} \mid K \text{ is analytic in } D_\rho, K \in C^0(\overline{D_\rho}),\ \|K\|_{\underline{\rho},c,\Gamma} < \infty\} \tag{5.31}$$

Similarly for embedding W of the stable manifold, we will assume we have expressions

$$(W)_i(\theta, s) = \sum_{n,m \ge 0} (W^{(n,m)})_i(\theta_1, \ldots, \theta_n, s_1, \ldots, s_m) \tag{5.32}$$

where $(W^{(n,m)})_i$ is analytic and we we give it the sup norm

$$\|(W)_i\|_{\underline{\rho}_1,\rho_2} = \sum_{n,m\geq 0} \|(W^{(n,m)})_i\|_{\rho_{1_n},\rho_2} \tag{5.33}$$

We define a norm on W as

$$\|W\|_{\underline{\rho}_1,\rho_2,\underline{c},\Gamma} = \sup_{i\in\mathbb{Z}^d} \min_{k\in\mathcal{K}} \Gamma^{-1}(i-c_k)\|W_i\|_{\underline{\rho}_1,\rho_2} \tag{5.34}$$

The space of analytic localized embeddings of the product of a torus and a ball in ℓ^∞ is the space

$$\begin{aligned}&\mathcal{A}_{\underline{\rho}_1,\rho_2,\underline{c},\Gamma}((\mathbb{T}^l)^{\mathbb{N}}\times B_{\rho_2})\\ &= \left\{W : D_{\underline{\rho}_1}\times B_{\rho_2}\to\mathcal{M} \mid \begin{array}{c} W \text{ is analytic in } D_{\underline{\rho}_1}\times B_{\rho_2},\\ W\in C^0(\overline{D_{\underline{\rho}_1}\times B_{\rho_2}}) \text{ and } \|W\|_{\underline{\rho}_1,\rho_2,c,\Gamma}<\infty\end{array}\right\}\end{aligned} \tag{5.35}$$

Remark 5.2.2. For the embeddings of the tori K we can assume nonuniform radius ρ for the domain of analyticity of $K_i^{(n)}$. The methods of this paper allow us to prove that we can choose an embedding of the stable manifold which has an expansion as in (5.32) for which the domain of analyticity in the s variable is uniform among $W^{(n)}$, which is why are definitions of the embeddings W have a uniform domain in s.

□

Finally we give the definition of a whiskered embedding of a torus that is localized near infinitely many lattice sites $c_n, n\in\mathbb{N}$ and decays like Γ. Definition 5.3.1 is based on the growth and decay rates of $F\circ DK(\theta)$, where K is the embedding of the torus. This is a generalization of the notion of a whiskered embedding in [33]. In Section 5.2.2, we provide an equivalent

notion of hyperbolicity based on the spectral properties of operators associated to DK.

Definition 5.2.4. (**Growth and decay rate formulation of hyperbolicity**) Let $\underline{\rho} = \{\rho_n \mid n, \rho_n \geq 0\}$ be a sequence of radii, $\omega \in \mathbb{R}^\infty$ a frequency vector, $\underline{c} = \{c_n \in \mathbb{Z}^n \mid n \geq 0\}$ a collection of lattice sites, Γ a decay function and a map $F : \mathcal{M} \to \mathcal{M} \in C^2_\Gamma$. We say that $K : D_{\underline{\rho}} \to \mathcal{M} \in \mathcal{A}_{\underline{\rho},\underline{c},\Gamma}$ is a whiskered embedding for F when we have:

1) The tangent space has an invariant splitting

$$T_{K(\theta)}\mathcal{M} = \mathcal{E}^s_{K(\theta)} \oplus \mathcal{E}^c_{K(\theta)} \oplus \mathcal{E}^u_{K(\theta)} \tag{5.36}$$

where $\mathcal{E}^{s,c,u}_{K(\theta)}$ satisfy $DF(K(\theta))\mathcal{E}^{s,c,u}_\theta = \mathcal{E}^{s,c,u}_{\theta+\omega}$

2) The projections $\Pi^{s,c,u}_{K(\theta)}$ associated to this splitting are in $S^1_{\underline{\rho},\underline{c},\Gamma}$.

3) The splitting (5.75) is characterized by asymptotic growth conditions: there are $0 < \mu_1, \mu_2 < 1, \mu_3 > 1$ such that $\mu_1\mu_3 < 1$, $\mu_2\mu_3 < 1$ and $C_h > 0$ such that for all $n \geq 1$ $\theta \in D_{\underline{\rho}}$

$$\|DF \circ K \circ T_\omega^{n-1} \times \cdots \times DF \circ Kv\|_{\underline{\rho},\underline{c},\Gamma} \leq C_h\mu_1^n\|v\|_{\underline{\rho},\underline{c},\Gamma} \iff v \in \mathcal{E}^s_{K(\theta)}. \tag{5.37}$$

and

$$\|DF^{-1} \circ K \circ T_\omega^{n-1} \times \cdots \times DF^{-1} \circ Kv\|_{\underline{\rho},\underline{c},\Gamma} \leq C_h\mu_2^n\|v\|_{\underline{\rho},\underline{c},\Gamma} \iff v \in \mathcal{E}^u_{K(\theta)}. \tag{5.38}$$

The center subspace is characterized by:

$$\|DF \circ K \circ T_\omega^{n-1} \times \cdots \times DF \circ Kv\|_{\underline{\rho},\underline{c},\Gamma} \leq C_h \mu_3^n \|v\|_{\underline{\rho},\underline{c},\Gamma}$$

$$\|DF^{-1} \circ K \circ T_\omega^{n-1} \times \cdots \times DF^{-1} \circ Kv\|_{\underline{\rho},\underline{c},\Gamma} \leq C_h \mu_3^n \|v\|_{\underline{\rho},\underline{c},\Gamma} \tag{5.39}$$

$$\iff v \in \mathcal{E}^c_{K(\theta)}$$

Remark 5.2.3. The notion of a whiskered torus that is considered in the paper is slightly more general that the one considered in [33]. Even if the torus is finite, we can allow for $\mathcal{E}^c_{K(\theta)}$ to be infinite, which is not done in [33]. Also, we work directly with infinite dimensional tori, whereas in [33] infinite dimensional tori are obtained by taking limits of tori of increasing dimension. However, the proofs of the results in this paper do not require that the map F is symplectic and hence it is natural to consider a more general notion of a whiskered torus.

However, Definition 5.3.1 does have the same flavor as the whiskered tori as constructed in [33] in the sense that the conditions for a torus to be whiskered are on growth and decay rates. The proof we give suggests to consider a more general notion for a torus to be whiskered based on spectral assumptions, which is done in Section 5.2.2

□

Spectral formulation of hyperbolicity

In this section we describe a more general notion of hyperbolicity than described in Definition 5.3.1 based on spectral properties of operators associated to DK. One can weaken the hypothesis that K is a whiskered embedding by considering the more general notion of non-resonant subspaces, similar to what is done in [16].

To this end, let $A, B : (\mathbb{T}^l)^{\mathbb{N}} \times \to \ell^\infty_{\underline{c},\Gamma}$ be in $S^1_{\underline{\rho},\underline{c},\Gamma}$ and consider the operators $\mathcal{L}^\omega_B$, $\mathcal{R}^k_A$ acting on the space $S^k_{\underline{\rho},\underline{c},\Gamma}$ that are defined by

$$\begin{aligned}(\mathcal{L}^\omega_B M)(\theta)(x_1,\ldots,x_k) &= B(\theta-\omega)M(\theta-\omega)(x_1,\ldots,x_k)\\ (\mathcal{R}^{k,\omega}_A M)(\theta)(x_,\ldots,x_k) &= M(\theta)(x_1,\ldots,A(\theta-\omega)x_k,\ldots,x_k)\end{aligned} \tag{5.40}$$

Instead of assuming that K is a whiskered embedding in the sense of Definition 5.3.1, one can replace condition 3) in Definition 5.3.1 by assuming

3*) $\mathrm{Spec}(\mathcal{L}_{A^c}) \subset \{\mu^{-1} \leq |z| \leq \mu_3\}$

$\mathrm{Spec}(\mathcal{L}_{A^s}) \subset \{0 \leq |z| \leq \mu_1\}$

$\mathrm{Spec}(\mathcal{L}_{A^u}) \subset \{0 \leq |z| \leq \mu_2^{-1}\}$

That the spectral formulation 3$*$) is equivalent to the asymptotic rate formulation in Definition 5.3.1 follows from the Spectral Radius Theorem, which states that

$$\lim_{n\to\infty} \|A^n\|^{1/n} = \rho(A) \tag{5.41}$$

where A is a bounded linear operator on a Banach space and $\rho(A)$ is the spectral radius of A. Indeed, from Equation (5.41) it follows that, for every $\epsilon > 0$

$$\|A^n v\| \leq C_\epsilon(\rho(A)+\epsilon)^n \|v\| \tag{5.42}$$

Applying Equation (5.42) to the operators $\mathcal{L}_{A^{s,c,u}}$ shows that the 3*) is equivalent to condition 3 of Definition 5.3.1.

5.2.3 Other spaces of functions used in the paper

In this section we define spaces of C^r embeddings that have decay, and those which are also localized. These spaces are used in the fixed point arguments in Sections 5.4.1 and 5.4.2.

We define the space $C^r_\Gamma(D_{\underline{\rho}_1} \times B_{\rho_2})$ as

$$C^r_\Gamma(D_{\underline{\rho}_1} \times B_{\rho_2}) = C^r_{\Gamma,\underline{\rho}_1,\rho_2}$$
$$= \{f : D_{\underline{\rho}_1} \times B_{\rho_2} \to \ell^\infty(\mathbb{Z}^N) \mid D^i f \in C^0(D_{\underline{\rho}_1} \times B_{\rho_2}, \mathcal{L}^i_\Gamma(\ell^\infty(\mathbb{Z}^N)), i = 1, \dots, r\} \tag{5.43}$$

A norm on $C^r_\Gamma(D_{\underline{\rho}_1} \times B_{\rho_2})$ is given by

$$\|f\|_{C^r_{\underline{\rho}_1,\rho_2,\Gamma}} := \max_{i=1,\dots,r} \sup_{(\theta,s)\in D_{\underline{\rho}_1}\times B_{\rho_2}} \|D^i f\|_{C^0_{\underline{\rho}_1,\rho_2,\Gamma}}$$

where we view $D^k f$ to be a map from $D_{\underline{\rho}_1} \times B_{\rho_2}$ to $\mathcal{L}^k_\Gamma(\ell^\infty(\mathbb{Z}^N))$

We define the space $C^r_{\underline{\rho}_1,\rho_2,\underline{c},\Gamma}$ by

$$C^r_{\underline{c},\Gamma}(D_{\underline{\rho}_1} \times B_{\rho_2}) = C^r_{\underline{\rho}_1,\rho_2,\underline{c},\Gamma}$$
$$= \{f : D_{\underline{\rho}_1} \times B_{\rho_2} \to \ell^\infty_{\underline{c},\Gamma}(\mathbb{Z}^N) \mid D^i f \in C^0(D_{\underline{\rho}_1} \times B_{\rho_2}, \mathcal{L}^i_{\underline{c},\Gamma}(\ell^\infty(\mathbb{Z}^N)), i = 1, \dots, r\} \tag{5.44}$$

A norm on $C^r_{\underline{c},\Gamma}(D_{\underline{\rho}_1} \times B_{\rho_2})$ is given by

$$\|f\|_{C^r_{\underline{\rho}_1,\rho_2,\underline{c},\Gamma}} := \max_{i=1,\dots,r} \sup_{(\theta,s)\in D_{\underline{\rho}_1}\times B_{\rho_2}} \|D^i f\|_{C^0_{\underline{\rho}_1,\rho_2,\underline{c},\Gamma}}$$

where we view $D^k f$ a map from $D_{\underline{\rho}_1} \times B_{\rho_2}$ to $\mathcal{L}^k_{\underline{c},\Gamma}(\ell^\infty(\mathbb{Z}^N))$.

The following proposition concerning the composition of functions in $C^r_{\underline{\rho}_1,\rho_2,\underline{c},\Gamma}$ will be used later. The statement and proof is similar to Proposition 2.17 in [31], though with slightly different function spaces.

Proposition 5.2.3. *If $F, G \in C^r_{\underline{\rho}_1,\rho_2,\underline{c},\Gamma}$ and $F(D_{\underline{\rho}_1} \times U_{\rho_2}) \subset D_{\underline{\rho}_1} \times U_{\rho_2}$, then $G \circ F \in C^r_{\underline{\rho}_1,\rho_2,\underline{c},\Gamma}$ and*

$$\|G \circ F\|_{C^r_{\underline{\rho}_1,\rho_2,\underline{c},\Gamma}} \le C_r(1 + \|F\|^r_{C^r_{\underline{\rho}_1,\rho_2,\underline{c},\Gamma}})\|G\|_{C^r_{\underline{\rho}_1,\rho_2,\underline{c},\Gamma}} \tag{5.45}$$

The proof follows from the Faa-di-Bruno formula and Lemma 5.2.2. □

5.3 Statement of results

We state two versions of the stable manifold theorem for localized whiskered tori, one with assumptions on growth and decay rates, and another version based on the spectral formulation of hyperbolicity and non-resonance conditions.

In [33] it was shown that given an approximate whiskered embedding, a true one exists nearby. In [33], their notion of a whiskered torus is similar to Definition 5.3.1, and hence it is desirable to state a theorem that applies directly to the tori constructed in [33]. This is the content of Theorem 5.3.1.

We then state a more general version of the theorem using the spectral formulation of hyperbolicity as done in Section 5.2.2. This is the version of the stable manifold theorem we will prove.

The proof we give follows the ideas in [16], where a proof of the stable manifold is given for fixed points and normally hyperbolic invariant manifolds in the context of general Banach spaces. Note that, by definition, a whiskered torus is not normally hyperbolic. Indeed, there are neutral directions not tangent to the torus (c.f. Definition 5.3.1).

First, we will consider a map $F : \mathcal{M} \to \mathcal{M}$ that has a whiskered embedding of a torus K and prove that it has a stable and unstable manifold, written $W^s(K((\mathbb{T}^l)^{\mathcal{K}}))$ and $W^u(K((\mathbb{T}^l)^{\mathcal{K}}))$, respectively. The stable manifold of $K((\mathbb{T}^l)^{\mathcal{K}})$ is characterized by the following: for each $\theta \in (\mathbb{T}^l)^{\mathcal{K}}$ there is a

manifold

$$\begin{aligned} W^s_{K(\theta)} &= \{x \in \mathcal{M} \mid d(F^n(x), F^n(K(\theta + n\omega))) \leq C_{x,\theta}\mu_1^n, n \geq 0\} \\ W^u_{K(\theta)} &= \{x \in \mathcal{M} \mid d(F^n(x), F^n(K(\theta + n\omega))) \leq C_{x,\theta}\mu_1^n, n \leq 0\} \end{aligned} \tag{5.46}$$

and then $W^{s,u}(K(\mathbb{T}^d))$ are given by

$$\begin{aligned} W^s((\mathbb{T}^l)^{\mathbb{N}}) &= \bigcup_{\theta \in (\mathbb{T}^l)^{\mathcal{K}}} W^s_{K(\theta)} \\ W^u((\mathbb{T}^l)^{\mathbb{N}}) &= \bigcup_{\theta \in (\mathbb{T}^l)^{\mathcal{K}}} W^u_{K(\theta)} \end{aligned} \tag{5.47}$$

$W^s_{K(\theta)}$ and $W^u_{K(\theta)}$ are called the stable and unstable fibers of the stable and unstable manifold.

We will prove that there is a parameterization

$$W(\theta, s) : D_{\underline{\rho}} \times (B_{\rho_2} \subset \ell^\infty_{\underline{c},\Gamma}) \to \ell^\infty_{\underline{c},\Gamma}$$

of the local stable manifold, where by local we mean in a neighborhood of the origin in the s variable. We will construct W by solving the functional equation

$$F(W(\theta, s)) = W(\theta + \omega, P(\theta + \omega, s)) \tag{5.48}$$

where P is a polynomial in s that describes what the dynamics are in the stable direction. The following result is a theorem for discrete maps of the lattice to itself. In Section 5.3.2 we show how to extend Theorem 5.3.1 in the case of whiskered tori for flows on lattices.

Theorem 5.3.1. *Let $F : \mathcal{M} \to \mathcal{M}$ be a map belonging to $C^r_\Gamma(\mathcal{B})$ for any ball $\mathcal{B} \subset \mathcal{M}$ and some decay function Γ and let $K : D_{\underline{\rho}_1} \to \mathcal{M} \in \mathcal{A}_{\underline{\rho}_1,\underline{c},\Gamma}((\mathbb{T}^l)^{\mathbb{N}})$ be an analytic whiskered embedding for F. Suppose that F has a complex analytic*

extension in a neighborhood of the torus $K((\mathbb{T}^l)^{\mathbb{N}})$*, i.e. there exists* ρ_2 *such that* F *is analytic on*

$$\{z \in \mathcal{M} \mid |z - K(\theta)| \leq \rho_2 \text{ for some } \theta \text{ with } \mid Im\ (\theta_n)| < \rho_{1,n} \text{ for all } n\} \quad (5.49)$$

Define $A(\theta) := DF(K(\theta))$ *and the operators* $A^{c,s,u}(\theta)$*, all of which act on the space of localized vectors* $\ell^\infty_{\underline{c},\Gamma}$*, by*

$$A^{c,s,u}(\theta) := \Pi^{c,s,u}_{K(\theta+\omega)} DF(K(\theta))|_{\mathcal{E}^{c,s,u}_{K(\theta)}} \quad (5.50)$$

Since the embedding is whiskered, we know that for some integer L*,*

$$\|A^s\|^{L+1}_{\underline{\rho}_1,\underline{c},\Gamma} \|A^{-1}\|_{\underline{\rho}_1,\underline{c},\Gamma} < 1 \quad (5.51)$$

We will assume that:

$A(\theta)$ *is invertible for any* $\theta \in D_{\underline{\rho}_1}$

Under these assumptions, we can find analytic maps $P, W : D_{\underline{\rho}_1} \times (B_{\rho_2} \subset \ell^\infty_{\underline{c},\Gamma}(\mathbb{Z}^d)) \to \ell^\infty_{\underline{c},\Gamma}(\mathbb{Z}^d)$ *where* B_{ρ_2} *is a neighborhood of the origin,* P *is a polynomial in* s*,* $W, P \in \mathcal{A}_{\underline{\rho}_1,\rho_2,\underline{c},\Gamma}(D_{\underline{\rho}_1} \times B_{\rho_2})$

$$F(W(\theta, s)) = W(\theta + \omega, P(\theta + \omega, s)) \quad (5.52)$$

holds in $D_{\underline{\rho}_1} \times B_{\rho_2}$ *and*

$$W(\theta, 0) = K(\theta) \quad (5.53)$$

$$P(\theta, 0) = 0 \quad DP(\theta, 0) = A^s(\theta - \omega) \quad (5.54)$$

Finally, the stable fiber $W^s_{K(\theta)} := W(\{\theta\} \times B_{\rho_2})$ *is the unique analytic invariant manifold that is tangent to the linear subspace* $\mathcal{E}^s_{K(\theta)}$ *and as a consequence of Equation 5.48 the stable fibers satisfy the invariance property that*

$$F(W^s_{K(\theta)}) = W^s_{K(\theta+\omega)} \tag{5.55}$$

Example 1. The main example we have in mind are Hamiltonian systems with infinite degrees of freedom where the interaction amont the sites decays. More specifically, consider the Hamiltonian

$$H(q,p) = \sum_{n\in\mathbb{Z}^N} \left(\frac{1}{2} p_n^2 + W(q_n) \right) + \sum_{j\in\mathbb{Z}^N} \sum_{n\in\mathbb{Z}^N} V_j(q_n - q_{n+j}) \tag{5.56}$$

where we have assumed that the system

$$\ddot{q} + W'(q) = 0 \tag{5.57}$$

has a hyperbolic fixed point. This assumption yields whiskered tori for the uncoupled system, that is the system without the interacting terms $V_j(q_n - q_{n+j})$. Moreover, suppose that the coupling potential V_k satisfy

$$\|V_k\|_{C^2_\rho} \leq C_V \Gamma(k) \tag{5.58}$$

i.e. the interaction decays according to the decay function Γ. Note that finite range interactions, which is equivalent to saying Γ is compactly supported, of any arbitrary length are included in this example.

In [33] it was shown that a whiskered torus exists for the coupled system under the assumption that an approximate whiskered torus exists. In particular, when the coupling is small, the tori of the uncoupled system persist. In

this paper, we assume that a whiskered torus exists and show that they have stable and unstable manifolds that are localized near the torus.

We can generalize the assumptions of Theorem 5.3.1 to include non-resonant manifolds. More specifically, instead of assuming that K is a whiskered embedding as in Definition 5.3.1, one can assume spectral properties related DK.

Theorem 5.3.2. *Let $F : \mathcal{M} \to \mathcal{M}$ be a map belonging to $C^r_\Gamma(\mathcal{B})$ for any ball $\mathcal{B} \subset \mathcal{M}$ and some decay function Γ and let $K : D_{\underline{\rho}_1} \to \mathcal{M} \in \mathcal{A}_{\underline{\rho}_1,\underline{c},\Gamma}((\mathbb{T}^l)^{\mathbb{N}})$ be an analytic embedding for of a torus for F.*

Furthermore, suppose that F has a complex analytic extension in a neighborhood of the torus $K((\mathbb{T}^l)^{\mathbb{N}})$, i.e. there exists ρ_2 such that F is analytic on

$$\{z \in \mathcal{M} \mid |z - K(\theta)| \leq \rho_2 \text{ for some } \theta \text{ with } \mid Im\ (\theta_n)| < \rho_{1,n} \text{ for all } n\} \quad (5.59)$$

Define $A(\theta) := DF(K(\theta))$ and the operators $A^{c,s,u}(\theta)$, all of which act on the space of localized vectors $\ell^\infty_{\underline{c},\Gamma}$, by

$$A^{c,s,u}(\theta) := \Pi^{c,s,u}_{K(\theta+\omega)} DF(K(\theta))|_{\mathcal{E}^{c,s,u}_{K(\theta)}} \quad (5.60)$$

Suppose that there is an integer L such that

$$\|A^s\|^{L+1}_{\underline{\rho}_1,\underline{c},\Gamma} \|A^{-1}\|_{\underline{\rho}_1,\underline{c},\Gamma} < 1 \quad (5.61)$$

We will assume that:

1) $A(\theta)$ is invertible for any $\theta \in D_{\underline{\rho}_1}$

2) The tangent space splits as

$$T_{K(\theta)}\mathcal{M} = \mathcal{E}^s_{K(\theta)} \oplus \mathcal{E}^c_{K(\theta)} \oplus \mathcal{E}^u_{K(\theta)} \tag{5.62}$$

where $\mathcal{E}^{s,c,u}_{K(\theta)}$ *satisfy:*

4) The projections $\Pi^{s,c,u}_{K(\theta)}$ *associated to this splitting are in* $S^1_{\underline{\rho},\underline{c},\Gamma}$.

5) We have the following non-resonance condition on the transfer operators $\mathcal{L}$ *and* $\mathcal{R}$ *defined in Section 5.2.2*

$$Spec(\mathcal{L}^\omega_{(A^{c\oplus u})}, S^1_{\underline{\rho},\underline{c},\Gamma}) \cap Spec(\mathcal{R}^{1,\omega}_{A^s}, S^1_{\underline{\rho},\underline{c},\Gamma}))^i = \emptyset \tag{5.63}$$

for $i = 1, \ldots, L$. *In particular, if* K *is a whiskered embedding for* F, *then* K *satisfies assumptions* $3 - 5$.

Under these assumptions, we can find analytic maps $P, W : D_{\underline{\rho}_1} \times (B_{\rho_2} \subset \ell^\infty_{\underline{c},\Gamma}(\mathbb{Z}^d)) \to \ell^\infty_{\underline{c},\Gamma}(\mathbb{Z}^d)$ *where* B_{ρ_2} *is a neighborhood of the origin,* P *is a polynomial in* s, $W, P \in \mathcal{A}_{\underline{\rho}_1,\rho_2,\underline{c},\Gamma}(D_{\underline{\rho}_1} \times B_{\rho_2})$

$$F(W(\theta, s)) = W(\theta + \omega, P(\theta + \omega, s)) \tag{5.64}$$

holds in $D_{\underline{\rho}_1} \times B_{\rho_2}$ *and*

$$W(\theta, 0) = K(\theta) \tag{5.65}$$

$$P(\theta, 0) = 0 \quad DP(\theta, 0) = A^s(\theta - \omega) \tag{5.66}$$

Moreover, if we suppose that

$$(Spec(\mathcal{R}^\omega_{A^s}))^i \cap Spec(\mathcal{L}^\omega_{A^s}) = \emptyset \tag{5.67}$$

for $1 \leq i \leq L$, *then we can chose* P *to be linear.*

Finally, the stable fiber $W^s_{K(\theta)} := W(\{\theta\} \times B_{\rho_2})$ *is the unique analytic invariant manifold that is tangent to the linear subspace* $\mathcal{E}^s_{K(\theta)}$ *and as a consequence of Equation 5.48 the stable fibers satisfy the invariance property that*

$$F(W^s_{K(\theta)}) = W^s_{K(\theta+\omega)} \tag{5.68}$$

Remark 5.3.1. We will prove Theorem 5.3.2, which generalizes Theorem 5.3.1, in Section 5.4. We state Theorem 5.3.1 since it is the most natural theorem to state to show the existence of localized stable manifolds for the whiskered tori constructed in [33]. This generalization also yields non-resonant manifolds, slow manifolds, and gives conditions that allow to choose P linear, namely condition 5.67.

Moreover, the fact that P satisfies $DP(\theta, 0) = A^s(\theta - \omega)$ implies that $W((\mathbb{T}^l)^{\mathbb{N}} \times B_{\rho_2})$ satisfies Equation 5.46.

Although Theorem 5.3.2 only gives the construction of the stable manifold for a whiskered embedding, we can use Theorem 5.3.2 to construct the unstable manifold $W^u((\mathbb{T}^l)^{\mathbb{N}})$ by noting that the unstable manifold for the torus $K(\mathbb{T}^d)$ under the map F is simply the stable manifold for $K((\mathbb{T}^l)^{\mathbb{N}})$ under the map F^{-1}.

The stable fibers $W^s_{K(\theta)}$ also satisfy the usual graph property, namely that $W^s_{K(\theta)}$ is, in a neighborhood of $K(\theta)$, a graph over $\mathcal{E}^s_{K(\theta)}$. Indeed, since Theorem 5.3.2 implies that

$$T_{K(\theta)} W^s_{K(\theta)} = \mathcal{E}^s_{K(\theta)} \tag{5.69}$$

and hence if we write $W = (W^s, W^{c\oplus u})$, where $W^s = \Pi^s_{K(\theta)} W$ and $W^{c\oplus u}_{K(\theta)} = \Pi^{c\oplus u}_{K(\theta)} W$, then (5.69) implies that $D_s W^s(\theta, 0)$ is invertible and hence by the implicit function theorem $W^s(\theta, s)$ is invertible in s in a neighborhood of $s = 0$. Thus, if $H_\theta(s) := W^{c\oplus u} \circ (W^s)^{-1}$ then the point $(s, H(s))$ is in the image of W, which means that $W^s_{K(\theta)}$ is the graph of H_θ.

5.3.1 Uniqueness Result

The parameterization W and the function P of Theorems 5.3.1 and 5.3.2 are not unique as the theorems are stated, though the image of W is unique. However, if we impose stronger conditions on W and P, we can show that they are in fact unique. The goal of this section is to state a theorem that states that the image of W is unique, and to state conditions that lead to unique functions W and P.

Theorem 5.3.3. *Under the setup of Theorem 5.3.1 or Theorem 5.3.2 the fibers $W(\{\theta\} \times B_{\rho_2})$ are unique in the sense that any localized analytic invariant manifold tangent to $\mathcal{E}^s_{K(\theta)}$ coincides with $W(\{\theta\} \times B_{\rho_2})$ in a neighborhood of $K(\theta)$.*

If, in addition, we suppose the following:

1) $W(\theta, 0) = K(\theta)$

2) The image of $DW(K(\theta, 0))$ is $\mathcal{E}^s_{K(\theta)}$ and is specified

3) $P(\theta, 0) = 0$ and $DP(\theta, 0) = A^s(\theta - \omega)$

4) $W^s_{i,\theta} = 0$, where $W^s_{i,\theta} := \Pi^s_{K(\theta)} D^i_s W(\theta, 0)$

Then the parameterization W and the function P are unique in $W, P \in \mathcal{A}_{\underline{\rho}_1,\rho_2,\underline{c},\Gamma}(D_{\underline{\rho}_1} \times B_{\rho_2})$

We will prove Theorem 5.3.3 in Section 5.4.3. For now, we note that Theorem 5.3.3 is important to prove the result for flows, which we do in Section 5.3.2.

Moreover, a corollary of Theorem 5.3.3 is that *the stable manifold the whiskered torus K is the same for the map F^n and F, that is*

$$W^s_{K(\theta)}(F^n) = W^s_{K(\theta+n\omega)}(F) \tag{5.70}$$

More precisely we can prove the following: If W and P are the unique functions that satisfy Theorem 5.3.3 and Equation (5.48) for the map F^n, then W and P solve the Equation (5.48) for the map F.

5.3.2 Stable manifolds for flows

In this section we will explain how one can extend Theorem 5.3.1 to the case of flows for lattice systems.

In [33] it was proven that a decay vector field $X \in C^r_\Gamma(\mathcal{B})$ generates a flow $\{S_t\}_{t\in\mathbb{R}}$ such that S_t is a decay diffeomorphism for all t. More precisely they proved the following result.

Proposition 5.3.4. *Let X be a C^r vector field, $r \geq 1$, on an open subset $\mathcal{B} \subset \mathcal{M}$ and consider the differential equation*

$$\dot{x} = X(x) \tag{5.71}$$

Let $\mathcal{B}_1 \subset \mathcal{B}$ be an open set such that $d(\mathcal{B}_1, \mathcal{B}^c) = \eta > 0$.

Then there exist $T > 0$ such that for all initial conditions $x_0 \in \mathcal{B}_1$ there is a unique solution S_t of the Cauchy problem corresponding to Equation (5.71) *defined for $|t| < T$. We denote by $S_t(x_0) = x_t$. Note that, by uniqueness, we have that $S_{t+s} = S_t \circ S_s$ when all the maps are defined and the composition makes sense. Moreover*

(1)For all $t \in (-T, T)$, $S_t : \mathcal{B}_1 \to \mathcal{B}$ is a diffeomorphism onto its image. (2) If $X \in C^r_\Gamma(\mathcal{B}_1)$ then $S_t \in C^r_\Gamma(\mathcal{B}_1)$ for all $t \in (-T, T)$. Moreover, there exist $C, \mu > 0$ such that

$$\|DS_t(x)\|_\Gamma \leq Ce^{\mu t} \tag{5.72}$$

for $x \in \mathcal{B}_1$ and $t \in (-T, T)$. When $\mathcal{B} = \mathcal{M}$ we have $T = \infty$.

Note that C^r_Γ functions are uniformly bounded, which is important to point out especially in the case $\mathcal{B}$ is unbounded, e.g. when $\mathcal{B} = \mathcal{M}$. Without the assumption that the vector field is uniformly bounded, we would not be able to chose $T = \infty$ in the case $\mathcal{B} = \mathcal{M}$. We omit the proof of this result as it is given in [33]. Now that we have Proposition 5.3.4, we now explain how to extend Theorem 5.3.1 in the case for flows.

Let X be a analytic vector field with decay in $C^r_\Gamma(\mathcal{B}_1)$. The notion of a whiskered torus for a flow is that we have an analytic embedding $K : D_{\underline{\rho}} \to \ell^\infty(\mathbb{Z}^N)$ in $\mathcal{A}_{\underline{\rho},\underline{c},\Gamma}$ such that

$$S_t \circ K(\theta) = K(\theta + t\omega) \tag{5.73}$$

Or equivalently, if one takes the derivative of Equation (5.73) with respect to t at $t = 0$ one obtains an equivalent equation in terms of the vector field X

$$X \circ K(\theta) = \partial_\omega K(\theta) := DK(\theta)\omega \tag{5.74}$$

which is the equation that is solved in [33]. We now state the definition of a localized whiskered torus for the flow S_t.

Definition 5.3.1. (**Whiskered tori for flows**) Let $\underline{\rho} = \{\rho_n \mid n, \rho_n \geq 0\}$ be a sequence of radii, $\omega \in \mathbb{R}^\infty$ a frequency vector, $\underline{c} = \{c_n \in \mathbb{Z}^n \mid n \geq 0\}$ a collection of lattice sites, Γ a decay function and a vector field X that is in $C^2_\Gamma(\mathcal{B})$ for every ball $\mathcal{B}$ of $\mathcal{M}$. Suppose that the flow S_t exists for all time t. We say that $K : D_{\underline{\rho}} \to \mathcal{M} \in \mathcal{A}_{\underline{\rho},\underline{c},\Gamma}$ is a whiskered embedding for the flow S_t when we have:

1) The tangent has an invariant splitting

$$T_{K(\theta)}\mathcal{M} = \mathcal{E}^s_{K(\theta)} \oplus \mathcal{E}^c_{K(\theta)} \oplus \mathcal{E}^u_{K(\theta)} \tag{5.75}$$

where $\mathcal{E}^{s,c,u}_{K(\theta)}$ satisfy $DK(\theta)\mathcal{E}^{s,c,u}_\theta = \mathcal{E}^{s,c,u}_{\theta+t\omega}$. Moreover, we also assume

2) The projections $\Pi^{s,c,u}_{K(\theta)}$ associated to this splitting are in $S^1_{\underline{\rho},\underline{c},\Gamma}$.

3) The splitting (5.75) is characterized by asymptotic growth conditions: Define $A(\theta, t) := DS_t(K(\theta))$ and

$$A^{s,c,u}(\theta, t) := A(\theta, t)|_{\mathcal{E}^{s,c,u}_\theta} \tag{5.76}$$

We assume that there are $0 < \mu_1, \mu_2 < 1, \mu_3 > 1$ such that $\mu_1\mu_3 < 1$, $\mu_2\mu_3 < 1$ and $C_h > 0$ such that for all $n \geq 1$ $\theta \in D_{\underline{\rho}}$

$$\begin{aligned}
&\|A^s(\theta,t)A^s(\theta,t_0)^{-1}\|_{\underline{\rho}_1,\rho_2,\underline{c},\Gamma} \leq C_h e^{-\mu_1(t-t_0)} \text{ for } t > t_0 \geq 0 \\
&\|A^u(\theta,t)A^u(\theta,t_0)^{-1}\|_{\underline{\rho}_1,\rho_2,\underline{c},\Gamma} \leq C_h e^{\mu_2(t-t_0)} \text{ for } t < t_0 \leq 0 \\
&\|A^c(\theta,t)A^c(\theta,t_0)^{-1}\|_{\underline{\rho}_1,\rho_2,\underline{c},\Gamma} \leq C_h e^{\mu_3|t-t_0|} \text{ for all } t_0, t
\end{aligned} \tag{5.77}$$

We now state the analogy of Theorem 5.3.1 in the case of flows, which is a straight-forward consequence of Theorem 5.3.1.

Theorem 5.3.5. *Let $X : \mathcal{M} \to \mathcal{M}$ be a vector field belonging to $C^r_\Gamma(\mathcal{B})$ for any ball $\mathcal{B} \subset \mathcal{M}$ and and some decay function Γ. By Proposition 5.3.4 the flow S_t exists and is a decay diffeomorphism for an interval $(-T.T)$, we will assume that $T = \infty$.*

Suppose that $K : D_{\underline{\rho}_1} \to \mathcal{M} \in \mathcal{A}_{\underline{\rho}_1,\underline{c},\Gamma}((\mathbb{T}^l)^{\mathbb{N}})$ is an analytic whiskered embedding for S_t. Suppose that X has a complex analytic extension in a neighborhood of the torus $K((\mathbb{T}^l)^{\mathbb{N}})$, i.e. there exists ρ_2 such that X is analytic on

$$\{z \in \mathcal{M} \mid |z - K(\theta)| \leq \rho_2 \text{ for some } \theta \text{ with } \mid Im\ (\theta_n)| < \rho_{1,n} \text{ for all } n\} \tag{5.78}$$

Define $A(\theta) := DF(K(\theta))$ and the operators $A^{c,s,u}(\theta)$, all of which act on the space of localized vectors $\ell^\infty_{\underline{c},\Gamma}$, by

$$A^{c,s,u}(\theta) := \Pi^{c,s,u}_{K(\theta+\omega)} DS_t(K(\theta))|_{\mathcal{E}^{c,s,u}_{K(\theta)}} \tag{5.79}$$

Since the embedding is whiskered, we know that for some integer L,

$$\|A^s\|^{L+1}_{\underline{\rho}_1,\underline{c},\Gamma}\|A^{-1}\|_{\underline{\rho}_1,\underline{c},\Gamma} < 1 \tag{5.80}$$

We will assume that:

1) $A(\theta)$ is invertible for any $\theta \in D_{\underline{\rho}_1}$

2) $L + 1 \leq r$

Under these assumptions, we can find analytic maps $P, W : D_{\underline{\rho}_1} \times (B_{\rho_2} \subset \ell^\infty_{\underline{c},\Gamma}(\mathbb{Z}^d)) \to \ell^\infty_{\underline{c},\Gamma}(\mathbb{Z}^d)$ where B_{ρ_2} is a neighborhood of the origin, P is a polynomial in s, $W, P \in \mathcal{A}_{\underline{\rho}_1,\rho_2,\underline{c},\Gamma}(D_{\underline{\rho}_1} \times B_{\rho_2})$

$$W(\theta, 0) = K(\theta) \tag{5.81}$$

$$P(\theta, 0) = 0 \quad DP(\theta, 0) = A^s(\theta - \omega) \tag{5.82}$$

Finally, the stable fiber $W^s_{K(\theta)} := W(\{\theta\} \times B_{\rho_2})$ is the unique analytic invariant manifold that is tangent to the linear subspace $\mathcal{E}^s_{K(\theta)}$ and as a consequence of Equation 5.48 the stable fibers satisfy the invariance property that

$$S_t(W^s_{K(\theta)}) = W^s_{K(\theta+t\omega)} \tag{5.83}$$

Remark 5.3.2. The proof of Theorem 5.3.5 only requires that S_{t_0} satisfies the conditions of Theorem 5.3.2 for a time t_0. We chose to state 5.3.5 the way we did since it uses the same notion of a whiskered torus in the case of flows for lattice systems with localized interactions considered in [33].

Proof: Our assumptions imply that K is a whiskered embedding for S_{t_0} for any t_0. Fix $t_0 \in \mathbb{R}$ and denote by W^s the stable manifold for the torus constructed in Theorem 5.3.1, and let $\{W^s_{K(\theta)} \mid \theta \in (\mathbb{T}^l)^{\mathbb{N}}\}$ be the corresponding stable fibers, that is $W^s_{K(\theta)} = W(\{\theta\}, B_{\rho_2})$ where W is the parameterization constructed in Theorem 5.3.1.

We wish to show that W^s is in fact the stable manifold of $K((\mathbb{T}^l)^{\mathbb{N}})$ for the flow S_t. For this, it suffices to show that $S_t W^s_{K(\theta)} = W^s_{K(\theta+t\omega)}$.

Fix $t \in \mathbb{R}$ and define

$$M(\theta) := S_t(W^s_{K(\theta)}) \tag{5.84}$$

We exploit the uniqueness assertions in Theorem 5.3.1 to prove that $M(\theta) = W^s_{K(\theta+t\omega)}$. Indeed, first notice that

$$T_{K(\theta)}M(\theta) = DS_t(K(\theta)T_{K(\theta)})W^s_{K(\theta)} = E^s_{K(\theta+t\omega)} \tag{5.85}$$

Moreover, we also have

$$S_{t_0}M(\theta) = S_t \circ S_{t_0}W^s_{K(\theta)} = S_t(W^s_{K(\theta+t_0\omega)}) = M(\theta + t_0\omega) \tag{5.86}$$

Thus $M(\theta)$ satisfies both

$$\begin{aligned} T_{K(\theta)}M(\theta) &= E^s_{K(\theta+t\omega)} \\ S_{t_0}M(\theta) &= M(\theta + t_0\omega) \end{aligned} \tag{5.87}$$

and hence the uniqueness assertions of Theorem 5.3.1 imply that $S_t W^s_{K(\theta)} = W^s_{K(\theta+t\omega)}$ as needed.

□

5.4 Proof of Theorem 2

We will prove Theorem 5.3.1 for F^n for fixed $n > 0$ instead of F itself. The reason we do this is because we have better estimates on DF^n. For example, we know that

$$\|A^s\|_{\underline{\rho},\underline{c},\Gamma} \leq C_h \mu_1^n$$

where $\mu_1 < 1$, and hence if n is large enough, $A^s(\theta)$ is a contraction for each θ. Moreover, the stable manifold the whiskered torus K is the same for the map F^n and F, that is

$$W^s_{K(\theta)}(F^n) = W^s_{K(\theta+n\omega)}(F) \tag{5.88}$$

Thus, we will need the following lemma

Lemma 5.4.1. $W^s_F = W^s_{F^n}$

Proof: Let $a_m = d(F^m(x), F^m(K(\theta)))$, where x is a point on $W^s_{F^n}$. It suffices to show that $a_m \to 0$ as $m \to \infty$.

We are assuming that $a_{mn} \to 0$ as $m \to 0$, so for any $\epsilon > 0$ there is an M such that $a_{mn} < \epsilon$ for $m > M$. Now notice that

$$a_{Mn+1} = d\left(F\left(F^{Mn}(x)\right), F^{Mn+1}(K(\theta))\right) < L_f\epsilon \tag{5.89}$$

where $L_f = \sup_{d(z,\mathbb{T}^{\mathbb{N}})<1} \|DF(z)\|$ is the Lipschitz norm for all points of distance 1 from the torus. It then follows that

$$a_{Mn+j} < L^j_f\epsilon \tag{5.90}$$

for $j = 1, \cdots, n-1$.

We know that $a_{Mn+n} = a_{(M+1)n} < \epsilon$ and hence we can repeat the same argument to obtain $a_{(M+1)n+j} < L^j_f\epsilon$ for $j = 1, \cdots, n-1$. We can assume that $L_f > 1$, otherwise $a_{Mn+j} \to 0$ as $j \to \infty$ and we are done. Thus, we obtain the uniform estimate

$$a_{Mn+j} < L^n_f\epsilon \tag{5.91}$$

for *all* $j \in \mathbb{N}$ since $L_f > 1$. Thus for every $\epsilon > 0$ there is an M such that $a_k < L_f^n \epsilon$ for $k > Mn$, which proves the claim.

□

We assume that a solution $W(\theta, s)$ of (5.48) exists and that we can write

$$\begin{aligned} W(\theta, s) &= W^{\leq} + W^{>} = \sum_{i=0}^{L} W_{\theta,i}(s, \ldots, s) + W^{>} \\ P(\theta, s) &= \sum_{i=0}^{L} P_{\theta,i}(s, \ldots, s) \end{aligned} \tag{5.92}$$

Where $W_{\theta,i}, P_{\theta,i}$ are polynomials in s, which is to say that they are $i-$multi-linear functions in s and $W^{>}$ vanishes up to order L in s.

The following Proposition is fundamental for our purposes. It states that we can solve (5.48) up to order L.

Proposition 5.4.2. *Assuming the hypotheses of Theorem 5.3.1, then we can find polynomials in s*

$$\begin{aligned} W^{\leq} &= \sum_{i=1}^{L} W_{i,\theta}(s, \ldots, s) \\ P &= \sum_{i=1}^{L} P_{i,\theta}(s, \ldots, s) \end{aligned} \tag{5.93}$$

Where $W_{i,\theta}, P_{i,\theta}$ are homogeneous polynomials of degree i in $S^i_{\underline{\rho}_1,\underline{c},\Gamma}$. $W^{\leq}$ and P are of degree not larger than L, are in $\mathcal{A}_{\underline{\rho}_1,\rho_2,\underline{c},\Gamma}$ for any $\rho_2 > 0$ and $\underline{\rho}_1$ satisfying $K \in \mathcal{A}_{\underline{\rho}_1,\underline{c},\Gamma}$ and

$$F(W^{\leq}(\theta, s)) = W^{\leq}(\theta + \omega, P^{\leq}(\theta + \omega, s)) + o(|(\theta, s)|^L) \tag{5.94}$$

Finally, we also have that

$$W(\theta, 0) = K(\theta) \tag{5.95}$$

$$P(\theta, 0) = 0 \quad DP(\theta, 0) = A^s(\theta - \omega) \tag{5.96}$$

To prove Proposition 5.4.2 we will need the following

Lemma 5.4.3. *Let $A, B : (\mathbb{T}^l)^{\mathbb{N}} \times \to \ell^\infty_{\underline{c},\Gamma}$ be in $S^1_{\underline{\rho},\underline{c},\Gamma}$ and consider the operators $\mathcal{L}^\omega_B$, $\mathcal{R}^k_A$ and $\mathcal{L}^\omega_{k,A,B}$ acting on the space $S^k_{\underline{\rho},\underline{c},\Gamma}$ that are defined by*

$$\begin{aligned}
&(\mathcal{L}^\omega_B M)(\theta)(x_1, \ldots, x_k) = B(\theta - \omega)M(\theta - \omega)(x_1, \ldots, x_k) \\
&(\mathcal{R}^{k,\omega}_A M)(\theta)(x_, \ldots, x_k) = M(\theta)(x_1, \ldots, A(\theta - \omega)x_k, \ldots, x_k) \\
&(\mathcal{L}^\omega_{k,A,B} M)(\theta)(x_1, \ldots, x_k) = B(\theta - \omega)M(\theta - \omega)(A(\theta - 2\omega)x_1, \ldots, A(\theta - 2\omega)x_k)
\end{aligned} \tag{5.97}$$

We have the following spectral inclusion

$$Spec(\mathcal{L}^\omega_{k,A,B}, S^k_{\underline{\rho},\underline{c},\Gamma}) \subset Spec(\mathcal{L}^\omega_B, S^1_{\underline{\rho},\underline{c},\Gamma}) Spec(\mathcal{R}^{1,\omega}_A, S^1_{\underline{\rho},\underline{c},\Gamma})^k \tag{5.98}$$

Moreover, we also have that $1 \notin Spec(\mathcal{L}^\omega_{i,A^s,(A^{c\oplus u})^{-1}})$.

Remark 5.4.1. Lemma 5.4.3 is an important way in which our proof differs from [16]. In the present work, Lemma 5.4.3 states that we are able to deduce spectral properties about $\mathcal{L}^\omega_{k,A,B}$ knowing the spectral properties of $\mathcal{L}^\omega_B$ and $\mathcal{R}^{1,\omega}_A$.

In contrast, since the main theorems in [16] are stated for fixed points and normally hyperbolic invariant manifolds and not whiskered tori, the analogy of Lemma 5.4.3 is easier to state. Indeed, Proposition 3.2 in [16] relates the

spectrum of certain operators $\mathcal{L}_B$, $\mathcal{L}_{k,A,B}$ and $\mathcal{R}_A^k$ in terms of the spectrum of A and B directly. More specifically, the operators considered in [16] do not depend on θ, and this allows them to prove $\mathrm{Spec}(\mathcal{L}_{k,A,B}) \subset \mathrm{Spec}(B)(\mathrm{Spec}(A))^k$. In our case one cannot directly relate the spectrum of $\mathcal{L}^{\omega}_{k,A,B}$ to the spectrum of A and B. Nevertheless, Lemma 5.4.3 in the present paper is sufficient for our purposes since the crucial property that is needed to prove an inductive result such as Proposition 5.4.2 both in this paper and in [16] is that $1 \notin \mathrm{Spec}(\mathcal{L}^{\omega}_{i,A^s,(A^{c\oplus u})^{-1}})$.

□

Proof of Lemma 5.4.3: The fact that the range of $\mathcal{L}^{\omega}_B, \mathcal{R}^{k,\omega}_B, \mathcal{L}^{\omega}_{k,A,B}$ lies in $S^k_{\underline{\rho}_1,\underline{c},\Gamma}$ follows from Lemma 5.2.2. Notice that $\mathcal{L}^{\omega}_{n,A,B} = \mathcal{L}^{\omega}_B \mathcal{R}^{1,\omega}_A \cdots \mathcal{R}^{k,\omega}_A$, and moreover the operators $\mathcal{L}^{\omega}_B, \mathcal{R}^{k,\omega}_A$ commute. Moreover, $\mathrm{Spec}(\mathcal{R}^{k,\omega}_A) = \mathrm{Spec}(\mathcal{R}^{1,\omega}_A)$. Hence using the general fact that $\mathrm{Spec}(AB) \subset \mathrm{Spec}(A)\mathrm{Spec}(B)$ [65] for any commuting elements of a Banach algebra, we obtain

$$\mathrm{Spec}(\mathcal{L}^{\omega}_{k,A,B}, S^k_{\underline{\rho},\underline{c},\Gamma}) \subset \mathrm{Spec}(\mathcal{L}^{\omega}_B, S^k_{\rho,\underline{c},\Gamma})\mathrm{Spec}(\mathcal{R}^{1,\omega}_A, S^k_{\underline{\rho},\underline{c},\Gamma})^k$$

It remains to show that $\mathrm{Spec}(\mathcal{L}^{\omega}_B, S^k_{\underline{\rho},\underline{c},\Gamma}) \subset \mathrm{Spec}(\mathcal{L}^{\omega}_B, S^1_{\underline{\rho},\underline{c},\Gamma})$ and $\mathrm{Spec}(\mathcal{R}^{1,\omega}_A, S^n_{\underline{\rho},\underline{c},\Gamma}) \subset \mathrm{Spec}(\mathcal{R}^{1,\omega}_A, S^1_{\underline{\rho},\underline{c},\Gamma})$. To show that $\mathrm{Spec}(\mathcal{L}^{\omega}_B, S^k_{\underline{\rho},\underline{c},\Gamma}) \subset \mathrm{Spec}(\mathcal{L}^{\omega}_B, S^1_{\underline{\rho},\underline{c},\Gamma})$ suppose that $\lambda \notin \mathrm{Spec}(\mathcal{L}^{\omega}_B, S^k_{\underline{\rho},\underline{c},\Gamma})$, that is we can solve

$$M_n(\theta)(B(\theta-\omega)x_1,\ldots,x_k) - \lambda M_k(\theta)(x_1,\ldots,x_k) = N_k(\theta)(x_1,\ldots,x_k) \quad (5.99)$$

where M_k is the unknown. We now show that this implies that we can solve

$$M_1(\theta)(B(\theta-\omega)x_1) - \lambda M_1(\theta)(x_1) = N_1(\theta)(x_1) \quad (5.100)$$

for M_1. To this end, we extend N_1 to a multi-linear operator $\tilde{N}_1$ as follows: choose a linear functional f_θ such that $f(x^*) = 1$ for some x^*. Then

$$\tilde{N}_1(x_1, \ldots, x_k) := N_1(x_1)f(x_2)\cdots f(x_k) \tag{5.101}$$

Note that $\|\tilde{N}\| = \|N\|$, and hence this extension is bounded. We can solve (5.99) where N_k is taken to be $\tilde{N}_1$, and let the solution be called $\tilde{M}_1$. Then plugging in x^* into the last $k-1$ arguments into $\tilde{M}_1, \tilde{N}_1$ we have

$$\tilde{M}_1(\theta - \omega)(x_1, x^*, \ldots, x^*) - \tilde{M}(\theta)(x_1, \ldots, x_k) = N_1(\theta)(x_1)f(x_2)\cdots f(x_k) \tag{5.102}$$

Then $M_1(\theta)(x) := \tilde{M}_1(\theta)(x, x^*, \ldots, x^*)$ solves (5.100). The same proof works for $\mathcal{R}^{k,\omega}_A$.

Finally, to show that $1 \notin \mathrm{Spec}(\mathcal{L}^{\omega}_{i,A^s,(A^{c\oplus u})^{-1}})$, it suffices to show, by (5.98) that

$$\lambda^{c\oplus u} \neq \lambda_1^s \cdots \lambda_n^s \tag{5.103}$$

where $\lambda^{c\oplus u} \in \mathrm{Spec}(\mathcal{L}^{\omega}_{(A^{c\oplus u})^{-1}}, S^1_{\underline{\rho},\underline{c},\Gamma})$ and $\lambda_i^s \in \mathrm{Spec}(\mathcal{R}^{1,\omega}_{A^s}, S^1_{\underline{\rho},\underline{c},\Gamma}), i = 1, \ldots, k$. Since we are working with F^n and not F, we have $\lambda_i^s \leq C_h(\mu_1)^n$ and $\frac{1}{2C_h(\mu_3)^n} \leq \lambda^{c\oplus u}$ Thus if $\lambda^{c\oplus u} = \lambda_1^s \cdots \lambda_n^s$, then $\frac{1}{2C_h(\mu_3)^n} \leq C_h^k(\mu_1)^{kn}$, that is

$$\frac{1}{2C_h^{k+1}} \leq (\mu_3\mu_1^k)^n \tag{5.104}$$

However, $(\mu_3\mu_1^k)^n \to 0$ as $n \to \infty$ since $\mu_1\mu_3 < 1$, which is a contradiction. $\square$

Proof of Proposition 5.4.2: That we can solve for the $i = 0, 1$ terms is, as we now explain, a consequence of our assumption that K is a whiskered

embedding. More precisely, to solve for $W_{\theta,0}, P_{\theta,0}$ we substitute (5.92) into (5.48) and evaluate at $s = 0$, and we obtain

$$F \circ W_{\theta,0} = W_{\theta+\omega,0} \circ P_{\theta+\omega,0} \tag{5.105}$$

Which is solved by taking $W_{\theta,0} = K(\theta)$ and $P_{\theta,0} = 0$.

To solve for $W_{\theta,1}, P_{\theta,1}$ we differentiate (5.48) at a point $(\theta, 0)$ to obtain

$$DF \circ W_{\theta,1} = W_{\theta+\omega,1} P_{\theta+\omega,1} \tag{5.106}$$

Recall that the projections $\Pi^s_{K(\theta)}$ satisfy

$$DF(K(\theta))\Pi^s_{K(\theta)} = \Pi^s_{K(\theta+\omega)} DF(K(\theta)) \tag{5.107}$$

Thus to solve (5.106) it suffices to take $W_{\theta,1} = \Pi^s_{K(\theta)}$ and $P_{\theta,1} = A^s(\theta - \omega)$, both of which are in $S^1_{\underline{\rho}_1,\underline{c},\Gamma}$. Note that this choice for $W_{\theta,1}$ is not unique since, for instance, we could have also chosen $W_{\theta,1} = \sigma\Pi^s_{K(\theta)}$, for $\sigma \in \mathbb{R}$.

For $i > 1$, we will solve for $W_{i,\theta}$, $P_{i\theta}$ inductively. Taking the i^{th} derivative of (5.48) we obtain

$$\begin{aligned} DF(K(\theta))W_{\theta,i} + r_i &= W_{\theta+\omega,i} P^{\otimes i}_{\theta+\omega,1} + W_{\theta+\omega,1} P_{\theta+\omega,i} \\ &= W_{\theta+\omega,i}(A^s(\theta))^{\otimes i} + P_{\theta+\omega,i} \end{aligned} \tag{5.108}$$

where r_i is a polynomial expression in $W_{\theta,j}, P_{\theta,j}, j \leq i-1$, and F and its derivatives up to order i. The fact that each term in (5.108) belongs to $S^k_{\underline{\rho}_1,\underline{c},\Gamma}$ is a consequence of Lemma 5.2.2. We will consider the projections of the equations onto $\mathcal{E}^s_{K(\theta)}$ and $\mathcal{E}^c_{K(\theta)} \oplus \mathcal{E}^u_{K(\theta)}$. If we let $W^s_{i,\theta} = \Pi^s_{K(\theta)} W_{i,\theta}, W^{c\oplus u}_{i,\theta} = \Pi^c_{K(\theta)} \oplus \Pi^u_{K(\theta)} W_{i,\theta}$ and similarly for P_i and r_i, then the projected equations become

$$\begin{aligned} A^s(\theta)W^s_{i,\theta} - W^s_{i,\theta+\omega}(A^s(\theta))^{\otimes i} - P_{i,\theta+\omega} &= r^s_i \\ A^{c\oplus u}(\theta)W^{c\oplus u}_{i,\theta} - W^{c\oplus u}_{i,\theta+\omega}(A^s(\theta))^{\otimes i} &= -r^{c\oplus u}_i \end{aligned} \tag{5.109}$$

The first of these equations can be solved by taking $W^s_{i,\theta} = 0$ and $P^s_{i,\theta} = -r_i$, while the second equation requires a bit more work. We first start by rewriting the equation as

$$\mathcal{L}_{A^{c\oplus u}} W^{c\oplus u}_{i,\theta} - \mathcal{L}^{\omega}_{i,A^s,\mathrm{Id}} W^{c\oplus u}_{i,\theta} = -r^{c\oplus u}_i \tag{5.110}$$

Thus if we show that $\mathcal{L}_{A^{c\oplus u}} - \mathcal{L}^{\omega}_{i,A^s,\mathrm{Id}}$ is invertible then we can conclude that choosing $W^s_{i,\theta} = 0$ allows us to uniquely determine $W^{c\oplus u}_{i,\theta}$. Using the general fact that $((\mathcal{L}_B)^{-1}W)(\theta) = (B(\theta))^{-1}W(\theta)$ we have

$$\mathcal{L}_{A^{c\oplus u}} - \mathcal{L}^{\omega}_{i,A^s,\mathrm{Id}} = \mathcal{L}_{A^{c\oplus u}} \left(\mathrm{Id} - \mathcal{L}^{\omega}_{i,(A^s),(A^{c\oplus u})^{-1}} \right) \tag{5.111}$$

Thus, by Lemma 5.4.3 and the assumptions of Theorem 5.3.1 imply that $1 \notin \mathrm{Spec}(\mathcal{L}^{\omega}_{i,(A^s),(A^{c\oplus u})^{-1}})$, it follows that $\mathcal{L}_{A^{c\oplus u}} - \mathcal{L}^{\omega}_{i,A^s,\mathrm{Id}}$ is invertible. □

5.4.1 Formulation as a fixed point problem

In this section we will use the fact that we can write $W = W^{\leq} + W^{>}$, where $W^{>}$ vanishes up to order L in the variable s. We will solve an equivalent form of (5.48), namely if we let $G(s,\theta) = F(K(\theta)+s)$, then we will solve

$$G(\theta, W_1(\theta,s)) = G(\theta,0) + W_1(\theta+\omega, P(\theta+\omega,s)) \tag{5.112}$$

Where $W_1(\theta, 0) = 0$ for all θ. Note that W_1 solves (5.112) if and only if $W := K(\theta) + W_1$ solve (5.48). The advantage of working with (5.112) is that there is a nice scaling of this equation that is not present in (5.48). Namely if we consider $G^\delta(\theta, x) := \frac{1}{\delta} G(\theta, \delta x)$ and similarly for W_1 and P we have that (5.112) holds in $D_{\underline{\rho}_1} \times B_\delta$ if and only if

$$G^\delta(\theta, W_1^\delta(\theta, s)) = G^\delta(\theta, 0) + W_1^\delta(\theta + \omega, P^\delta(\theta + \omega, s)) \tag{5.113}$$

holds in $D_{\underline{\rho}_1} \times B_1$. The idea is to scale only in the directions non-tangential to the torus, which does have a natural interpretation for G, W_1 and P, though does not have a natural interpretation for F, which is one important subtlety in why we chose to slightly modify the problem.

This choice of scaling also has the following crucial property: let $N(\theta, s) := G(\theta, s) - G(\theta, 0) - D_s G(\theta, 0)s$. Then $\|N\|_{C_s^r((\mathbb{T}^l)^{\mathbb{N}}_{\underline{\rho}} \times B(1))} \to 0$ as $\delta \to 0$. This will allow us to obtain better estimates when solving the fixed point equation we consider. Note also that the domain of analyticity of G is $D_{\rho_1} \times B_{\rho_2}$ while the domain of analyticity was $\{z \in \mathcal{M} \mid |z - K(\theta)| \leq \rho_2$ for some θ with $|\text{ Im } (\theta_n)| < \rho_{1,n}$ for all $n\}$

Note that solving (5.48) up to order L is equivalent to solving (5.112) up to order L. Thus we can assume that we have $W_1^{\leq}$ and P, polynomials in s that solve (5.112) up to order L. Now we will write a fixed point equation for a function $W_1^{>}$ such that $W_1 := W_1^{\leq} + W_1^{>}$ solves (5.112). To this end we note that we have the following Taylor expansion for G

$$G(\theta, W_1(\theta, s)) = G(\theta, 0) + D_x G(\theta, 0)(W_1^{\leq} + W_1^{>}) + N(\theta, W_1^{\leq} + W_1^{>}) \tag{5.114}$$

Assuming that W_1 solves (5.112) then

$$\begin{aligned} &G(\theta,0) + W_1(\theta+\omega, P(\theta+\omega,s)) \\ &= G(\theta,0) + D_x G(\theta,0)(W_1^{\leq} + W_1^{>}) + N(\theta, W_1^{\leq} + W_1^{>}) \end{aligned} \tag{5.115}$$

Rearranging terms and defining $Q_\omega := (\mathrm{Id}, P) \circ (T_\omega, \mathrm{Id})$ we have

$$DF(K(\theta))W_1^{>} - W_1^{>} \circ Q_\omega = -N \circ (0, W_1^{\leq} + W_1^{>}) - DF(K(\theta))W_1^{\leq} + W_1^{\leq} \circ Q_\omega \tag{5.116}$$

If we define the operator S by

$$SH := DF(K(\theta))H - H \circ Q_\omega$$

then the idea to formulate the problem of finding $W_1^{>}$ via a fixed point argument becomes clear: If we can show that S is invertible then (5.116) becomes

$$W_1^{>} = S^{-1}[-N \circ (\theta, W_1^{\leq} + W_1^{>}) - DF(K(\theta))W_1^{\leq} + W_1^{\leq} \circ Q_\omega] \tag{5.117}$$

The invertibility of S

We start by defining an appropriate space functions in which $W^{>}$ lies to guarantee that S is invertible. Given a decay function Γ and an positive integer ℓ we will consider the norm on functions that vanish up to order l in the variable s

$$\|H\|_{\Omega^{\underline{\rho}}_{\underline{c},\Gamma,\ell}} := \max_{0 \leq i \leq \ell+1} \|D_s^i H\|_{C^0_{\underline{c},\Gamma}(D_{\underline{\rho}} \times B_1)} \tag{5.118}$$

and consider the space

$$\Omega^{\rho}_{\underline{c},\Gamma,\ell} = \left\{ \begin{array}{c} H : D_{\underline{\rho}} \times B_1 \to \mathcal{M} \mid H \text{ is analytic on } D_{\underline{\rho}} \times B_1, \\ D_s^k H(,\overline{\theta},0) = 0 \text{ for } k \leq 0 \leq \ell \text{ and } \|H\|_{\Omega^{\underline{\rho}}_{\underline{c},\Gamma,\ell}} < \infty \end{array} \right\} \tag{5.119}$$

where by D_s we mean the derivative with respect to the s component. As the following lemmas shows, the operator S is invertible on $\Omega^{\underline{\rho}}_{\Gamma,\ell}$

Lemma 5.4.4. *Under the assumptions of Theorem 5.3.1, the operator S preserves the space $\Omega^{\underline{\rho}_1}_{\underline{c},\Gamma,L}$ (i.e. $x \in \Omega^{\underline{\rho}_1}_{\underline{c},\Gamma,L}$ implies that $S(x) \in \Omega^{\underline{\rho}_1}_{\underline{c},\Gamma,L}$). Moreover, the map $S : \Omega^{\underline{\rho}_1}_{\underline{c},\Gamma,L} \to \Omega^{\underline{\rho}_1}_{\underline{c},\Gamma,L}$ is a bounded invertible operator, with a bounded inverse and $\|S^{-1}\|$ can be bounded by a constant independent of the scaling parameter δ.*

Proof: We first need to check that $S(H) \in \Omega^{\underline{\rho}_1}_{\underline{c},\Gamma,L}$ if $H \in \Omega^{\underline{\rho}_1}_{\underline{c},\Gamma,L}$. It is clear that $D^i_s(SH)(\theta, 0) = 0$ for $i = 1, \ldots, L$ since H has this property and $Q(\theta, 0) = 0$. Moreover, we claim that the $\Omega^{\underline{\rho}_1}_{\underline{c},\Gamma,L}$ norm of each term defining S, namely $DF(K(\theta))H$ and $H \circ Q_\omega$, are finite. Indeed, $\|DF(K(\theta))H\|_{\Omega^{\underline{\rho}_1}_{\underline{c},\Gamma,L}} < \infty$ since the multiplicative factor of $DF(K(\theta))$ is independent of s and $\|DF(K(\theta))\|_{\underline{\rho}_1,\underline{c},\Gamma} < \infty$.

For the $H \circ Q_\omega$ term note that $Q_\omega(\theta, 0) = 0$ and $DQ_\omega(\theta, 0) = A^s(\theta - \omega)$, which is a contraction. Hence, for a small enough scaling parameter, the image of Q_ω lies in the domain of H, and hence Proposition 5.2.3 implies that $H \circ Q_\omega \in \Omega^{\underline{\rho}_1}_{\underline{c},\Gamma,L}$.

We solve the equation

$$SH = \eta \tag{5.120}$$

where H is the unknown and η is known. This is equivalent to

$$H = A(\theta)^{-1} H \circ Q_\omega + A(\theta)^{-1}\eta \tag{5.121}$$

At least formally, we see that

$$H = \sum_{j=0}^{\infty} A(\theta)^{-j+1} \eta \circ Q^j_\omega \tag{5.122}$$

is a solution. We justify this formal solution by showing that

$$\sum_{j=0}^{\infty} \|A^{-(j+1)}\eta \circ Q_\omega^j\|_{\Omega^{\underline{\rho}_1}_{\underline{c},\Gamma,L}} \leq C\|\eta\|_{\Omega^{\underline{\rho}_1}_{\underline{c},\Gamma,L}} \tag{5.123}$$

By the Faa-di-Bruno formula we have

$$D_s^k(\eta \circ Q_\omega^j) = \sum_{i=0}^{k} \sum_{k_1+\cdots+k_i=k} \sigma^{i,k}_{k_1,\ldots,k_i}([D_s^i\eta] \circ Q_\omega^j) D_s^{k_1} Q_\omega^j \cdots D_s^{k_i} Q_\omega^j \tag{5.124}$$

where $\sigma^{i,k}_{k_1,\ldots,k_i}$ are explicit combinatorial coefficients. Using (5.124) with $k = L+1$ we will obtain the desired estimates. First, we need to estimate each term and factor appearing in (5.124). Since $Q_\omega(\theta,0) = 0$ and $DQ_\omega(\theta,0) = A^s(\theta-\omega)$ we can, by our scaling assumptions, choose a scaling parameter and $\epsilon > 0$ small enough so that both

$$\|DQ_\omega\|_{C^0_{\underline{c},\Gamma}(D_{\underline{\rho}_1}\times B_1)} \leq \|A^s\|_{\underline{\rho}_1,\underline{c},\Gamma} + \epsilon < 1 \tag{5.125}$$

and

$$\|DQ_\omega\|^{L+1}_{C^0_{\underline{c},\Gamma}(D_{\underline{\rho}_1}\times B_1)} \|A^{-1}\|_{\underline{\rho}_1,\underline{c},\Gamma} \leq (\|A^s\|_{\underline{\rho}_1,\underline{c},\Gamma} + \epsilon)^{L+1} \|A^{-1}\|_{\underline{\rho}_1,\underline{c},\Gamma} \tag{5.126}$$

Recall that $(\|A^s\|_{\underline{\rho}_1,\underline{c},\Gamma})^{L+1}\|A^{-1}\|_{\underline{\rho}_1,\underline{c},\Gamma} < 1$ by our assumption on L. Since we want estimates on $D^k Q_\omega^j$ we use the fact that Q is a polynomial in s to say that, for $(\theta, s) \in D_{\underline{\rho}_1} \times B_1$

$$\|D^k Q_\omega^j(\theta,s)\|_{\underline{\rho}_1,\underline{c},\Gamma} \leq C_k(\|A^s\|_{\underline{\rho}_1,\underline{c},\Gamma} + \epsilon)^j, \tag{5.127}$$

for $k = 0, 1, \ldots, L$ and $j = 0, 1, 2, \ldots$ Now we need to estimate the factor $(D_s^i\eta) \circ Q_\omega^j$. Since $D_s^i\eta(\theta,0) = 0$ for $i = 0, 1, \ldots, L$ we have, by Taylor's Theorem

$$\|D_s^i\eta\|_{C^0_{\underline{\rho}_1,\rho_2,\underline{c},\Gamma}} \leq C\|D_s^{L+1}\eta\|_{C^0_{\underline{\rho}_1,1,\underline{c},\Gamma}} \rho_2^{L-k} \tag{5.128}$$

From (5.127) we deduce that the image of $D_{\underline{\rho}_1} \times B_1$ under the map Q_ω^j is contained in $D_{\underline{\rho}_1} \times B_{\rho_2}$ where $\rho_2 = (\|A\|_{\underline{\rho}_1,\underline{c},\Gamma} + \epsilon)^j$. From (5.127) and (5.128) we deduce that

$$\|(D_s^i \eta) \circ Q_\omega^j\|_{C^0_{\underline{\rho}_1,1,\underline{c},\Gamma}} \leq C\|D_s^{L+1}\eta\|_{C^0_{\underline{\rho}_1,1,\underline{c},\Gamma}} \|(\|A\|_{\rho_1,\underline{c},\Gamma} + \epsilon)^{(L+1-i)j} \tag{5.129}$$

Finally using (5.124), (5.127) and (5.129) we have

$$\begin{aligned}
&\|D^{L+1}(A^{-(j+1)}\eta Q_\omega^j)\|_{C^0_{\underline{\rho}_1,1,\underline{c},\Gamma}} \\
&\leq C\sum_{i=0}^{L+1} \|D_s^{L+1}\eta\|_{C^0_{\underline{\rho}_1,1,\underline{c},\Gamma}} \|\|A^{-1}\|^{j+1}_{\underline{\rho}_1,\underline{c},\Gamma} (\|A\|_{\underline{\rho}_1,\underline{c},\Gamma} + \epsilon)^{(L+1-i)j} (\|A^s\|_{\rho_1,\underline{c},\Gamma} + \epsilon)^{ij} \\
&\leq C\|D_s^{L+1}\eta\|_{C^0_{\underline{\rho}_1,1,\underline{c},\Gamma}} [\|A^{-1}\|_{\underline{\rho}_1,\underline{c},\Gamma} (\|A\|_{\underline{\rho}_1,\underline{c},\Gamma} + \epsilon)^{L+1}]^j
\end{aligned} \tag{5.130}$$

Since $(\|A^s\|_{\underline{\rho}_1,\underline{c},\Gamma})^{L+1}\|A^{-1}\|_{\underline{\rho}_1,\underline{c},\Gamma} < 1$ we conclude that (5.123) holds.

□

5.4.2 Solving the fixed point equation

Now that we have shown that S is invertible, recall that we wish to solve the equation

$$W_1^> = \mathcal{T}(W_1^>) \tag{5.131}$$

where $\mathcal{T}$ is defined by

$$\mathcal{T}(W_1^>) = S^{-1}[-N \circ (\theta, W_1^\leq + W_1^>) - DF(K(\theta))W_1^\leq + W_1^\leq \circ Q_\omega] \tag{5.132}$$

We now show that $\mathcal{T}$ is a contraction is a suitably chosen space of functions.

Lemma 5.4.5. *Under the assumptions of Theorem 5.3.1 and under the scaling assumptions,* $\mathcal{T}$ *sends the closed ball of radius* $\frac{\rho_2}{3}$ *,* $\overline{B}_{\frac{\rho_2}{3}}$*, of* $\Omega^{\rho_1}_{\underline{c},\Gamma,L}$ *into itself and is a contraction. Therefore* $\mathcal{T}$ *has a fixed point* $W^{>}$ *in the closed unit ball of* $\Omega^{\rho_1}_{\underline{c},\Gamma,L}$*.*

Proof: First we show that $\mathcal{T}$ maps points in $\overline{B}_{\frac{\rho_2}{3}}$ to $\Omega^{\rho_1}_{\underline{c},\Gamma,L}$. The more refined estimate that $\mathcal{T}$ maps $\overline{B}_{\frac{\rho_2}{3}}$ to itself will be proven later. By choosing a small enough scaling parameter, we can assume that $W_1^{\leq}$ is arbitrarily close to the identity and Q_ω to be arbitrarily close to A^s. Thus if $W_1^{>}$ is in $\overline{B}_{\frac{\rho_2}{3}}$, then the image of $W_1^{\leq} + W_1^{>}$ lies in the ball of radius $\overline{B}_{\rho_2}$, and recall that $N(\theta, s)$ is assumed to be analytic on $D_{\rho_1} \times B_{\rho_2}$. Thus, by Proposition 5.2.3 we can conclude that $N \circ (\theta, W_1^{\leq} + W_1^{>})$ is in $\Omega^{\rho_1}_{\underline{c},\Gamma,L}$.

The other terms $DF(K(\theta))W_1^{\leq}$ is in $\Omega^{\rho_1}_{\underline{c},\Gamma,L}$ because the multiplying factor of $DF(K(\theta))$ does not depend on s, and since $Q_\omega(\theta, 0) = 0$ and $DQ_\omega(\theta, 0) = A^s(\theta - \omega)$ it follows that $W^{\leq} \circ Q_\omega$ is also in $\Omega^{\rho_1}_{\underline{c},\Gamma,L}$.

We show that $\mathcal{T}$ is a contraction. For $W_1^{>}$ and $W_1^{>} + \Delta$ in the closed until ball of $\Omega^{\rho}_{\underline{c},\Gamma,L}$ We have the incremental formula

$$\begin{aligned} \mathcal{T}(W_1^{>} + \Delta) - \mathcal{T}(W_1^{>}) &= \int_0^1 \frac{d}{d\tau}[\mathcal{T}(W_1^{>} + \tau\Delta)]d\tau \\ &= -\int_0^1 S^{-1} D_x N(\theta, W_1^{\leq} + W_1^{>} + \tau\Delta)\Delta d\tau \end{aligned} \tag{5.133}$$

Taking the $(L+1)$-derivative of (5.133) in the s variable we obtain

$$\|\mathcal{T}(W_1^{>} + \Delta) - \mathcal{T}(W_1^{>})\|_{\Omega^{\rho}_{\underline{c},\Gamma,L}} \leq C\|N\|_{C_x^{L+2}}\|\Delta\|_{\Omega^{\rho}_{\underline{c},\Gamma,L}} \tag{5.134}$$

Since $\|N\|_{C_x^{L+2}} \to 0$ as the scaling parameter goes to zero, we conclude that $\mathcal{T}$ is a contraction for sufficiently small values of the scaling parameter.

Now we show that $\mathcal{T}$ maps $\overline{B}_{\frac{\rho_2}{3}} \subset \Omega^{\rho}_{\underline{c},\Gamma,L}$ into itself. For $\|W_1^>\|_{\Omega^{\rho}_{\underline{c},\Gamma,L}} \leq 1$ we have

$$\begin{aligned}\mathcal{T}(W_1^>) &= \mathcal{T}(0) + (\mathcal{T}(W_1^>) - \mathcal{T}(0)) \\ &= (S^{-1}[-G(\theta, W_1^\leq) + G(\theta, 0) + W_1^\leq \circ Q_\omega]) + (\mathcal{T}(W_1^>) - \mathcal{T}(0))\end{aligned} \tag{5.135}$$

Since $\|S^{-1}\|$ is independent of the scaling parameter, we can say that the first term can be made as small as we wish with a small enough scaling parameter, and the second term has norm smaller than $\frac{\rho_2}{3}$ since $W_1^>$ does and $\mathcal{T}$ is a contraction.

□

5.4.3 Proof of the uniqueness of the manifold and the functions P and W

In this section we prove the uniqueness result stated in Section 5.4.3. In the proof of Proposition 5.4.2, we saw that there was a lack of uniqueness in solving for $W_{i,\theta}$. However once we chose $W_{i,\theta}$ and $P_{i,\theta}$ for $1 = 1, \ldots, L$ we found a unique $W^>$ such that

$$W = \sum_{i=1}^{L} W_{i,\theta} + W^> \tag{5.136}$$

and P that satisfy the conclusions of Theorem 5.3.2. That conditions 1-4 of Theorem 5.3.3 guarantee that W and P thus follows from the proof of Proposition 5.4.2 and the fact that $W^>$ is unique.

Now we want show that uniqueness of the manifold itself. Indeed, let W be the analytic solution of Equation (5.48) constructed from Theorem 5.3.2

and write

$$W_\theta = (W_\theta^s, W_\theta^{c\oplus u}) = (\Pi^s_{K(\theta)} W_\theta, \Pi^{c\oplus u}_{K(\theta)} W_\theta) \tag{5.137}$$

Moreover, consider the Taylor series up to order L and write $W_\theta = \sum_i^L W_{i,\theta} + W^>$. If we suppose that $W^s_{1,\theta} = \Pi^s_\theta$ and $W^s_{i,\theta} = 0$ for $i = 2, \ldots, L$, then the proof of Proposition 5.4.2 implies that this choice of $W^s_{i,\theta}, i = 1, \ldots, L$ determines uniquely $W^{c\oplus u}_{i,\theta}$ for $i = 1, \ldots, L$, and the proof of Lemma 5.131 then implies that $W^>$ is also determined uniquely by $W^s_{i,\theta}, i = 1, \ldots, L$.

We now want to use this observation to prove that the manifold $W(\{\theta\} \times B_1)$ constructed in the proof of Theorem 5.3.1 is unique amont all manifolds that are invariant under F and, tangent to $\mathcal{E}^s_{K(\theta)}$ and admit an analytic parameterization that decay like Γ. Indeed, suppose that $V_\theta \in \mathcal{A}_{\rho_1,\rho_2,\underline{c},\Gamma}$ is an embedding of an invariant manifold, the image of $DV_\theta(0)$ is $\mathcal{E}^s_{K(\theta)}$ and the dependence on θ is analytic. If we write $V_\theta = (V^s_\theta, V^{c\oplus u}_\theta)$then by the implicit function theorem we know that V^s_θ is invertible in a neighborhood of the origin. Thus if we let $H = V^{c\oplus u}_\theta \circ (V^s_\theta)^{-1}$, then the image of V_θ is the same as the graph of H. Since the graph of H is invariant we can conclude that

$$F^{c\oplus u} \circ (\mathrm{Id}, H) = H \circ F^s \circ (\mathrm{Id}, H) \tag{5.138}$$

Thus, it follows that Equation (5.48) holds if we take $W = (\mathrm{Id}, H)$ and $R = F^s \circ W$. Moreover, $W = (\mathrm{Id}, H)$ satisfies $W^s_{1,\theta} = \Pi^s_\theta$ and $W^s_{i,\theta} = 0$ for $i = 2, \ldots, L$ and hence W coincides with the solution given in the proof of Theorem 5.3.1.

Appendix

Appendix A

Appendix on Deformation Theory

In this section we recall some facts from deformation theory that we used. The treatment here follows [19] and we refer the reader to [74] for more details on the subject. Let M be a manifold. Suppose we have a family of diffeomorphisms $f_a : M \to M$, where a lies in some (possibly infinite) interval. In the context of proving Theorem 2.2.1 the variable a corresponded to the time variable t, whereas in the context of Theorem 2.3.3 we used the perturbation parameter ϵ. Hence, we use a as a neutral symbol for the parameter of the family in this section to avoid confusion in our two different uses of deformation theory.

Given a family of diffeomorphisms f_a we can obtain a vector field $\mathcal{F}_a$ defined by

$$\frac{d}{da} f_a = \mathcal{F}_a \circ f_a \tag{A.1}$$

Conversely, given a C^1 vector field $\mathcal{F}_a$ and some initial conditions f_0, we can determine uniquely f_a by the theory of ODE's.

Note that we can think of $\mathcal{F}_a$ as an "infinitesimal diffeomorphism".

Many functional equations that are non-linear and non-local when formulated in terms of f_a become linear and local when formulated in terms of $\mathcal{F}_a$. Hence, it is equivalent to speak of the family f_a or of $(\mathcal{F}_a, f_0)$.

Proposition A.0.6. *If $f_a, g_a : M \to M$ are diffeomorphisms and $\mathcal{F}_a$, $\mathcal{G}_a$ are their generators, then we have*

(1) If we define $h_a = g_a \circ f_a$, then its generator $\mathcal{H}_a$ is given by

$$\mathcal{H}_a = \mathcal{G}_a + (g_a)_* \mathcal{F}_a$$

where $(g_a)_*$ is the push-forward:

$$(g_a)\mathcal{F}_a = Dg_a \circ g_a^{-1}\mathcal{F}_a \circ g_a^{-1} = (Dg_a\mathcal{F}_a) \circ g_a^{-1}$$

(2) If $g_a \circ f_a = Id$ then

$$\mathcal{G}_a + (g_a)_* \mathcal{F}_a = 0$$

The proof of this proposition simply involves recalling the definition of $\mathcal{H}_a$. With this, we can now state the following proposition, that asserts that the existence of a Hamiltonian F_a that generates f_a. We used this proposition several times to prove Theorems 2.2.1 and 2.3.1.

We will now consider the case when f_a are exact symplectic and show that they have an associated Hamiltonian.

Proposition A.0.7. *Let f_a be a smooth family of exact symplectic diffeomorphisms. We have*

If f_0 is exact symplectic, then f_a is exact symplectic if and only if there exists a family of functions $F_a : M \to \mathbb{R}$ such that:

$$i_{\mathcal{F}_a}\omega = dF_a$$

Proof:

By the definition of f_a being exact symplectic, we know that there exists a family of primitive functions P^{f_a} which satisfy

$$f_a^*(\alpha) = \alpha + P^{f_a}$$

and hence we have that

$$d\left(\frac{d}{da}P^{f_a}\right) = \frac{d}{da}f_a^*(\alpha)$$

The right side of the equation is the Lie derivative of α with respect to the vector field $\mathcal{F}_a$. Thus we can use Cartan's formula to say that

$$d\left(\frac{d}{da}P^{f_a}\right) = f_a^*(i_{\mathcal{F}_a}d\alpha + di_{\mathcal{F}_a}\alpha)$$

And hence, by rearranging terms we have that

$$f^*(i_{\mathcal{F}_a}\omega) = d\left[\frac{d}{da}P^{f_a} - f^*I_{\mathcal{F}_a}\alpha\right] = d\psi_a$$

where $\psi_a = \frac{d}{da}P^{f_a} - f^*I_{\mathcal{F}_a}\alpha$. Since f_a is a diffeomorphism, we can say that

$$i_{\mathcal{F}_a}\omega = d\left[(f_a)_*\left(\frac{d}{da}P^{f_a}\right) - i_{\mathcal{F}_a}\alpha\right]$$

where, recall that $(f_a)_* = (f_a^{-1})^*$. Hence we can take

$$F_a = (f_a)_*\left(\frac{d}{da}P^{f_a}\right) - i_{\mathcal{F}_a}\alpha$$

□

Now we derive a formula for the Hamiltonian generating $h_a = g_a \circ f_a$ in terms of F_a and G_a.

With this we can now state the following proposition that tells us how to compute the Hamiltonian of the composition and inverses of families of exact symplectic diffeomorphisms was needed in both Theorems 2.2.1 and 2.3.3

Proposition A.0.8. *If $f_a : M \to M$ and $g_a : M \to M$ are exact symplectic diffeomorphisms generated by their Hamiltonians $F_a : M \to \mathbb{R}$ and $G_a :\to \mathbb{R}$ respectively, then we have:*

(1) *If we define $h_a = g_a \circ f_a$, its Hamiltonian H_a is given by*

$$H_a = G_a + F_a \circ g_a^{-1}$$

(2) *If $g_a \circ f_a = Id$ then*

$$G_a + F_a \circ g_a^{-1} = 0$$

Proof: By Prop. A.0.7 we have that

$$i_{\mathcal{H}_a}\omega = i_{\mathcal{G}_a + (g_a)_*\mathcal{F}_a}\omega = G_a + i_{(g_a)_*\mathcal{F}_a}\omega$$

Now we compute that

$$(i_{(g_a)_*\mathcal{F}_a}\omega)(v) = \omega(Dg_a \circ g_a^{-1}\mathcal{F}_a \circ g_a^{-1}, v)$$

Since g_a^{-1} is symplectic we can furthermore say that

$$\begin{aligned}\omega(Dg_a \circ g_a^{-1}\mathcal{F}_a \circ g_a^{-1}, v) &= \omega(Dg_a^{-1}Dg_a \circ g_a^{-1}\mathcal{F}_a \circ g_a^{-1}, Dg_a^{-1}v) \\ &= \omega(\mathcal{F}_a \circ g_a^{-1}, Dg_a^{-1}v)\end{aligned} \tag{A.2}$$

However, by the definition of F_a we have that

$$\omega(\mathcal{F}_a \circ g_a^{-1}, Dg_a^{-1}v) = dF_a \circ g_a^{-1} \cdot Dg_a^{-1}v = d(F_a g_a^{-1}) \cdot v$$

Thus we have proven that

$$i_{(g_a)_*\mathcal{F}_a}\omega = d(F_a g_a^{-1})$$

which thus completes the proof of the proposition. □

Bibliography

[1] Iupac compendium of chemical terminology – the gold book, 2009.

[2] Ralph Abraham and Joel Robbin. *Transversal mappings and flows*. An appendix by Al Kelley. W. A. Benjamin, Inc., New York-Amsterdam, 1967.

[3] V. I. Arnol′d. Small denominators and problems of stability of motion in classical and celestial mechanics. *Uspehi Mat. Nauk*, 18(6 (114)):91–192, 1963.

[4] V. I. Arnol′d. Instability of dynamical systems with many degrees of freedom. *Dokl. Akad. Nauk SSSR*, 156:9–12, 1964.

[5] V. I. Arnol′d. *Mathematical methods of classical mechanics*, volume 60 of *Graduate Texts in Mathematics*. Springer-Verlag, New York, 199? Translated from the 1974 Russian original by K. Vogtmann and A. Weinstein, Corrected reprint of the second (1989) edition.

[6] Luis Barreira and Yakov B. Pesin. *Lyapunov exponents and smooth ergodic theory*, volume 23 of *University Lecture Series*. American Mathematical Society, Providence, RI, 2002.

[7] Peter W. Bates, Kening Lu, and Chongchun Zeng. Approximately invariant manifolds and global dynamics of spike states. *Invent. Math.*, 174(2):355–433, 2008.

[8] E. A. Belbruno and J. K. Miller. Sun-perturbed earth-to-moon transfers with ballistic capture. *Journal of Guidance Control Dynamics*, 16:770–775, 1993.

[9] D. Blazevski and C. Ocampo. Periodic orbits in the concentric circular restricted four-body problem and their invariant manifolds. *Physica D: Nonlinear Phenomena, available online*, 2012.

[10] Daniel Blazevski and Rafael de la Llave. Localized stable manifolds of whiskered tori in coupled map lattices with decaying interaction. *In preparation.*

[11] Daniel Blazevski and Rafael de la Llave. Time-dependent scattering theory for ODEs and applications to reaction dynamics. *Journal of Physics A: Mathematical and Theoretical*, 44(19):195101, 2011.

[12] Daniel Blazevski and Diego del Castillo-Negrete. parallel heat transport in reversed shear magnetic field configurations. *In preparation.*

[13] Daniel Blazevski and Diego del Castillo-Negrete. Slow diffusion across shearless cantori. *In preparation.*

[14] Daniel Blazevski and Jennifer Franklin. Using scattering theory to compute invariant manifolds in the laser-driven henon-heiles system. *In preparation.*

[15] M. V. Budyansky, M. Yu. Uleysky, and S. V. Prants. Detection of barriers to cross-jet lagrangian transport and its destruction in a meandering flow. *Phys. Rev. E*, 79(5):056215, May 2009.

[16] Xavier Cabré, Ernest Fontich, and Rafael de la Llave. The parameterization method for invariant manifolds. I. Manifolds associated to non-resonant subspaces. *Indiana Univ. Math. J.*, 52(2):283–328, 2003.

[17] C. C. Conley. Low energy transit orbits in the restricted three-body problem. *SIAM J. Appl. Math.*, 16:732–746, 1968.

[18] Stephen Coombes and Paul C. Bressloff, editors. *Bursting: the Genesis of Rhythm in the Nervous System.* World Scientific Publishing Co. Pte. Ltd., 2005.

[19] R. de la Llave, J. M. Marco, and R. Moriyón. Canonical perturbation theory of Anosov systems and regularity results for the Livšic cohomology equation. *Ann. of Math. (2)*, 123(3):537–611, 1986.

[20] R. de la Llave and R. Obaya. Regularity of the composition operator in spaces of Hölder functions. *Discrete Contin. Dynam. Systems*, 5(1):157–184, 1999.

[21] D. del Castillo-Negrete and L. Chacón. Parallel heat transport in integrable and chaotic magnetic fields. *submitted.*

[22] D. del Castillo-Negrete and L. Chacón. Local and nonlocal parallel heat transport in general magnetic fields. *Phys. Rev. Lett.*, 106(19):195004, May 2011.

[23] D. del Castillo-Negrete, J. M. Greene, and P. J. Morrison. Area preserving nontwist maps: periodic orbits and transition to chaos. *Physica D: Nonlinear Phenomena*, 91(1-2):1 – 23, 1996.

[24] D. del Castillo-Negrete, J. M. Greene, and P. J. Morrison. Renormalization and transition to chaos in area preserving nontwist maps. *Physica D: Nonlinear Phenomena*, 100(3-4):311 – 329, 1997.

[25] Diego del Castillo-Negrete and P. J. Morrison. Chaotic transport by rossby waves in shear flow. 5(4):948–965, 1993.

[26] Amadeu Delshams, Rafael de la Llave, and Tere M. Seara. A geometric mechanism for diffusion in Hamiltonian systems overcoming the large gap problem: heuristics and rigorous verification on a model. *Mem. Amer. Math. Soc.*, 179(844):viii+141, 2006.

[27] Philip Du Toit, Igor Mezić, and Jerrold Marsden. Coupled oscillator models with no scale separation. *Phys. D*, 238(5):490–501, 2009.

[28] G. Bard Ermentrout and David H. Terman. *Mathematical foundations of neuroscience*, volume 35 of *Interdisciplinary Applied Mathematics*. Springer, New York, 2010.

[29] Neil Fenichel. Persistence and smoothness of invariant manifolds for flows. *Indiana Univ. Math. J.*, 21:193–226, 1971/1972.

[30] E. Fermi, J. Pasta, and S. Ulam. Studies of nonlinear problems. i. In A. C. Newell, editor, *Nonlinear wave motion. Lectures in applied math-*

ematics, vol. 15, pages 143–156. Amer. Math. Soc., Providence, R.I., 1955.

[31] Ernest Fontich, Rafael de la Llave, and Pau Martín. Dynamical systems on lattices with decaying interaction I: a functional analysis framework. *J. Differential Equations*, 250(6):2838–2886, 2011.

[32] Ernest Fontich, Rafael de la Llave, and Pau Martín. Dynamical systems on lattices with decaying interaction II: hyperbolic sets and their invariant manifolds. *J. Differential Equations*, 250(6):2887–2926, 2011.

[33] Ernest Fontich, Rafael de la Llave, and Yannick Sire. Construction of invariant whiskered tori by a parameterization method. part II: Quasi-periodic and almost periodic breathers in coupled map lattices. *Submitted*, 2012.

[34] G. Friesecke and R. L. Pego. Solitary waves on FPU lattices. I. Qualitative properties, renormalization and continuum limit. *Nonlinearity*, 12(6):1601–1627, 1999.

[35] G. Friesecke and R. L. Pego. Solitary waves on FPU lattices. II. Linear implies nonlinear stability. *Nonlinearity*, 15(4):1343–1359, 2002.

[36] G. Friesecke and R. L. Pego. Solitary waves on Fermi-Pasta-Ulam lattices. III. Howland-type Floquet theory. *Nonlinearity*, 17(1):207–227, 2004.

[37] G. Friesecke and R. L. Pego. Solitary waves on Fermi-Pasta-Ulam lattices. IV. Proof of stability at low energy. *Nonlinearity*, 17, 2004.

[38] A. G. Suárez, D. Hestroffer, and D. Farrelly. Formation of the extreme Kuiper-belt binary 2001 QW_{322} through adiabatic switching of orbital elements. *Celestial Mech. Dynam. Astronom.*, 106(3):245–259, 2010.

[39] Antonio Gamboa Suárez, Daniel Hestroffer, and David Farrelly. Formation of the extreme Kuiper-belt binary 2001 QW_{322} through adiabatic switching of orbital elements. *Celestial Mech. Dynam. Astronom.*, 106(3):245–259, 2010.

[40] Wulfram Gerstner and Werner M. Kistler. *Spiking neuron models*. Cambridge University Press, Cambridge, 2002. Single neurons, populations, plasticity.

[41] G. Gòmez, A. Jorba, J. Masdemont, and C. Simò. Study of the transfer from the earth to a halo orbit around the equilibrium point L1;. *Celestial Mechanics and Dynamical Astronomy*, 56:541–562, 1993. 10.1007/BF00696185.

[42] John Guckenheimer and Philip Holmes. *Nonlinear oscillations, dynamical systems, and bifurcations of vector fields*, volume 42 of *Applied Mathematical Sciences*. Springer-Verlag, New York, 1990. Revised and corrected reprint of the 1983 original.

[43] Eugene Gutkin. Asymptotics of trajectories for cone potentials. *Phys. D*, 17(2):235–242, 1985.

[44] Eugene Gutkin. Integrable Hamiltonians with exponential potential. *Phys. D*, 16(3):398–404, 1985.

[45] J. Hadamard. Sur le module maximum d'une fonction et de ses derives. *Bull. Soc. Math. France*, 42:68–72, 1898.

[46] Jack K. Hale. *Ordinary differential equations*. Robert E. Krieger Publishing Co. Inc., Huntington, N.Y., second edition, 1980.

[47] M. W. Hirsch, C. C. Pugh, and M. Shub. *Invariant manifolds*. Lecture Notes in Mathematics, Vol. 583. Springer-Verlag, Berlin, 1977.

[48] Philip J. Holmes and Jerrold E. Marsden. Melnikov's method and Arnol′d diffusion for perturbations of integrable Hamiltonian systems. *J. Math. Phys.*, 23(4):669–675, 1982.

[49] Kathleen C Howell and David B Spencer. Periodic orbits in the restricted four-body problem. *Acta Astronautica*, 13(8):473–479, 1986.

[50] Andrea Hubacher. Classical scattering theory in one dimension. *Comm. Math. Phys.*, 123(3):353–375, 1989.

[51] Eugene M. Izhikevich. *Dynamical systems in neuroscience: the geometry of excitability and bursting*. Computational Neuroscience. MIT Press, Cambridge, MA, 2007.

[52] C. Jaff, S.D. Ross, M.W. Lo, J. Marsden, D. Farrelly, and T. Uzer. Statistical theory of asteroid escape rates. *Phys Rev Lett*, 89(1):011101, 2002.

[53] Miaohua Jiang and Rafael de la Llave. Smooth dependence of thermodynamic limitsof SRB-measures. *Communications in Mathematical Physics*, 211:303–333, 2000. 10.1007/s002200050814.

[54] T.J. Kalvouridis, M. Arribas, and A. Elipe. Parametric evolution of periodic orbits in the restricted four-body problem with radiation pressure. *Planetary and Space Science*, 55(4):475 – 493, 2007.

[55] S. Kawai, A. Bandrauk, C. Jaffe, T. Bartsch, J. Palacian, and T. Uzer. Transition state theory for laser-driven reactions. *The Journal of Chemical Physics*, 126(16):164306, 2007.

[56] Shinnosuke Kawai, Andre D. Bandrauk, Charles Jaffe, Thomas Bartsch, Jesus Palacian, and T. Uzer. Transition state theory for laser-driven reactions. *The Journal of Chemical Physics*, 126(16):164306, 2007.

[57] Papadakis K.E. Asymptotic orbits in the restricted four-body problem. *Planetary and Space Science*, 55(10):1368 – 1379, 2007.

[58] A. Kolmogoroff. On inequalities between the upper bounds of the successive derivatives of an arbitrary function on an infinite interval. *Amer. Math. Soc. Translation*, 1949(4):19, 1949.

[59] Wang Sang Koon, Jerrold E. Marsden, Shane D. Ross, and Martin W. Lo. Constructing a low energy transfer between Jovian moons. In *Celestial mechanics (Evanston, IL, 1999)*, volume 292 of *Contemp. Math.*, pages 129–145. Amer. Math. Soc., Providence, RI, 2002.

[60] Carl D. Murray and Stanley F. Dermott. *Solar system dynamics*. Cambridge University Press, Cambridge, 1999.

[61] Edward Nelson. *Topics in dynamics. I: Flows*. Mathematical Notes. Princeton University Press, Princeton, N.J., 1969.

[62] Roger G. Newton. *Scattering theory of waves and particles*. Dover Publications Inc., Mineola, NY, 2002. Reprint of the 1982 second edition [Springer, New York; MR0666397 (84f:81001)], with list of errata prepared for this edition by the author.

[63] Yakov B. Pesin. *Lectures on partial hyperbolicity and stable ergodicity*. Zurich Lectures in Advanced Mathematics. European Mathematical Society (EMS), Zürich, 2004.

[64] Michael Reed and Barry Simon. *Methods of modern mathematical physics. I.* Academic Press Inc. [Harcourt Brace Jovanovich Publishers], New York, second edition, 1980. Functional analysis.

[65] Walter Rudin. *Functional analysis*. International Series in Pure and Applied Mathematics. McGraw-Hill Inc., New York, second edition, 1991.

[66] Susumu Shinohara and Yoji Aizawa. Indicators of reconnection processes and
transition to global chaos in nontwist maps. *Progress of Theoretical Physics*, 100(2):219–233, 1998.

[67] Carles Simò. On the Analytical and Numerical Approximation of Invariant Manifolds. In D. Benest & C. Froeschle, editor, *Modern Methods in Celestial Mechanics, Comptes Rendus de la 13ieme Ecole Printemps d'Astrophysique de Goutelas (France), 24-29 Avril, 1989. Edited by Daniel Benest and Claude Froeschle. Gif-sur-Yvette: Editions Frontieres, 1990., p.285*, pages 285–+, 1990.

[68] Carles Simò. Effective computations in hamiltonian dynamics. *Cent annes après les Méthodes Nouvelles de H. Poincaré, Societe Mat. de France*, 1996.

[69] P. S. Soulis, K. E. Papadakis, and T. Bountis. Periodic orbits and bifurcations in the Sitnikov four-body problem. *Celestial Mech. Dynam. Astronom.*, 100(4):251–266, 2008.

[70] Yoshihiko Susuki, Igor Mezić, and Takashi Hikihara. Coherent swing instability of power grids. *J. Nonlinear Sci.*, 21(3):403–439, 2011.

[71] Victor G. Szebehely. *Theory of Orbits: the Restricted Problem of Three Bodies*. Academic Press, New York, 1967.

[72] Walter Thirring. *A course in mathematical physics. Vol. 3*. Springer-Verlag, New York, 1981. Quantum mechanics of atoms and molecules, Translated from the German by Evans M. Harrell, Lecture Notes in Physics, 141.

[73] Walter Thirring. *Classical mathematical physics*. Springer-Verlag, New

York, third edition, 1997. Dynamical systems and field theories, Translated from the German by Evans M. Harrell, II.

[74] R. Thom and H. Levine. Singularities of differentiable mappings. In C.T. Wall, editor, *Proceedings of Liverpool Singularities— Symposium. I (1 969/1970).*, pages 1–89. Springer-Verlag, Berlin, 1971.

[75] Dmitry Treschev and Oleg Zubelevich. *Introduction to the perturbation theory of Hamiltonian systems*. Springer Monographs in Mathematics. Springer-Verlag, Berlin, 2010.

[76] Holger Waalkens, Roman Schubert, and Stephen Wiggins. Wigner's dynamical transition state theory in phase space: classical and quantum. *Nonlinearity*, 21(1):R1–R118, 2008.

Vita

Daniel Blazevski was born in Detroit, Michigan, on July 18, 1984, the son of Krume Blazevski and Danca Marinkovska. After completing his High School studies in Harrison Township, Michigan, 2002, he entered Wayne State University. He later transfered to the University of Michigan where he received a (B. S.) in Mathematics with Highest Honors in 2006.

He then spent a semester studying mathematics and the Russian language in Moscow. He began his PhD studies in mathematics at the University of Texas at Austin in 2007. In June 2012, he plans on beginning a postdoctoral position at the Swiss Federal Institute of Technology in Zurich (ETH Z) under the mentorship of George Haller.

Permanent address: dblazevski@math.utexas.edu

This dissertation was typeset with LaTeX[‡] by the author.

[‡]LaTeX is a document preparation system developed by Leslie Lamport as a special version of Donald Knuth's TeX Program.